P-07-41

Oskarshamn site investigation

Structural analysis of brittle deformation zones in the Simpevarp-Laxemar area, Oskarshamn, southeast Sweden

Giulio Viola, Guri Venvik Ganerød
Geological Survey of Norway, N-7491 Trondheim, Norway

March 2007

Svensk Kärnbränslehantering AB
Swedish Nuclear Fuel
and Waste Management Co
Box 5864
SE-102 40 Stockholm Sweden
Tel 08-459 84 00
+46 8 459 84 00
Fax 08-661 57 19
+46 8 661 57 19

ISSN 1651-4416
SKB P-07-41

Oskarshamn site investigation

Structural analysis of brittle deformation zones in the Simpevarp-Laxemar area, Oskarshamn, southeast Sweden

Giulio Viola, Guri Venvik Ganerød
Geological Survey of Norway, N-7491 Trondheim, Norway

March 2007

Keywords: Oskarshamn, AP PS 400-05-096, Structural geology, Deformation zone, Fault zone, Cataclasite, Fault breccia, Kinematics.

Abstract

A study of predominantly brittle structures, i.e. brittle deformation zones, faults, fractures and associated fault rocks, was carried out in the Simpevarp-Laxemar area, Oskarshamn. The main aim of the study was to document from a geometric and kinematic point of view the brittle deformation history of the area. Moreover, the study deals with the detailed characterization of the observed deformation zones and fault rocks were systematically investigated in order to improve our understanding of the deformation mechanisms that controlled the local brittle structural evolution.

Structural data were obtained from field observations and from detailed logging of selected drill core sections from a variety of boreholes. These results were integrated with observations from thin sections prepared from carefully selected and structurally controlled samples.

The structures investigated in the area include low-grade brittle-ductile shear zones, proper brittle faults containing several generations of cataclasites and breccias cemented by diagenetic minerals and systematic sets of hybrid fractures of limited offset.

In most field localities and drill cores there are abundant joints and dilational fracture sets, commonly with only minor offset. These are in most cases coated or filled with a range of different minerals reflecting changing environmental conditions during successive deformation events.

Striated surfaces were used to constrain the kinematics of fault zones. Such data were obtained from outcrops and, to a variable extent, from several oriented deformation zones in the drill cores. In total, a considerable amount of new data has been acquired that is crucial to the understanding of the structural evolution of brittle faults, deformation zones and fractures on a local and regional scale and their complete characterization.

In detail, the Laxemar area is characterized by conjugate sets of steep strike-slip brittle faults and shear fractures whose orientation allows for their geometric correlation to the lineaments previously identified in the area by SKB. A prominent NS trending set, a ENE-WSW dextral set together with their respective Riedel shears and a well defined family of fractures trending ESE-WNW, whose kinematics remain as yet undetermined, are the most striking features observed in this subarea.

Moving eastward towards Simpevarp, the overall fracture/fault orientation pattern becomes more complex and heterogeneous. This is in part due to a gradual change of the lineaments' orientation, with a set of NNE-SSW and NE-SW trending lineaments becoming the most characteristic structural orientations. This orientation change may be possibly linked to the presence of the intervening NE-SW trending sinistral Äspö mylonite belt, which may have played a role in controlling the orientation of later brittle structures.

Very important is the identification of a set of small-scale, moderately to gently SSW and N/NNE dipping fault planes that are either normal or reverse faults. They occur in Laxemar as well as in the Simpevarp Peninsula and along its coastline.

Time relationships among the fractures/faults identified are difficult to constrain, although the general impression is that flat lying structures generally postdate the steep structures.

Several deformation zones were logged and characterized in drill cores. They contain very often fault rocks in their cores and they range from cohesive cataclasites to non-cohesive breccias, although cohesive fault rocks dominate.

Kinematic indications and the characteristics of the deformation zones found in the oriented cores correlate well with field observations.

Sammanfattning

En undersøkelse hovedsakelig rettet mot sprø strukturer, som sprø forkastninger, brudd og assosierte forkastningsbergarter, er utført i Simpevarp-Laxemar området, Oskarshamn. Hovedmålet for undersøkelsen er å dokumentere den sprø deformasjonshistorien i området basert på geometriske og kinematiske data. I tillegg er en detaljert karakterisering av observerte deformasjonssoner og forkastningsbergarter utført systematisk for å oppnå en bedre forståelse av deformasjonsmekanismen som kontrollerte den lokale, sprø deformasjonshistorien.

Strukturgeologiske data er samlet fra feltobservasjoner og fra detaljert kartlegging av utvalgte seksjoner fra borekjerner fra et utvalg borehull. Dette er integrert med observasjoner fra polerte tynnslip fra nøye utvalgte prøver fra felt og borekjerner. Tynnslipene som ble studert ved hjelp av standard petrografiske teknikker, og i noen tilfeller supplert med SEM (backscatter).

De undersøkte strukturene som finnes i området omfatter fra lavgrads, sprø-duktile skjærsoner til sprø forkastninger med flere generasjoner av kataklasitt og breksje sementert av diagenetiske mineraler, og systematiske sett av hybridbrudd med begrenset separasjon. Disse observasjonene er i samsvar med en rekke av hendelser med stadig mer sprø deformasjon som følger etter plastisk deformasjon.

I de fleste feltlokaliteter og borekjerner er det rikelig med sprekker og dilasjons-bruddsett, ofte med liten separasjon. Disse er i de fleste tilfeller dekket eller fylt med et utvalg av mineraler som gjenspeiler forandring i miljøet under suksessive deformasjonshendelser.

Bruddflater med striasjoner er brukt til å bestemme kinematikken til forkastningssoner. Slike data er samlet fra blotninger i felt og, i varierende grad, fra flere orienterte deformasjonssoner i borekjerner. Til sammen utgjør dette et betydelig antall nye data som er avgjørende for forståelsen for strukturell utvikling av sprø forkastninger, og en fullstendig beskrivelse av deformasjonssoner og brudd i lokal og regional skala.

Laxemar-området er karakterisert av konjugerte sett av steile strøk-slipp forkastninger og skjærbrudd, som har lignende orientering som lineamenter kartlagt av SKB. Et fremtredende (NS-gående) sett, et ØNØ-VSV høyrelengs sett med sine respektive Riedel-skjær, og et veldefinert bruddsett med ØSØ-VNV retning hvor kinematikken er ubestemt, er de mest fremtredende strukturene i subbområdet Laxemar.

Lenger øst mot Simpevarp blir den generelle orienteringen av brudd og forkastninger mer kompleks og heterogen. Dette er delvis på grunn av en gradvis endring i lineament-orientering, hvor et sett med NNØ-SSV og NØ-SV gående lineamenter er de mest fremtredende strukturene i området. Endringen i bruddorientering kan muligens relateres til det mellomliggende NØ-SV orienterte, med venstrelengs bevegelse, som muligens har spilt en kontrollerende rolle i orienteringen av senere, sprø strukturer.

En viktig observasjon er et sett av småskala forkastningsplan, med moderat til svakt fall mot SSV og N/NNØ, og med enten normal eller revers bevegelse. Disse forekommer i Laxemar, på Simpevarp-halvøya og langs kysten.

Tidsrelasjoner mellom identifiserte brudd/forkastninger er vanskelig å bestemme, selv om det generelle inntrykket er at flate strukturer postdaterer steile strukturer.

I det undersøkte området finnes det gode blotninger av forkastninger i vegskjæringer og langs kysten. Distinkte populasjoner og forkastningsbergarter kan identifiseres. Disse strukturene er trolig relatert til bevegelse langs store, regionale forkastninger. Forkastningene har gode ”slickensides” (lineasjoner) og har dermed potensiell nytte i en kinematisk analyse.

Forkastningsbergarter som er identifisert og beskrevet i borekjernene varierer fra kohesive kataklasitter til ikke-kohesive breksjer. De kohesive forkastningsbergartene dominerer, og har ofte en sentral kjerne av gouge. Spekteret av forkastningsbergarter reflekterer enten gradvis minkende trykk og temperatur under forkastningsaktiviteten, eller en reaktivering av eksisterende forkastninger. I de identifiserte forkastningssonene er forekomsten av forkastningsbergarter relativt tykk, fra noen få meter til titalls meter. Bredden på forkastningssonene reflekterer størrelsen på forkastningen, og dens mulige sammenheng med lineamenter kartlagt på overflaten.

Kinematiske data fra borekjernene samsvarer godt med det som er funnet i felt, og den generelle trenden for området.

Contents

1 Introduction

This document provides a detailed characterization, in terms of geometry, kinematics and overall deformation characteristics, of selected brittle deformation zones at the Oskarshamn investigation site (Figure 1-1). Deformation zones were studied at a number of outcrops so as to gain insights into the general field relationships, and in a series of chosen drill cores, selected due to the relevance of the deformation zones they intersected, identified in the geological single-hole interpretation.

This study forms one of the activities performed within the site investigation process at Oskarshamn. The work was carried out in accordance with activity plan AP PS 400-05-096. Controlling documents for performing this activity are listed in Table 1-1. Both activity plan and method descriptions are SKB's internal controlling documents.

Table 1-1. Controlling documents for the performance of the activity.

Activity plan	**Number**	**Version**
Karaktärisering av spröda deformationszoner	AP PS 400-05-086	1.0
Method descriptions	**Number**	**Version**
/Braathen 1999/	Tectonophysics 302, 99-121.	
/Braathen et al. 2002/	Norwegian Journal of Geology, 82, 225–241.	
/Braathen et al. 2004/	Tectonics, 23, TC4010, doi:10.1029/2003TC001558.	
/Munier et al. 2003/	SKB R-03-07	
/Nordgulen et al. 2002/	Norwegian Journal of Geology, 82, 299–316.	
/Osmundsen et al. 2003/	Journal of the Geological Society, London 160, 1–14.	
/Petit 1987/	Journal of Structural Geology 9, 597–608.	

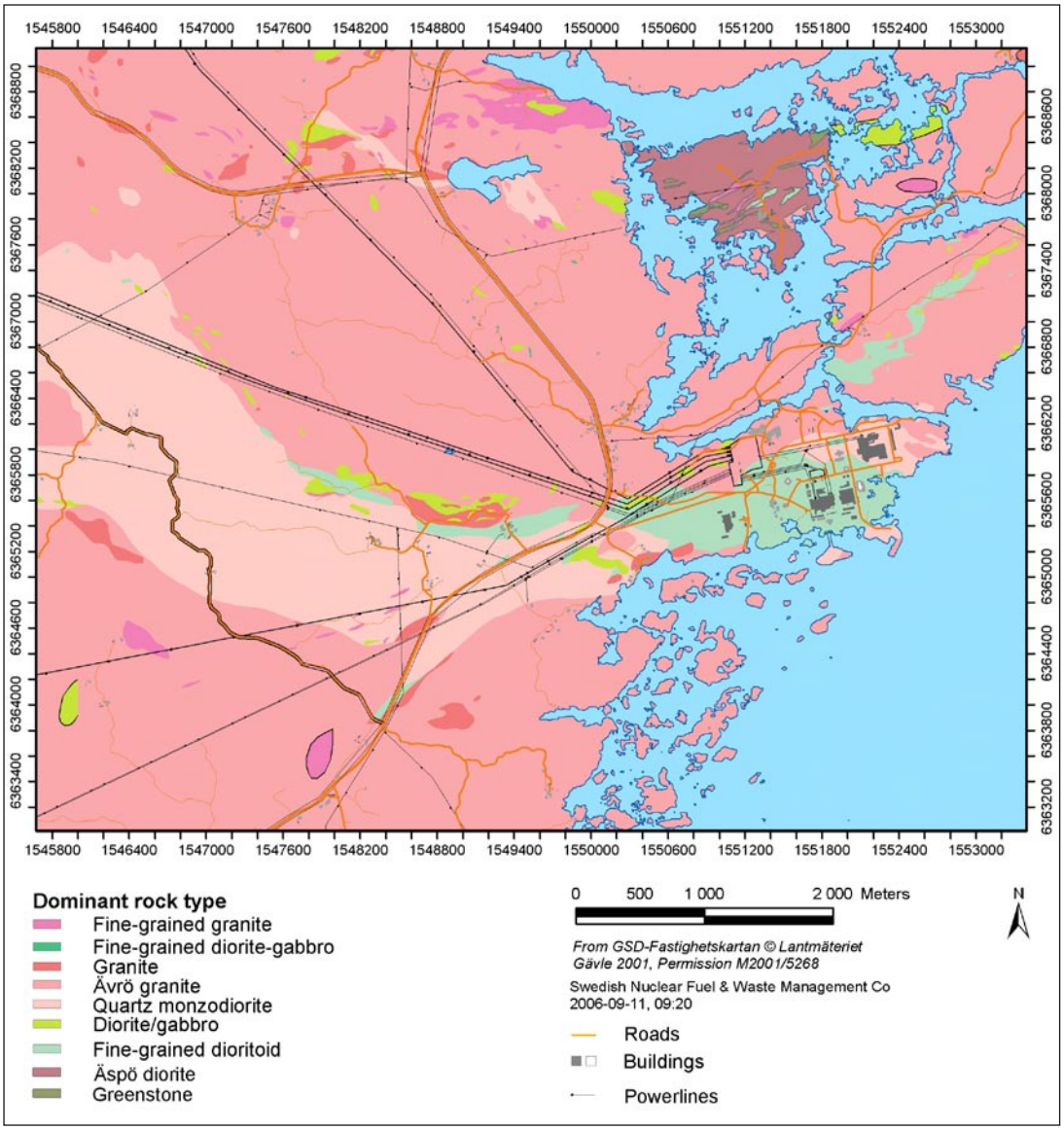

Figure 1-1. *Geology map of the Oskarshamn site investigation area.*

2 Objective and scope

The aim of this study is to document, describe and characterize geometrically and kinematically, by means of detailed and systematic geometric and kinematic structural analysis, several brittle deformation zones observed in the field and in a series of selected drill cores. The associated fault rocks, when present, were also investigated in order to improve our understanding of the deformation mechanisms that controlled the local brittle structural history. Data from the field and from drill cores, combined with observations from selected thin sections, form the basis for the results and conclusions of this study.

3 Equipment

3.1 Description of equipment/interpretation tools

During fieldwork and core inspection, we used the standard equipment for structural investigations, including hammer, compass, hand lens, diluted HCl, digital camera, and GPS for locating observation points according to SKB standards (Swedish Grid coordinate system). Samples collected in the field and from drill cores were cut in the laboratory, and selected oriented slabs were marked and sent in for preparation of polished, oriented thin sections. The thin sections were analysed petrographically.

4 Execution

4.1 Methodology

The project was carried out in conformity with the accepted activity plan AP PS 400-05-096. Literature studies preceded the investigations that were carried out at the Oskarshamn site on October 17–21, December 5–9, 2005 and March 20–23 2006.

Five days were devoted to fieldwork in the Laxemar, Simpevarp and Äspö areas and nine to the logging of individual deformation zones (DZ) in drill cores that were identified in the geological single-hole interpretation. The following drill cores (in brackets are reported the logged depth intervals) were inspected: KSH03A (160–275 m), KLX04 (873–973 m), KLX06 (368–390 m), KLX07 (111–180 m, 604–659 m and 816–838 m), KLX07B (120–175 m), KLX08 (100–165 m, 218–252 m and 760–781 m) and KLX10 (389–432,5 m and 471–499 m). The standard procedure for obtaining the true orientation of linear structures (lineations, striations, etc) on fault surfaces in drill cores of known orientation is as follows:

1. Fractures of potential interest are identified by visual inspection of drill cores from selected deformation zones, as defined previously by the geological single hole interpretations.
2. Individual fractures are identified on the BIPS image of the borehole wall, which provides a mirror image of the core itself. Care has to be taken to ensure that the fracture selected on the image matches the one from the drill core. In some cases this can be challenging, particularly where numerous fractures cut the core at different angles. Independent checks that the correct fracture is chosen can be carried out by using information contained in the drill core database, as, for example, the properties of the fracture itself, the acute angle α between the fracture and the core axis, and the angle β, which is the angle (measured counter-clockwise) from the lower intersection of the fracture with the core wall, to the top of the drill core.
3. Having identified the fracture of interest, the top of the drill core is marked based on visual inspection of the BIPS image and on the angle β. Fractures' orientation (strike and dip) is obtained using the information contained in the drill core database.
4. The core is positioned the right way up and at the true inclination using a core holder supplied by SKB. This device allows the accurate adjustment of the core inclination as given in the database.
5. The orientation of the linear structure is determined by measuring its plunge direction and plunge.
6. When the sense of slip can be determined with confidence, the true movement of the hanging wall with respect to the footwall of the fault is established.
7. Relevant data are recorded in a database.

Thin section samples were collected in the field and from some of the drill cores. A total of 48 polished sections were studied at the Geological Survey of Norway (Trondheim) using standard petrographic techniques, and in some cases also backscattered scanning electron microscopy (SEM).

4.2 Data handling and processing

Structural data were analysed at the Geological Survey of Norway (NGU) in Trondheim and plotted using standard techniques.

Thin sections were analysed in several steps:

1) Scanning at high resolution of the entire section using a standard slide scanner.
2) Printing of the scanned jpg-images as A4 colour prints that aid greatly in establishing general structural and textural relationships and are crucial in locating critical sites for further detailed study.
3) Petrographic analysis and documentation of textural and micro-structural relationships using a digital camera attached to the microscope.
4) Detailed studies of specific mineralogical and textural details using SEM in backscatter mode (not included in this report).

4.3 Analysis and interpretation

The working methods used during both fieldwork and structural data analysis and petrographic work are described in /Braathen 1999, Braathen et al. 2002, Nordgulen et al. 2002, Osmundsen et al. 2003/. In this report, the definition of fault rocks is done according to the classification in /Braathen et al. 2004/. Criteria for identifying kinematic indicators in the brittle regime are presented, for example, in /Petit 1987/.

A systematic analysis of fault slip data at the micro- and meso-scale has been made aiming towards an improved understanding of kinematic patterns in the area of interest. The approach consists in the analysis of strike and dip of fault planes and of azimuth and plunge of their striations. This allows the determination of the complete kinematics of fault trends (even major fault trends). It also provides the basis for paleo-stress inversion calculations that can aim at the reconstruction of the stress field evolution through time. Figure 4-1 provides the key to read the conventions used in the stereonets to represent the orientation and the kinematics of individual fault plane/striation pairs.

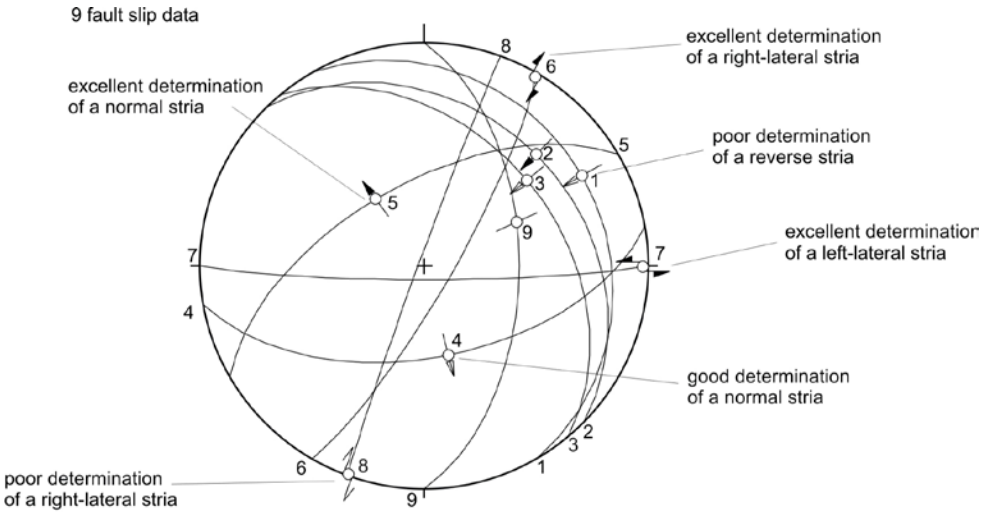

Figure 4-1. *Example of a stereonet plotting kinematic information for striated fault planes (Schmidt projection, lower hemisphere). Keys for striae: outward directed arrow: normal striation (numbers 4 and 5 on stereoplot); inward directed arrow: reverse striation (numbers 1, 2 and 3); couple of arrows: strike-slip striation (numbers 6, 7 and 8); full black arrowhead: excellent constraints on the sense of shear (numbers 2, 5, 6 and 7); empty arrowhead: good constraints on the sense of shear (numbers 3 and 4); open arrowhead: poor constraints on the sense of shear (numbers 1 and 8); thin line without any arrowhead: no constraints on the sense of shear (number 9).*

4.4 Nonconformities

No nonconformities have been noted.

4.5 Fault architecture and nomenclature

Faults occur on all scales in the lithosphere. They control the spatial arrangement of rock units, affect the topography, control the permeability of rocks and sediments and, more importantly, create deformation (strain, plus rotation plus translation) during plate interaction and intraplate movements. The term fault zone is generally used for brittle structures in which loss of continuity and slip occurs on several discrete faults within a band of definable width. Shear zones, on the other hand, are ductile structures, across which a rock body does not lose continuity so that strain is progressively distributed across a band of definable width. Based on this definition, a fault zone is a volume of rock where strain is highly localized.

Commonly fault zones can be divided into a series of distinctive constituent elements (Figure 4-2 and Figure 4-3). These are 1) the *undeformed host rock*, 2) the *transition zone* /Munier et al. 2003/ (corresponding to the "damage zone" of /Gudmundsson et al. 2001/) and 3) the proper *fault core* /e.g. Caine et al. 1996, Evens et al. 1997, Braathen and Gabrielsen 2000/. The host rock consists of undisturbed rock with low fracture frequency of < 4 fractures/m /Munier et al. 2003/ (Figure 4-2). The transition zone still contains undeformed rock, but the fracture frequency generally increases up to 9 fractures/m (Figure 4-2). Narrow zones or bands of fault rock may occur, especially closer to the transition to the fault core. The width of the transition zone varies with the size of the fault zone and the style of deformation, and can range from a few meters to tens of meters. The fault core is identified by the occurrence of fault rock or intensively fractured rock (Figure 4-2 and Figure 4-3). Fault rocks may occur in lenses alternating with pods of relatively undeformed rock /Caine et al. 1996, Braathen and Gabrielsen 2000/. The width of the fault core may vary from cm to m /Braathen and Gabrielsen 2000/.

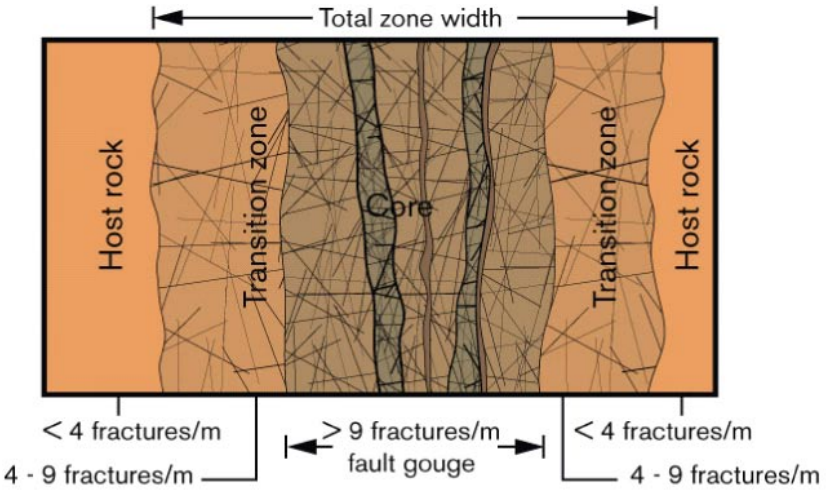

Figure 4-2. *Schematic illustration of a brittle deformation zone according to SKB definition /after Munier et al. 2003/*

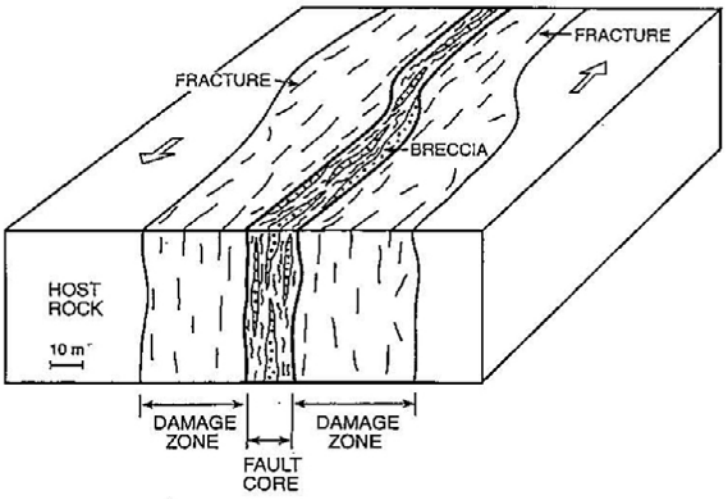

Figure 4-3. *Schematic illustration of the architecture of an idealized fault zone /Gudmundsson et al. 2001/. Note that the term "damage zone" corresponds conceptually to the term "transition zone" of Figure 4-2.*

Rocks that occur within fault zones provide primary evidence for the processes that have occurred there. It is therefore of great importance to fully characterize fault rock occurrences, so as to better understand faulting processes at all scales. Fault rocks form in response to strain localization within fault and shear zones and reflect the interplay of a variety of physical and environmental parameters such as the finite amount of strain, lithology, style of deformation (i.e. frictional or plastic flow), presence or absence of fluids, strain rate, temperature, pressure and so on. Figure 4-4 reports the classification scheme suggested by /Braathen et al. 2004/ that we will use in this study to classify fault rock occurrences.

Brittle ← *Deformation style* → **Ductile**									
Frictional flow ← *Dominant deformation mechanism* → **Plastic flow**									
Non-cohesive			Secondary cohesion		Primary cohesion				*% matrix and grain-size*
			Cemented HB	Indurated HB		*> 50% phyllosilicate*	*< 50% phyllosilicate*		
Hydraulic breccia (HB)	Breccia series	Proto-breccia	Cemented proto-breccia	Indurated proto-breccia	Cataclasite series	Proto-cataclasite	Proto-phyllonite	Proto-mylonite	Blastomylonite	*0-50% matrix*
		Breccia	Cemented breccia	Indurated breccia		Cataclasite	Phyllonite	Mylonite		*50-90% matrix*
		Ultra-breccia	Cemented ultra-breccia	Indurated ultra-breccia		Ultra-cataclasite	Ultra-phyllonite	Ultra-mylonite		*90-100% matrix*
		Gouge	Cemented gouge	Indurated gouge						*Sub-microscopic matrix*
			Pseudotachylyte							

Figure 4-4. *Fault rock classification scheme proposed by /Braathen et al 2004/.*

Table 4-1. Schematic description of different types of deformation mechanisms and fault rocks classified as per /Braathen et al. 2004/.

Term	Description	Note
Fault rocks or fault-related rocks	Commonly formed through strain concentration within a tabular or planar zone that experiences shear stress.	1
Frictional flow	Pressure, subordinate temperature and fluid controlled deformation mechanisms which have a brittle style: granulation of grains by inter, intra and transgranular micro fracturing, and intra or intergranular frictional sliding with abrasion of fracture walls and grain margins	2
Plastic flow	Mainly thermally activated, continuous deformation without rupture, with a ductile style of deformation: dislocation creep and glide, solid state diffusion creep, diffusional mass transfer, and viscous grain boundary sliding	
Non-cohesive	Not consolidated	3
Secondary cohesion	Consolidated after formation, either through cementation of the matrix, or through compaction, recrystallisation or neo-mineralisation (see indurated)	
Primary cohesion	Cohesion preserved during formation	3
Hydraulic fracturing	Fracturing caused by fluid pressure: commonly random orientation of fractures and rough fracture surfaces. The resulting hydraulic breccia may not be tabular or planar, however, it is tectonically induced and frequently fault-related.	4
Cemented	Consolidated through mineral precipitation in pores of the matrix	
Indurated	Consolidated basically by compaction due to directed pressure, annealing by recrystallisation of grains, or neomineralisation (e.g., muscovitisation, silicification, albitisation, epidotisation, saussuritisation). The term disregards cementation unless related to general neomineralisation	
Phyllosilicate content	Content of sheet-minerals (characterised by weak '001' bonds) of the phyllosilicate group	5
Matrix	Fine-grained material in a fault rock formed by granulation or dynamic recrystallisation of grains, filling the interstices between larger clasts of original rock	
Breccia	Mainly chaotic, non-cohesive fault rock, generated by frictional flow	3
Cataclasite	Mainly chaotic fault rock that developed with cohesion, which is generated by mainly frictional flow	6
Phyllonite	Phyllosilicate-rich fault rock with distinct mineral fabric, and dominated plastic flow	7
Mylonite	Fault rock with distinct mineral fabric, and dominated by plastic flow	8
Blasto-mylonite	Fault rock in which dynamic recrystallisation and/or neomineralisation causing grain-size increase of clasts, outpace grain-size reduction	8

1. For classification of fault rocks, see: *Higgins* [1971], *Bell & Etheridge* [1973], *Zeck* [1974], S*ibson* [1977a], *Wise et al.,* [1984], *Schmid & Handy* [1991].
2. Term introduced by *Schmid & Handy* [1991]. See also description of *Bell & Etheridge* [1973].
3. Concept introduced by *Higgins* [1971].
4. For hydraulic breccias, see e.g., *Clark & James* [2003]
5. Clay content as factor in classification of faults rocks in sedimentary units, e.g., *Fisher & Knipe* [1998].
6. Possible application of phyllosilicate content in the sub-division of fault rocks in sedimentary rocks, e.g., *Fisher & Knipe* [1998].
7. Definitions following *Knopf* [1931], however, adding a limit to the phyllosilicate content.
8. See definitions of *Sibson* [1977a].

We will now provide a brief characterization and description of each fault rock type:

Cataclastic rocks

Cataclastic rock is a general term for all rocks produced by cataclasis. Cataclastic rocks can be divided into two main types: (1) those without and (2) those with primary cohesion /Higgings 1971/.

(1) Cataclastic rocks without primary cohesion

Fault Breccia: A rock composed of angular to rounded fragments, formed by crushing or grinding along a fault. Most fragments are large enough to be visible to the naked eye, and they make up more than 30 percent of the rock. Coherence, if present, is due to secondary processes /Higgings 1971/.

Protobreccia – fragment size > 50 mm /Davis and Reynolds 1996/ and a matrix content of 0–50% /Braathen et al. 2004/.

Breccia - fragment size > 1 mm and < 50 mm /Davis and Reynolds 1996/ and a matrix content of 50–90% /Braathen et al. 2004/.

Ultrabreccia – fragment size > 0,1 mm and < 1 mm /Davis and Reynolds 1996/ and a matrix content of 90–100% /Braathen et al. 2004/.

Fault Gouge: Plasticine-like rock material formed by the extreme crushing or grinding of the host rock along a fault. Most individual fragments are too small to be visible to the naked eye and fragments larger than the average groundmass grains make up less than 30 percent of the rock. Coherence, if present, is due to secondary processes /Higgings 1971/.

Gouge – fragment size < 0,1 mm /Davis and Reynolds 1996/ and a sub-microscopic matrix /Braathen et al. 2004/. Gouge consists 100% of a sub-microscopic matrix that is by definition non-cohesive /Braathen et al. 2004/. Gouge can have different colours, but is commonly red to brownish-red in the drill cores and trench (PSM007637) in the Laxemar and Simpevarp areas.

(2) Cataclastic rocks with primary cohesion

Cataclasite: a chaotic, structureless cohesive rock in which most of the fragments are less than 0,2 mm, and make up less than about 30 percent of the rock. Essentially like a mylonite but lacks mineral fabric /Higgings 1971, Braathen et al. 2004/.

Protocataclasite – particle size > 10 mm and a matrix content of 0–50% /Braathen et al. 2004/.

Cataclasite – fragment size > 0,1 mm < 10 mm /Davis and Reynolds 1996/ and a matrix content of 50–90% /Sibson 1977, Braathen et al. 2004/.

Ultracataclasite – fragment size < 0,1 mm /Davis and Reynolds 1996/ and a matrix content of 90–100% /Sibson 1977, Braathen et al. 2004/.

Phyllonite: fault rock with primary cohesion that shows cataclastic deformation but is commonly foliated. Phyllonites consist of more than 50% phyllosilicate /Braathen et al. 2004/.

***Mylonite*:** is a fault rock with distinct mineral fabric and is dominated by plastic flow /Braathen et al. 2004/.

Pseudotachylyte: A glassy rock closely associated with brittle-ductile faults or fault zones. The groundmass of the rock is composed mainly of glass, which in some cases contains microlites of feldspar, vesicles, spherulites, amygdules, or partially melted rock and mineral fragments. The rock fragments may be cataclastic or undeformed. Pseudotachylytes are believed to form by localized partial melting resulting from frictional fusion during faulting /Higgings 1971/.

5 Results

The bedrock in the Oskarshamn investigation site belongs to the Transscandinavian Igneous Belt, and is dominated by c. 1800 Ma old, fairly massive granites to dioritoids, and subordinate bodies of gabbros (Figure 5-1) /Persson Nilsson et al. 2004, Wahlgren et al. 2004, Wahlgren et al. 2005/. In the following we describe first, outcrop by outcrop, our field observations, and then the results of the detailed core logging.

5.1 Field localities

5.1.1 Laxemar

PSM007630 (6367536/1547573), PSM007631 (6367218/1547636), PSM007632 (6367018/1547958) and PSM007633 (6367002/1547836)

These four observation stations (Figure 5-1) are discussed together. Figure 5-2 plots the orientation of several fractures and joints measured in order to obtain a fracture orientation background value for the area.

The two red great circles are the orientation of two small-scale brittle-ductile faults, characterized by polished surfaces and the presence of epidote veins and coating plus localized grain-size reduction. The general orientation of background fractures in this area varies from WNW-ESE to N-S and ENE-WSW (Figure 5-2).

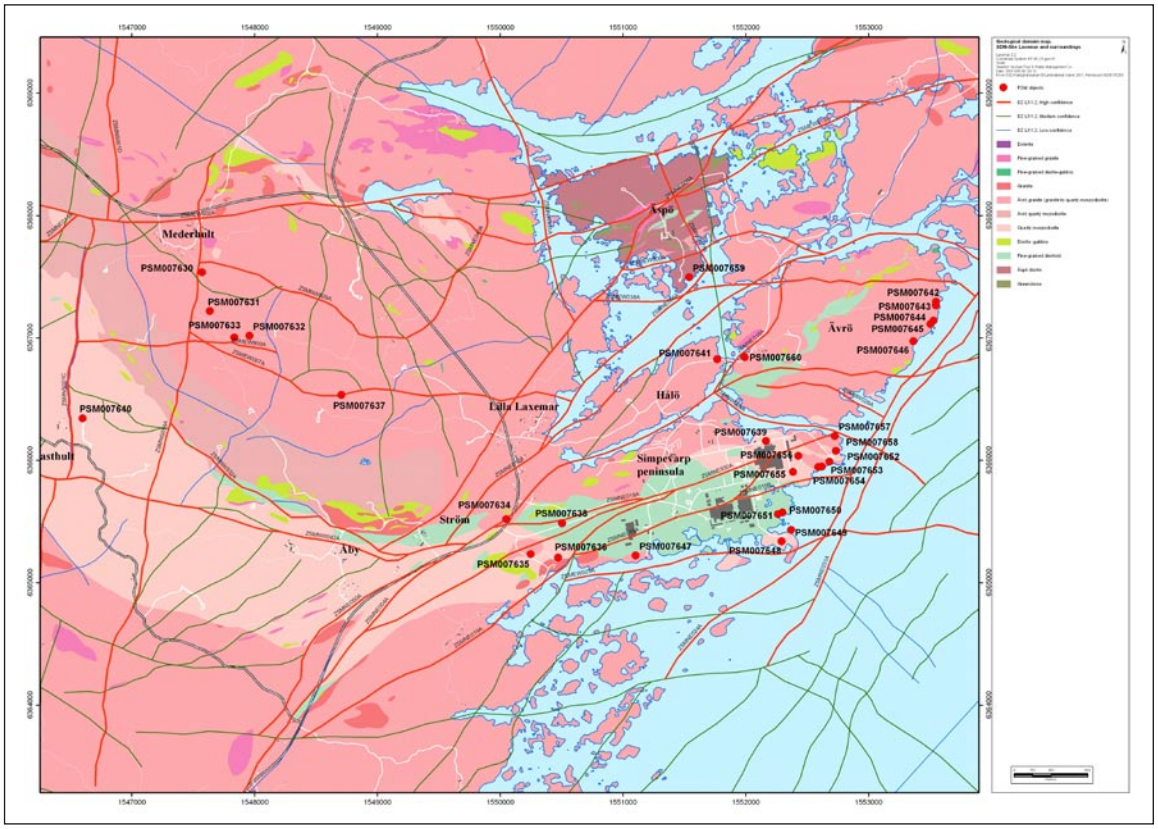

Figure 5-1. *Geology and lineament map of the area investigated and location of the studied outcrops.*

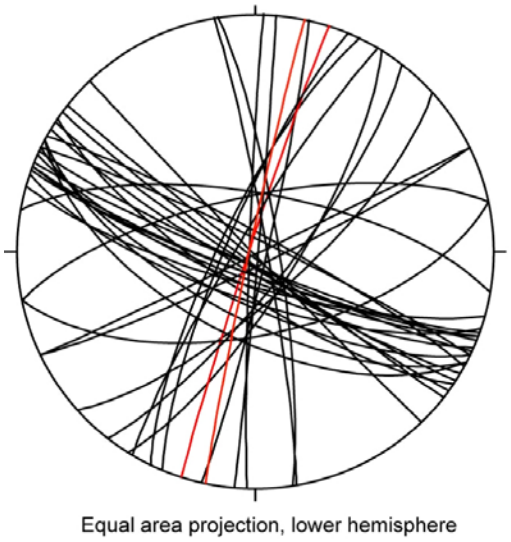

Figure 5-2. *Fracture and joint orientation for observation sites PSM007630, 31, 32 and 33. The two red great circles plot two small-scale brittle-ductile faults.*

PSM007634 (6365518/1550051)

The outcrop consists of rather heterogeneously distributed, strongly foliated quartz-feldspar protomylonites and mylonites that dip steeply to the NW. They belong to the Äspö shear zone. Stretching lineations plunge moderately to the SW (Figure 5-3). Oriented thin sections establish a consistent sinistral kinematics for the NE-SW-trending mylonite zone, as shown by abundant kinematic indicators such as asymmetric sigma and delta clasts and penetrative extensional crenulation cleavage (ECC, Figure 5-3).

The outcrop is characterized by later, overprinting brittle-ductile shear zones (Figure 5-4 and Figure 5-5) and several epidote-coated slickensided surfaces. The generally steep shear zones present a pervasive foliation, defined by epidote, and locally are reminiscent of proper low-grade ductile shear zones (Figure 5-4). They do not exploit geometrically the older ductile fabric. Field observations suggest an overall dextral kinematics for these shear zones. Cataclasites are present (Figure 5-4), deform the protomylonitic foliation and place the formation conditions at the brittle-ductile regime boundary.

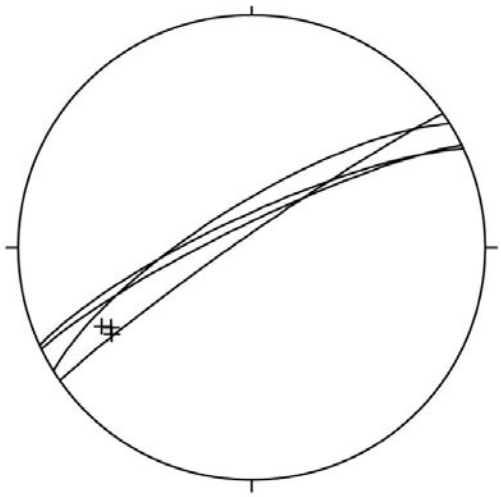

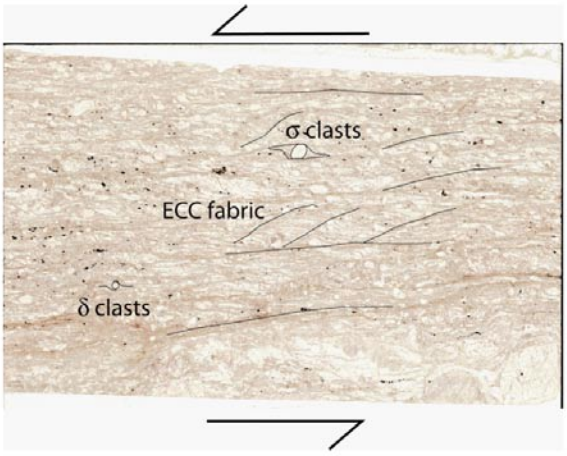

Figure 5-3. *To the left, orientation of the mylonitic foliation as great circles and its associated SW plunging stretching lineation (crosses); to the right, sinistral kinematic indicators constrain the sense of hear of PSM007634 mylonites.*

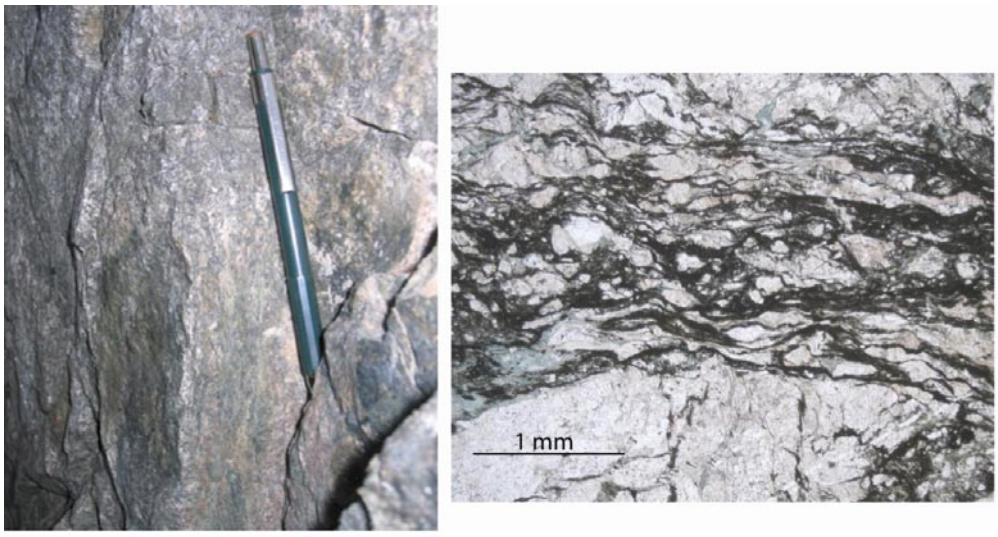

Figure 5-4. *Field view of a steep epidote-bearing brittle-ductile shear zone. To the right, microphotograph of foliated cataclasites, with strain accommodated by cataclastic flow mechanisms.*

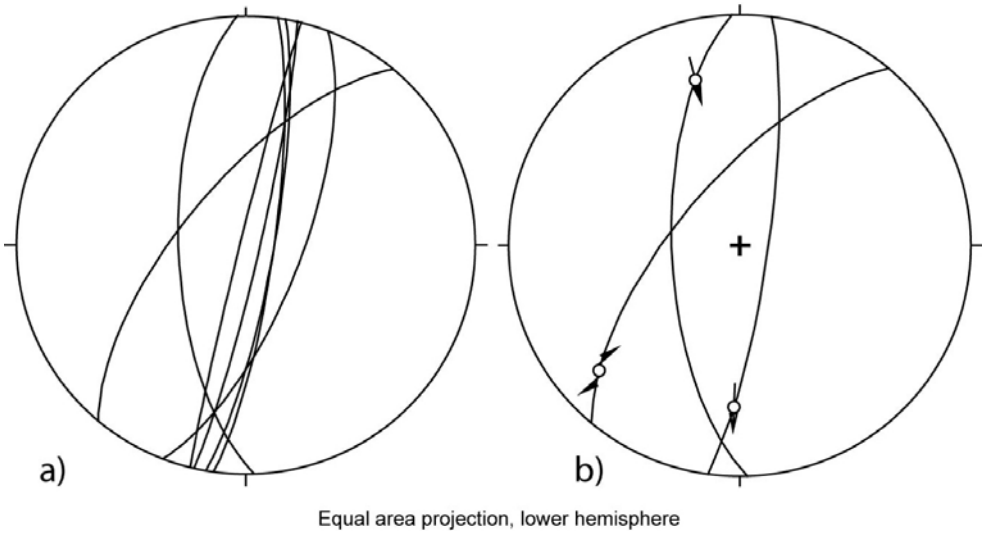

Figure 5-5 a and b. *Orientation and kinematics of the steep brittle faults at PSM007634.*

Figure 5-5a shows the orientation of all brittle-ductile shear zones measured at the outcrop, whereas Figure 5-5b plots only the surfaces that could be constrained kinematically. The general trend of the shear zones is NNE-SSW with a steep dip.

PSM007636 (6365205/1550473)

The stereonet plots the orientation of several subvertical joints observed at the outcrop. The dominant orientation of the joints is ENE-WSW with a steep dip (Figure 5-6).

PSM007637 (6366534/1548707)

The observations of PSM007637 refer to a c. 3 m deep trench recently dug across the east-west trending deformation zone ZSMEW007, first identified on the basis of geophysical data. In this section we characterize the exposed portion of the deformation zone based on outcrop- and thin section-scale observations.

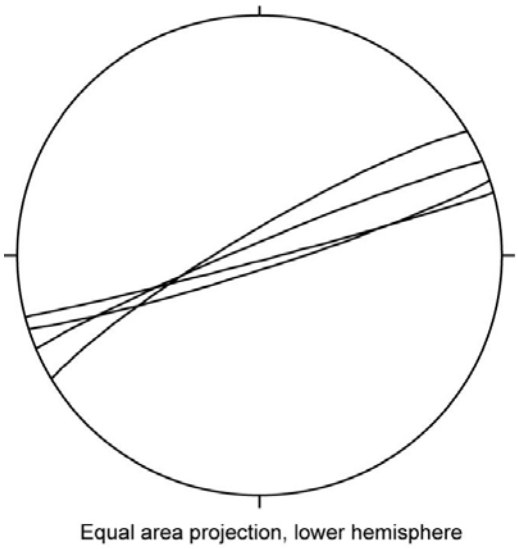

Figure 5-6. *Orientation of joints measured at site PSM007636.*

Fault zone anatomy

The brittle fault exposed in the trench deforms the Ävrö granite. It dips moderately (between 32° and 38°) to the N/NNE (Figure 5-7). No mesoscopic signs of ductile precursors were observed. A complex brittle deformation zone is exposed in the excavation site (Figure 5-8). It consists primarily of cataclasites that cover the complete structural/textural transition from proto- to ultracataclasites. The entire transition zone is estimated to be 5–6 m in true thickness, with the core consisting of ~ 3 m of ultracataclasites and cataclasites and a ~ 20 cm-thick inner core composed of gouge and ultrabreccia with a distinctive reddish-brown and light green colour. The reddish-brown gouge is continuous along the fault plane while the greenish gouge and the ultrabreccia are instead discontinuous and vary in thickness along the fault plane.

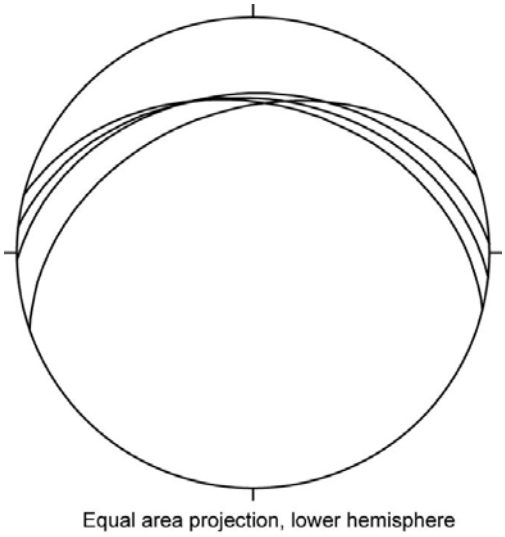

Figure 5-7. *Stereonet of the trench fault orientation.*

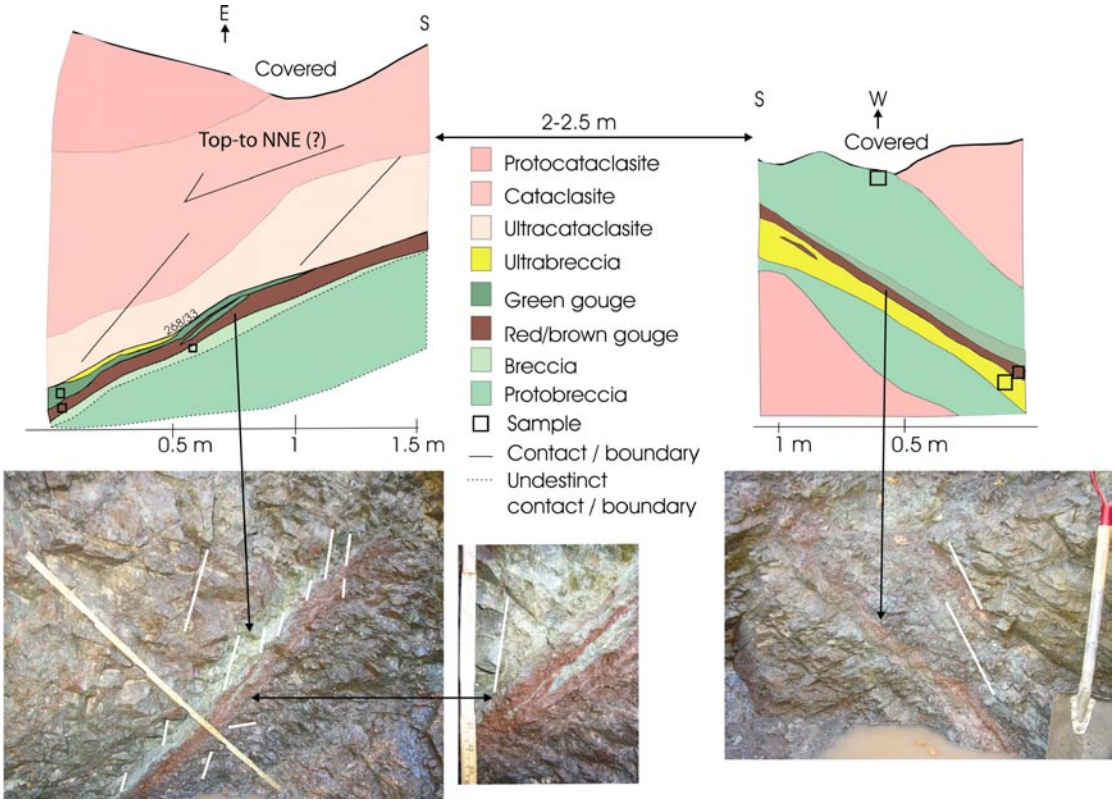

Figure 5-8. *Sketch and photographs of the trench walls with the exposed fault rocks.*

The spatial arrangement of Riedel type fractures in both the hanging wall and footwall suggests normal kinematics, with the hanging wall displaced to the north (Figure 5-8). However, the absence of clear slickenlines or stretching lineations prevents the exact extension direction to be established. Some of the Riedel shears are themselves decorated by mm-thick ultracataclastic injections (for example, sample E of Figure 5-12).

Several samples of gouge from within the fault core were analyzed in order to determine their exact grain-size distribution. Figure 5-9 shows the results of the granulometric tests and confirms the breccia to gouge composition of the deformation zone core.

As seen in Figure 5-8, the relationships between the green and red component are complex, with interfingering geometries. Thin sections from the two different gouge components were studied in order to constrain genetic relationships (if possible) between them. Figure 5-10a to d show microstructural textures of the red gouge. It contains millimetric, angular fragments of an hematite-impregnated, strongly foliated ultracataclasite (Figure 5-10 a in the centre of the image). Figure 5-10b and c show that the hematite-impregnation history is probably the result of a polyphase history (Figure 5-10b, with fragments of pale, red hematite-decorated cataclasite embedded in dark-red hematite cataclastic fragments), followed yet by another, subsequent phase of cataclastic deformation, which is not characterized by the presence of hematite (Figure 5-10c, where a large fragment of red cataclasite is split into several fragments by a later, hematite-barren cataclastic injection). Figure 5-10d shows the progressive strain spatial evolution of the original granitic protolith, represented by a large K-feldspar fragment at the bottom of the microphotograph.

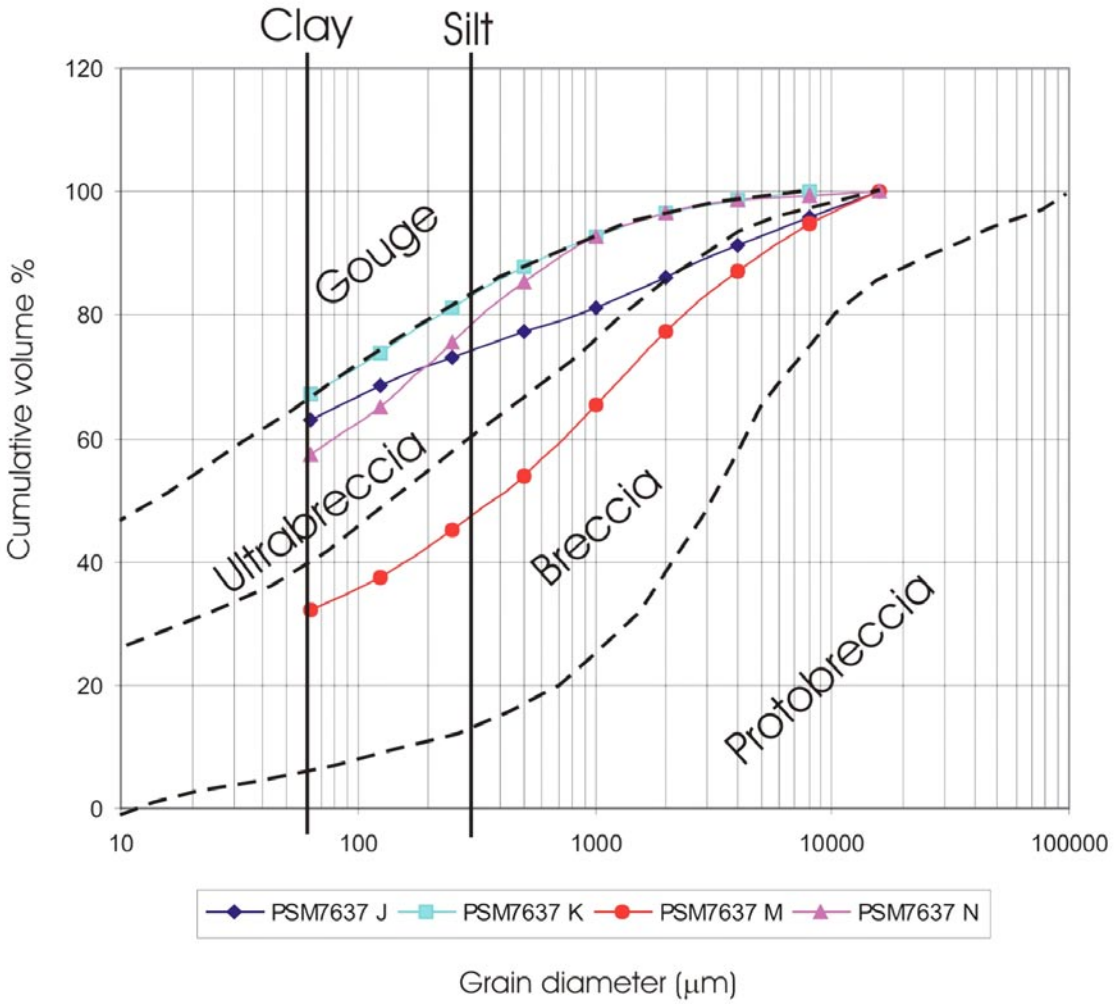

Figure 5-9. *Grain-size distribution of non-cohesive fault rocks in the trench. The blue line (J) plots the results of a sample of red gouge from the eastern side of the trench, the turquoise line (K) of a green gouge (or ultrabreccia) sample from the eastern side, the red line (M) of a green gouge (or ultrabreccia) sample from the western side of the trench and the pink line (N) of a sample of green breccia from the western wall of the trench.*

The large crystal represents a rigid fragment that is progressively reworked along its edges. Elongated fragments, which in proximity of the parent fragment form a foliation that wraps around the grain, are mechanically crushed to produce a very fine-grained, matrix-supported ultracataclasite. Red staining is visible along preferential fracture planes and highlights the afore-mentioned foliation.

Figure 5-10e and f show characteristic microtextures of the green gouge component. The widespread green colour is due to abundant chlorite (Figure 5-10e) that is itself mechanically comminuted in the areas of more intense cataclasis to generate the greenish appearance of the rock, together with the formation of abundant sericite formed at the expense of plagioclase. In the green gouge thin sections studied during this project there was no sign of foliated ultracataclasites, as opposed to the red gouge. These observations suggest a fundamental difference between the two fault rock components. The presence of inherited, foliated ultracataclasite fragments in the red gouge suggests that the gouge formed at least in part at the expense of a pre-existing foliated fault rock, whose presence is likely to have enhanced strain localization along the presently visible fault core. The green gouge is actually an ultracataclasite entirely derived from the granitic host rock. Anastomosing and interfingering relationships between the two components may indicate the original wavy and undulating geometry of the precursor

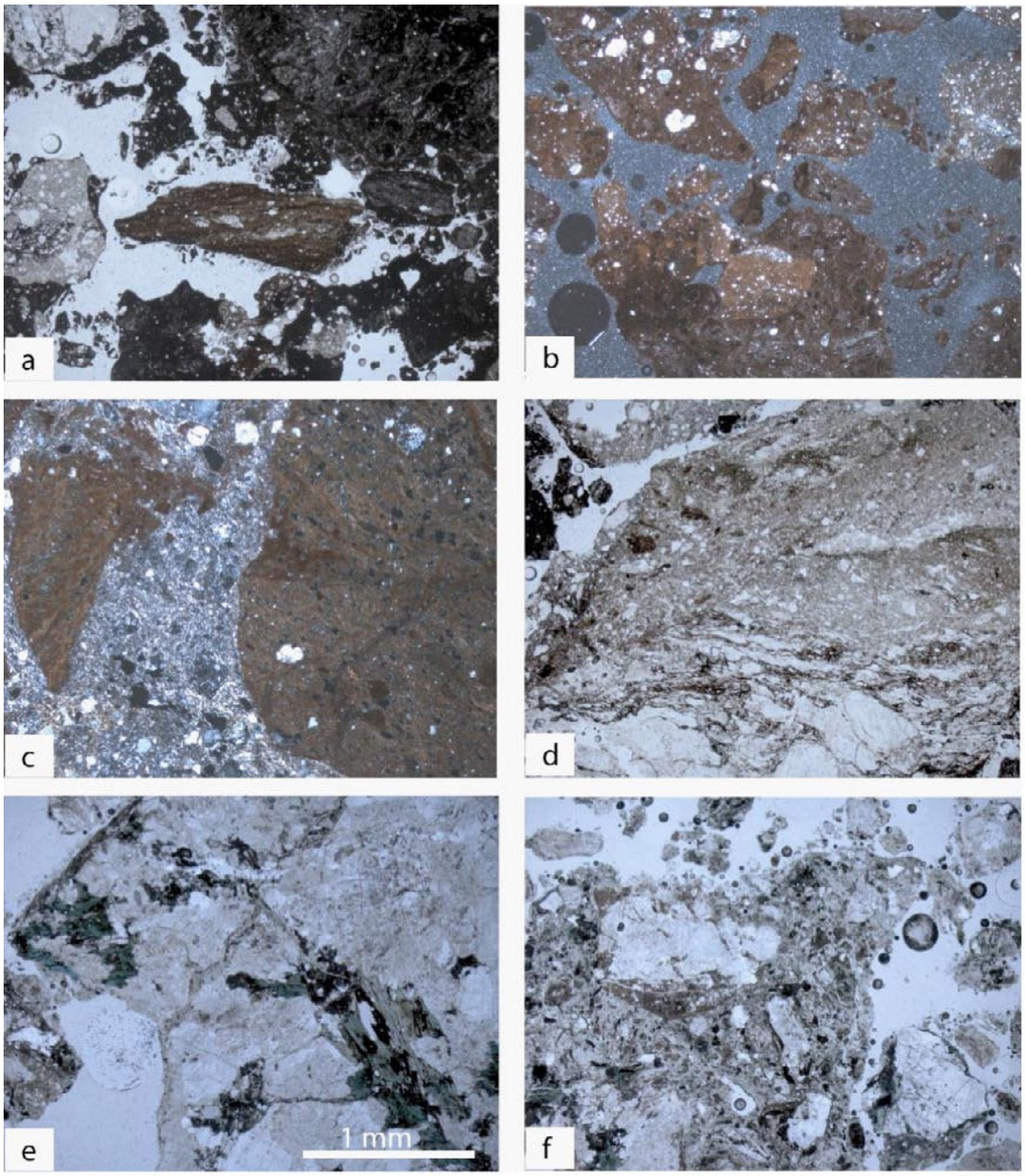

Figure 5-10. *Microphotographs of red (a-d) and green (e-f) gouge samples. a) Fragments of strongly foliated ultracataclasite occur as clasts within the red gouge. b) Hematite-impregnated fragments. c) Hematite-impregnated ultracataclasite crosscut by later hematite-barren ultracataclasite. d) Progressive strain evolution, from a large K-feldspar grain to an ultracataclasite through a foliated cataclasite. e) Characteristic microtexture of the green gouge component with large green chlorite crystals. f) Ultracataclastic texture of the green gouge component.*

foliated fault rock, which may have itself formed at the expense of the cataclastic granite. The remarkably different colour, which, as discussed above, is due to different weathering and finite strain amount, reflects the significant fluid-rock interaction that was controlled in its volumetric extent by the anisotropies of the faulted rocks. Red hematite staining can therefore represent the result of oxidation and fluid flow within and along the foliated fault rock precursor. These ideas remain only working hypotheses and more in-depth investigations would be needed in order to fully unravel the mechanisms that generated the gouge and the ultracataclasites.

In the footwall, immediately below the fault plane and along the southern side of the trench, there is an open, sub-horizontal fracture filled with clastic sediments (Figure 5-11). These sediments are well packed, but not consolidated. The largest grains or clasts are found at the openings of the fracture that also correspond to the narrowest parts of the fracture, whereas the finest grains are located farthest into the fracture and into small linked fractures (Figure 5-11). This is very likely the result of a Quaternary phenomenon, whereby overpressured and fluidized water-rich sediments at the base of an ice sheet were mobilized as forceful injections and either filled in pre-existing fractures or even opened new dilatant joints.

Thin section study

A set of 9 different samples (7 from the hanging wall and 2 from the footwall) were collected at increasing distance from the fault core in order to appreciate variations of strain and changes in deformation mechanisms in space. Figure 5-12 shows the relative location and textures of the samples.

Sample PSM007637A, the closest to the fault core in the hanging wall, is an ultracataclasite characterized by significant grain-size reduction, abundant intra- and intergranular fractures and discrete small-scale fault surfaces (Figure 5-13a and b).

As expected, strain decreases progressively with distance from the fault core. Sample PSM007637B and C (0.5 and 1 m from the fault core, respectively) show a significant decrease in the overall amount of cataclasis (Figure 5-12). The primary granite texture is mostly preserved, with large quartz, plagioclase and K-feldspar grains almost totally undeformed. Deformation is strongly partitioned into narrow, at times anastomosing cataclastic bands (Figure 5-13c and d) and a few randomly oriented fractures. The cataclastic horizons have very irregular shapes and geometries,

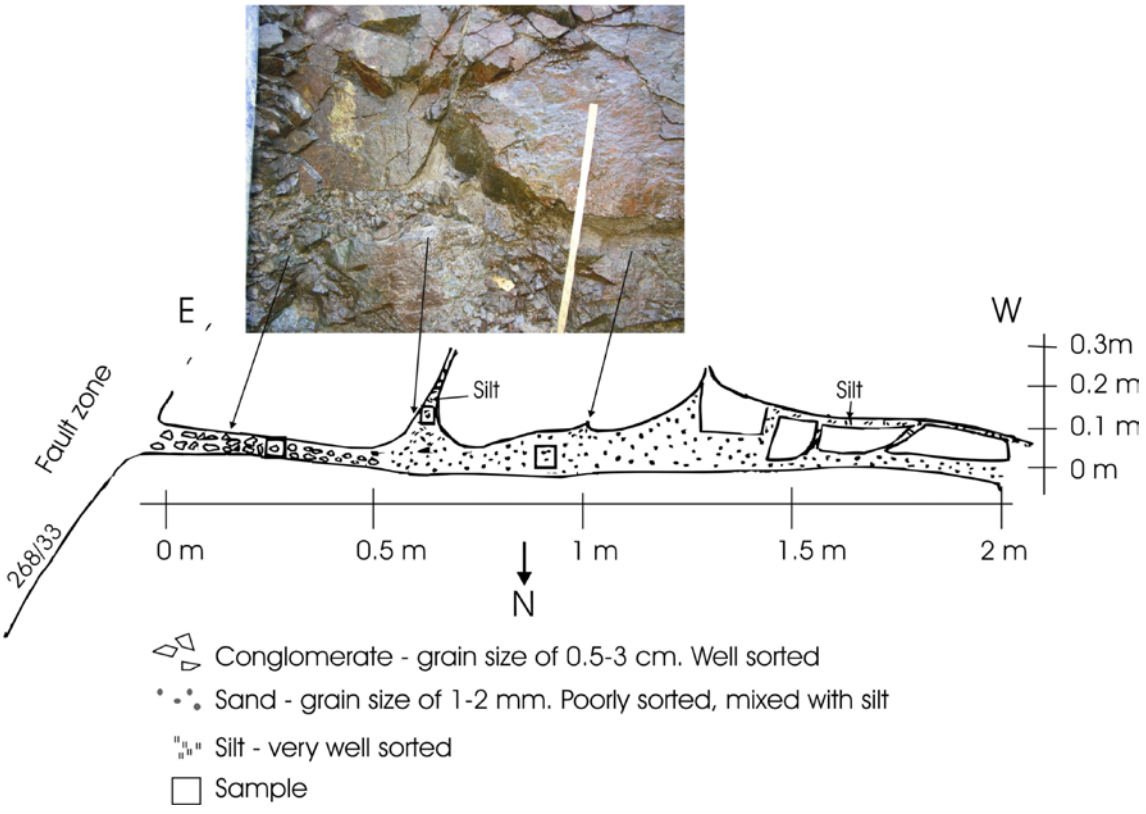

Figure 5-11. *Possible fluidized Quaternary sediments injected into a sub-horizontal fracture in the footwall. The largest grains are concentrated at the opening of the fracture, forming a conglomerate, while the finest grains are transported farther in, in the smallest openings.*

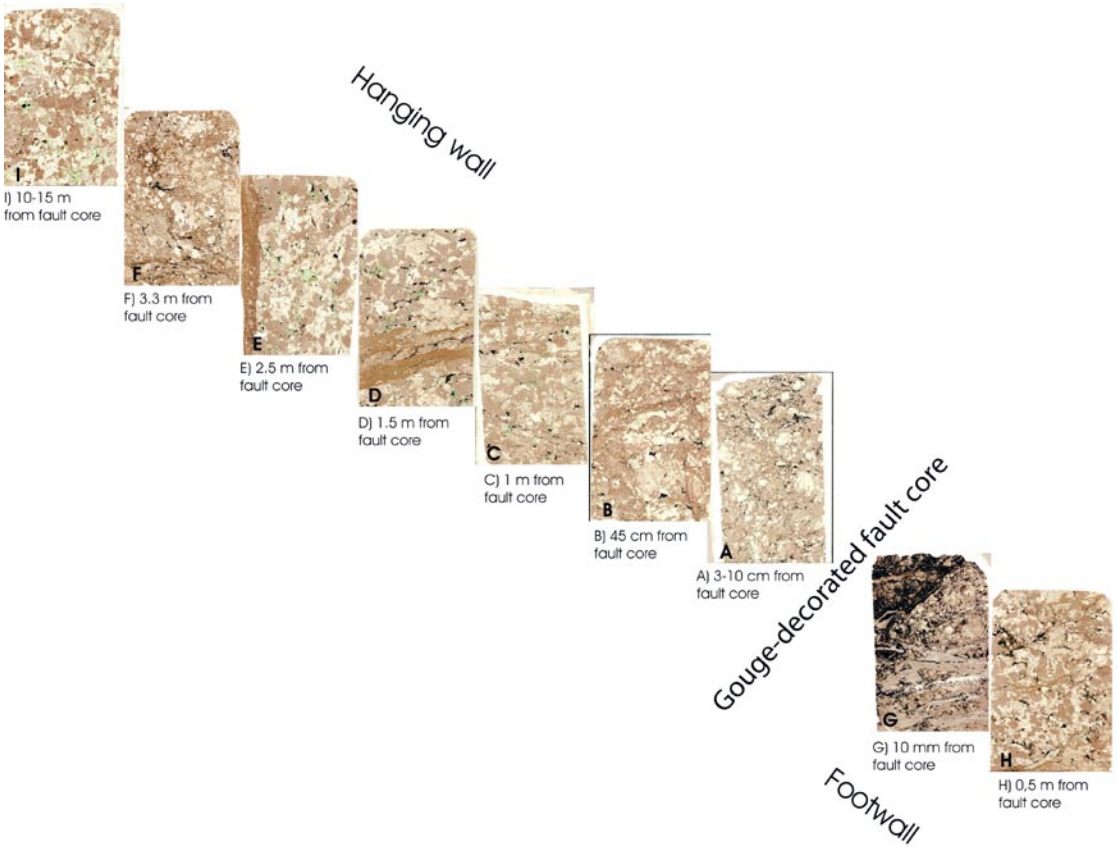

Figure 5-12. *Thin sections (with sample position with respect to the fault) from the trench.*

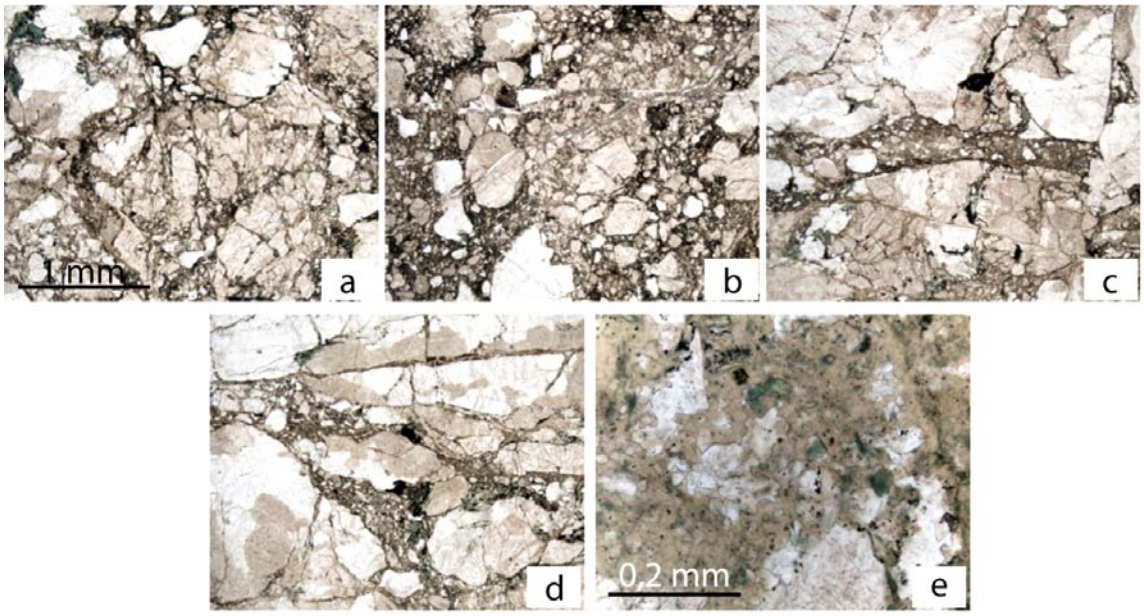

Figure 5-13. *a) Ultracataclasite texture defined by grain size reduction, clast rigid body rotation and intra- and intergranular fractures. b) Discrete fracture plane crosscutting an ultracataclastic ground mass. c) Fluidized ultracataclasite injection. d) Random distribution of fluidized ultracataclasites. e) Detail of highly irregular clast boundaries within fluidized ultracataclasites, supportive of significant fluid-rock interaction.*

which do not follow discrete fault surfaces, but are instead reminiscent of random fluidized cataclastic injections (Figure 5-13c and d). Fluidized cataclasites have been recently used to infer seismic activity /e.g. Rowe et al. 2005/.

Samples PSM007637E and F are basically undeformed granites, apart from thin veins of fluidized ultracataclasites. Figure 5-13e shows the details of one of these cataclastic injections. The highly irregularly-shaped fragments suggest important fluid-rock interaction in the form of resorbed grain boundaries, thus strengthening the idea of fluidized cataclasites.

The footwall is not exposed to the same extent within the trench and only 2 samples could be collected. PSM007637G (Figure 5-12), immediately below the fault core, is a strongly tectonised rock, characterized by a pervasive network of dilatant, cataclastic fractures. It is interesting to note that the sample contains abundant calcite veins that, based on geometric relationships, are interpreted as late features of the deformation history. No calcite veins were instead observed within the hanging wall, possibly suggesting preferential late fluid circulation in the footwall. Sample PSM007637H, only 0.5 below the fault zone is basically undeformed, with only very minor cataclastic horizons (Figure 5-12).

PSM007638 (6365484/1550505)

The stereonet plots the orientation and the kinematics of two epidote-chlorite coated slickensided planes found within a fine-grained dioritic outcrop. The NNE striking surface has a reverse top-to-E/ESE kinematics, whereas the W/WNW striking plane shows dextral transtensional kinematics (Figure 5-14).

PSM007640 (6366342/1546600)

Drilling site KLX11A was investigated before the actual drilling phase was initiated but after a thorough site cleaning process necessary to remove the otherwise very dense local vegetation. The dominant rock type within the c. 15×20 m pavement is quartzmonzodiorite, with only minor fine- to medium-grained granite and pegmatite intrusions.

The outcrop is intensively fractured and affected by systematic sets of hybrid fractures, showing variable amounts of shear and normal offsets (Figure 5-15). No fault rocks were observed. Geometric changes of the fracture trends lead to an increase of shear vs. normal component or vice versa, thus generating proper joints or shear fractures in addition to hybrid fractures. Only 2 epidote-coated slickensided surfaces were found, orientated 352/72 and 014/78 (~ N-S and steep) and with slickenlines oriented 152/28 and 192/42 respectively. The transport direction

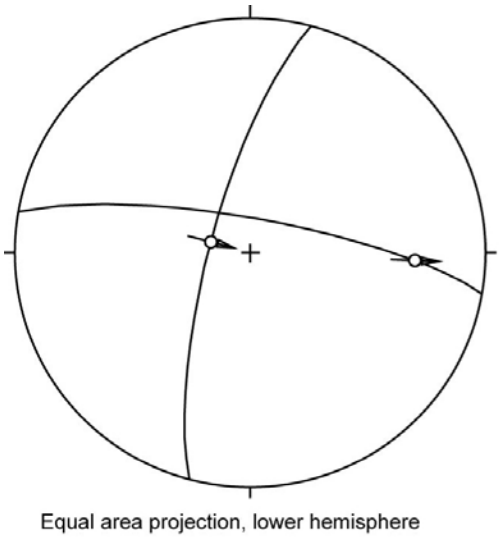

Figure 5-14. *Orientation and kinematics of 2 striated planes for PSM 007638.*

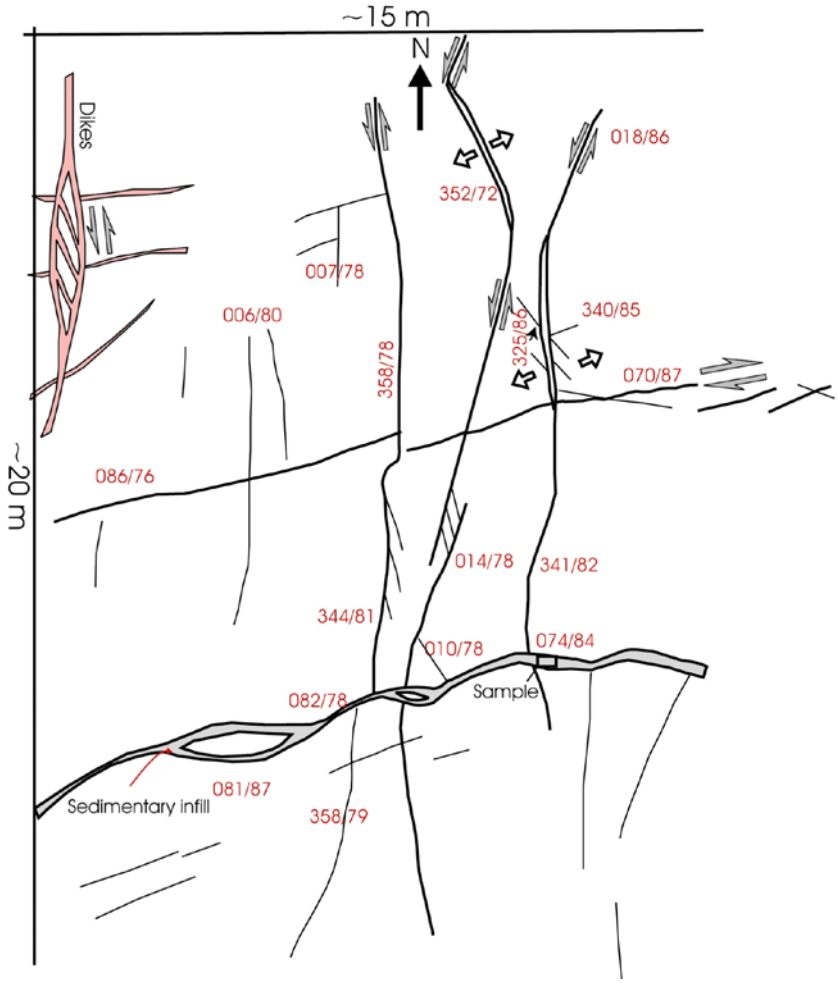

Figure 5-15. *Sketch fracture map of drilling site KLX11A.*

plunges thus moderately to the S, SSE. The subhorizontal pavement (thus the surface of observation) is at an angle to the relative movement direction vector and is therefore not ideally orientated for the kinematic analysis of the fractures. However, the mismatch angle is only moderate and several consistent observations at the outcrop scale make us confident of the reliability of the kinematic interpretations presented below.

Figure 5-15 is a sketch of the most important fractures and fracture sets mapped and characterized during the outcrop inspection. Two broad sets are recognized:

1) NS trending shear fractures, locally characterized by a significant component of orthogonal dilation, and
2) E/ENE trending shear fractures.

Fracture orientation is shown in the stereonets of Figure 5-16. The stereoplot Figure 5-16a reports contours to poles for 1,029 fracture planes, as established by a detailed fracture mapping study performed by /Cronquist et al. 2006/. The data set highlights two distinct maxima spread about the primitive circle that represent the strong preferential orientation of the two systematic sets discussed above and highlighted in our sketch of the polished rock pavement. Each maximum is slightly elongated along the primitive circle and defines a "tail" of orientations that is due to fractures slightly misoriented with respect to the dominant orientation (see below). Figure 5-16b shows the orientation of the fractures measured during the present study, while Figure 5-16c shows the orientation of only structurally controlled selected fractures and their kinematic interpretation based on their geometrical relationships.

The two fracture sets are discussed below individually.

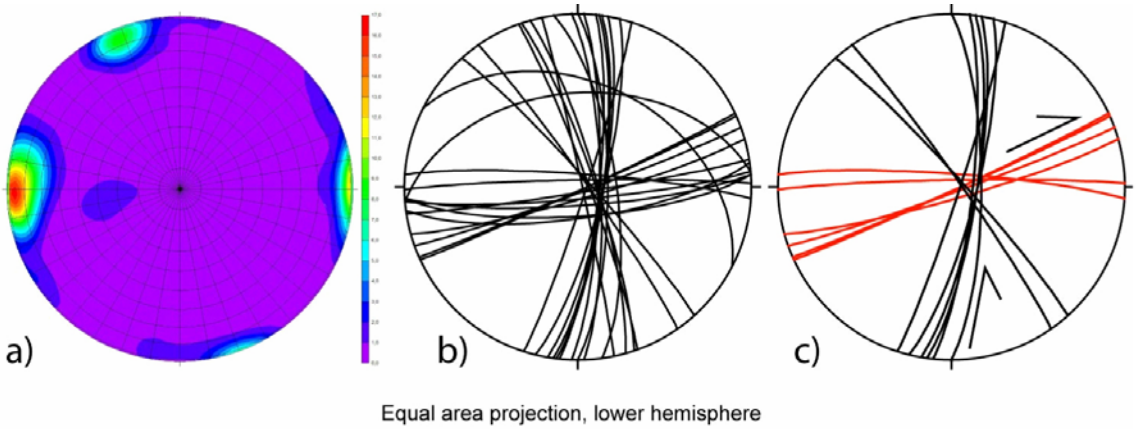

Figure 5-16. *a) Stereonets of 1,029 fractures measured at the site by /Cronquist et al. 2006/, b) of our own measurements and c) suggested kinematic interpretation of the dominant fracture patterns (right).*

NS trending set

The NS trending set is the most pervasive at the outcrop scale and is well defined in terms of orientation, continuity and kinematics. It is formed by planar, steep to sub-vertical, long and generally rather continuous shear fractures that strike NS to NNW-SSE (Figure 5-16), as shown by the subhorizontal pole maxima of Figure 5-16a and the great circles of Figure 5-16b and c. Specific structural features, such as releasing bends, en-echelon lateral stepping and Riedel shears, allowed the establishing of consistent kinematics for the set. The NS trending fracture set is interpreted as a series of predominantly sinistral fractures and faults. Figure 5-17 illustrates some of the kinematic criteria used in the analysis:

a) The two large NS fractures visible in the photograph are characterized by a localized change in strike from NNE to N/NNW (Figure 5-15 and Figure 5-17). This is in turn reflected in the local development of so-called releasing bends, that is, portions of the deformed rock volume where, due to the change in orientation of the fault/fracture that accommodates the offset with respect to the local, instantaneous stress field, there occurs a transition from dominant strike-slip to extensional conditions. Figure 5-15 and Figure 5-17 illustrate the phenomenon with sets of white arrows diverging from the fracture strand, which express the opening direction across the fault. The couple of black arrows along the remaining parts of the fractures indicate instead the sinistral kinematics. The orientation of the bend is such that, within a sinistral shear corridor, the sinistral horizontal component is transformed into a local extensional component, leading to overall dilation within the releasing bend and to the opening of a proper dilatant fracture or joint.

   Figure 5-17 shows the local orthogonal dilation (visible thanks to a significant increase of the opening of the fracture/fault walls) that characterizes the releasing bends. In the case of dextral shearing, similarly oriented faults would generate restraining bends, that is, regions of localized compression and shortening.

b) Synthetic and antithetic Riedel shears are numerous and confirm the sinistral kinematics (Figure 5-17).

c) The spatial arrangement of some of the fault segments, such as the case of en-echelon stepping, is consistent with sinistral shearing. Tension gashes within bridges separating individual fault segments also confirm the sinistral kinematics of the fractures/faults.

The plot of the structurally constrained fault segments confirms the sinistral kinematics of the NS trending structures (Figure 5-16c). Figure 5-16b and c, together with the inset of Figure 5-17, show that the cluster of roughly NS-trending fractures can actually be split into two distinct subgroups. A first, very systematic and dominant set is comprised of only NS striking features, which are the master faults at the outcrop scale. A second, subsidiary set of SSE/NNW trending fractures can instead be interpreted as sinistral Riedel shears kinematically linked to the master NS features.

Figure 5-17. *View to north of the polished drilling site and of the sinistral NS trending fracture set. Note the releasing bends and the associated dilation (shown by large white arrows).*

The overall spatial and geometric association of these two subsets suggests their cogenetic origin within the same sinistral shear corridor. The spread of orientations in the pole-to-fracture stereonet (Figure 5-16a) is due to the geometric relationship between master and subsidiary Riedel shears.

To the west of the outcrop there occurs an interesting structural feature. Thin leucocratic dykes (possibly aplitic) trend generally NS, but, within a zone of en-echelon lateral stepping, they become oblique to the overall fault strike and perpendicular to the local stretching direction (Figure 5-15 and Figure 5-17). The geometry of this structure is consistent with the sinistral kinematics defined for the brittle regime of the outcrop fractures. It would seem therefore that similar kinematic conditions (in response to a similarly oriented stress field) were present at the time of dyke emplacement, thus under higher T conditions than those of the fracture-formation episode. This evidence may suggest a long-lived, kinematically consistent sinistral shearing episode that continued during the progressive exhumation of the rocks into the brittle portion of the crust.

E/ENE trending set

The E/ENE -trending fracture set is less pervasive than the NS system and of more difficult interpretation. Two main fracture/fault strands were investigated. The southernmost fracture (Figure 5-15) is very continuous (except a couple of sites where the fracture steps laterally) but not straight. It is instead characterized by an undulating geometry, with an overall ENE trend. The fracture is locally anastomosing and isolates pockets of undeformed host rock. Noclear kinematic indicators were found. The fracture is open and about 30–50 mm wide. It is filled by clastic sediment, which was sampled at the site shown on Figure 5-15 for microscopic analysis.

Figure 5-18A illustrates the clastic nature of the fracture infill, characterized by a variety of grain shapes ranging from well-rounded to angular. Figure 5-18 A and B show the heterogeneous composition of the clasts, with metamorphic quartz clasts derived from a source other

than the magmatic host rocks. Hand specimens suggest a faint clast size grading parallel to the fracture walls. Figure 5-18D and E illustrate features of possible pressure-solution processes, whereby well-rounded quartz grains impinge into each other with very smooth, rounded grain boundaries, sealed by very thin seams of insoluble material. /Röshoff and Cosgrove, 2002/ describe numerous subvertical sedimentary dykes in the Oskarshamn-Västervik area and conclude that their majority was emplaced as forceful injections of fluidized sediments. They suggested that the appropriate model for the generation of the dykes is that of external fluid fracturing and that the fluid pressure during dyke emplacement was probably considerably in excess of that required to open ideally oriented basement fractures. The stress boundary conditions are likely to have been those of a vertical maximum principal compression and an increasing horizontal stress with depth. Several lines of evidence indicate that the dykes are relatively old features i.e. that they are not associated with Quaternary glaciations.

A second, continuous NNE-SSW trending fracture is found a few meters north of the sandstone-decorated fracture. Its kinematics was established to be dextral on the ground of the en-echelon arrangement of individual fracture segments and the presence of dextral Riedel shears. The amount of lateral offset could not be determined due to the lack of suitable structural markers.

The stereographic analysis of structurally selected portions of the E/ENE-W/WSW trending fractures also confirms an overall dextral kinematics. The stereonet of Figure 5-16c shows the great circles (in red) of several fracture orientations. The obtained geometric relationship can be interpreted as a set of E/ENE-W/WSW trending master fault segments associated with subsidiary EW trending Riedel shears, indicative of dextral shear.

Relative crosscutting relationships between the two sets of fractures/faults are not clear-cut and the kinematic information is not consistent. Locally, the NS trending fractures offset sinistrally the E/ENE-W/WSW trending fractures, but are in turn offset along a E/ENE-W/WSW direction in other parts of the outcrop (Figure 5-15).

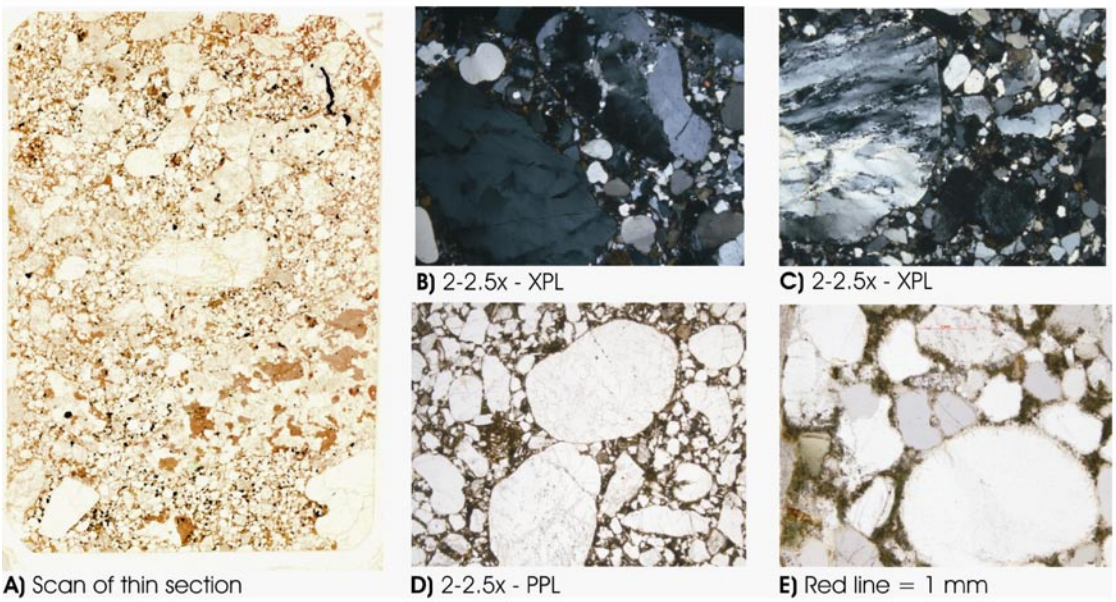

Figure 5-18. *A) Scan of the fracture infill thin section. B and C) Microphotographs of metamorphic quartz in the clastic sediment B): quartz grain with deformation bands; C): rounded clast of metamorphic, dynamically recrystallized quartz). D and E) Pressure-solution features of the clastic infill, with impinging quartz grains, pairs of concave/convex sub rounded grain boundaries and thin films of insoluble material along the grain boundaries.*

5.1.2 Ävrö coastline

PSM007641 (6366825/1551768)

The outcrop presents numerous epidote/chlorite-coated striated fault planes. Most readings refer to roughly NS-trending steep faults with striations plunging moderately to the south and either dextral or sinistral oblique strike-slip kinematics (Figure 5-19).

PSM007643 (6367266/1553550)

A small-scale steep brittle fault zone containing a heavily crushed and fractured core that lacks any distinctive fault rock characterizes the outcrop. The dextral sense of shear was established thanks to the presence of Riedel shears (average orientation 218/60) and striations (Figure 5-20).

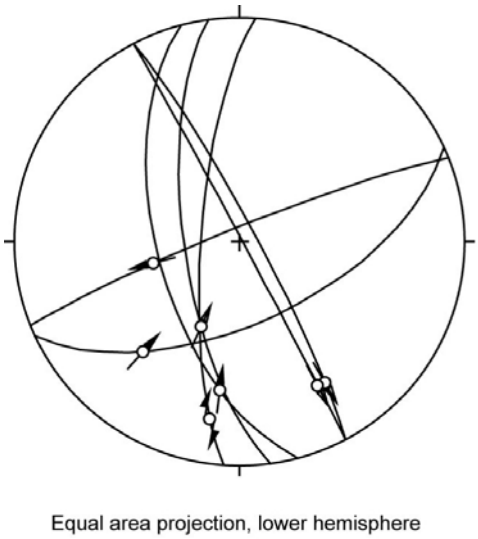

Figure 5-19. *Stereoplot of PSM007641 fault slip data.*

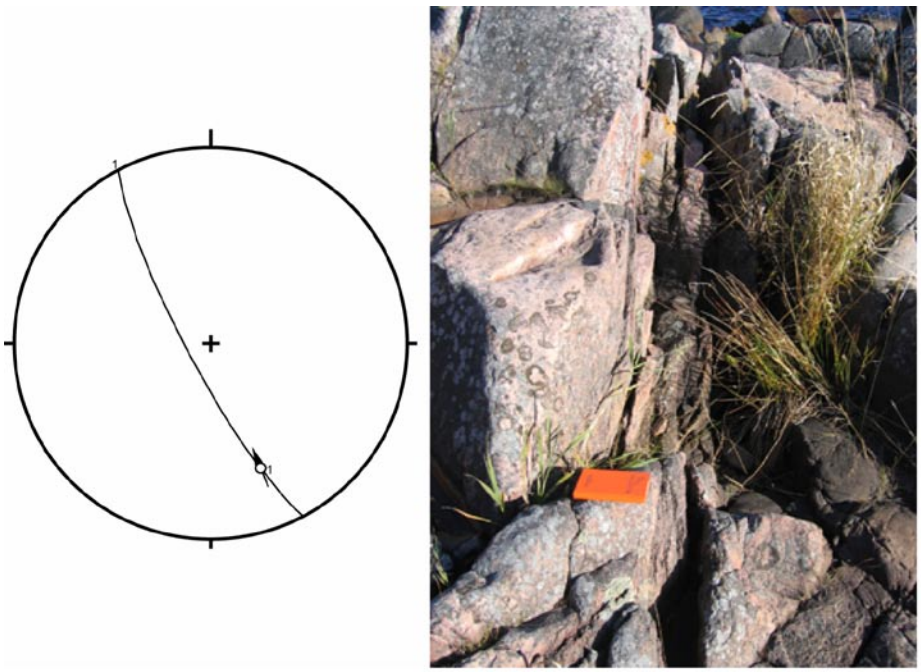

Figure 5-20. *Orientation and kinematics of the brittle fault shown in the photograph of PSM007643.*

PSM007644 (6367141/1553530)

The outcrop contains a c. 0.5 m thick, strongly foliated EW-trending brittle-ductile shear zone (Figure 5-21). Riedel shears associated with it suggest dextral kinematics (see the dextral Riedel shown on the stereonet of Figure 5-21). Figure 5-22 B shows the moderately foliated texture of a sample collected in the shear zone.

A brittle cataclastic fault zone cuts across the brittle-ductile shear zone.

Thin section analysis of the brittle fault (Figure 5-22A) shows a relatively undeformed, medium-grained granite characterized by narrow and localized cataclastic deformation bands (visible as thin black dilatant linear features on the microphotograph). Their random distribution and spatial arrangement suggests hydrofracturing as their possible formation mechanism.

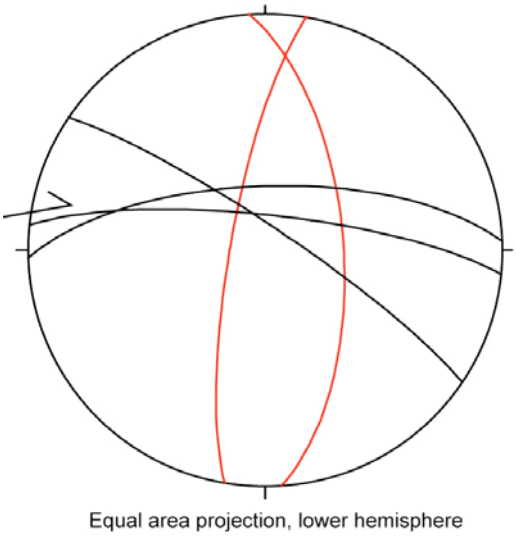

Figure 5-21. *Orientation of significant structural features of site PSM007644. Red great circles represent a NS-trending brittle fault that cuts across the dextral EW-trending brittle-ductile fault shown by the black great circles.*

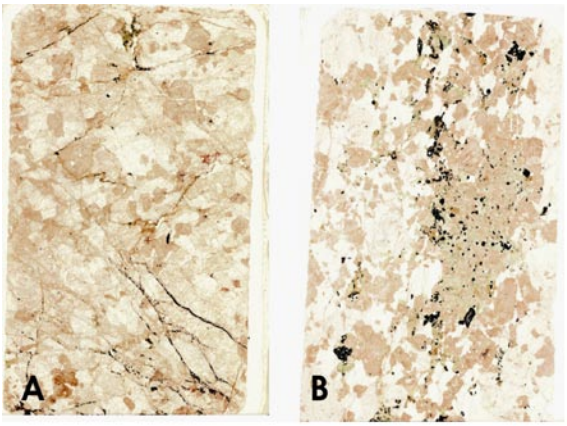

Figure 5-22. *A) Thin cataclastic bands coalesce in a dilatant network in a sample of the NS trending brittle fault zone of PSM007644. B) Faint foliation (trending roughly NS in the microphotograph) of the brittle-ductile shear zone.*

PSM007646 (6366972/1553367)

This locality along the coast offers a set of interesting crosscutting relationships among different generations of faults. Moreover, the presence of a microgranite dyke that, undeformed, crosscuts a cataclastic fault zone, but is in turn cut by a different brittle fault, offers the unique possibility to add some absolute geochronological constraints to the deformation history of the area.

An E/ENE-W/WSW striking, NNW dipping brittle fault zone (Figure 5-23) up to 1.5 m thick is the dominant feature of the outcrop. It comprises an ultracataclastic core and a strongly cataclastic deformation zone (Figure 5-24). The ultracataclasite is dark brown, black in colour; it is locally foliated and generally defined by anastomosing zones of extreme grain size reduction that surround lenses of the still relatively undeformed protolith, a medium-grained pink granite (Figure 5-24). Epidote veining (commonly random in orientation) is very abundant. No kinematic indicators were observed.

Thin sections from samples PSM007646B and C (Figure 5-24 for location and Figure 5-25) provide insights into the brittle deformation mechanisms of this deformation zone.

Anastomosing networks of epidote-decorated ultracataclasites deform pervasively the rock together with injected brown-yellow fluidised ultracataclasites. Strain is partitioned between areas with little or no finite deformation and others characterized instead by extreme grain-size reduction by mechanical comminution of the host rock. Figure 5-26 illustrates that the brittle history is complex, with several episodes of brecciation, rock dilation and late calcite veining, with multiple crosscutting relationships. The epidote-decorated cataclasite formation is a relatively early phase of the brittle history.

Figure 5-26a shows a cataclastic vein that deforms epidote crystals (genetically linked to an earlier cataclasite) and breaks them up into small fragments, pointing to post-epidote growth deformation. Figure 5-26b presents even stronger evidence in support of a polyphase brittle deformation history. Several brownish ultracataclasite injections deform the epidotised granite. The NS trending vein crosscuts a previously formed EW trending ultracataclasite, but is in turn cut by a series of systematic NE-trending thinner injections of the same brown ultracataclasite. Figure 5-26c adds further elements to this complex evolution, illustrating a “late” dilational calcite vein that cuts across the brownish ultracataclasites.

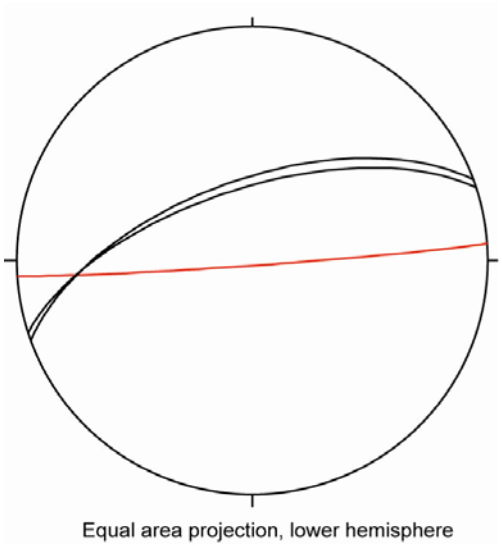

Figure 5-23. *Black great circles represent the orientation of the large ultracataclastic brittle fault that is crosscut by the dyke. The red, EW-trending steep great circle represents the discrete brittle fault that cuts through the dyke.*

The dyke shown in Figure 5-24 is not deformed by this brittle history. In fact it cuts discordantly the ultracataclastic/cataclastic outcrop, thus placing a maximum age constraint on the formation of the E/ENE-W/WSW striking brittle deformation zone (Figure 5-27). However, a steep, EW striking brittle dextral fault cuts across and offsets it by c. 0.2 m, thus clearly postdating its intrusion. Slickenlines along the fault plane plunge 12° toward 092.

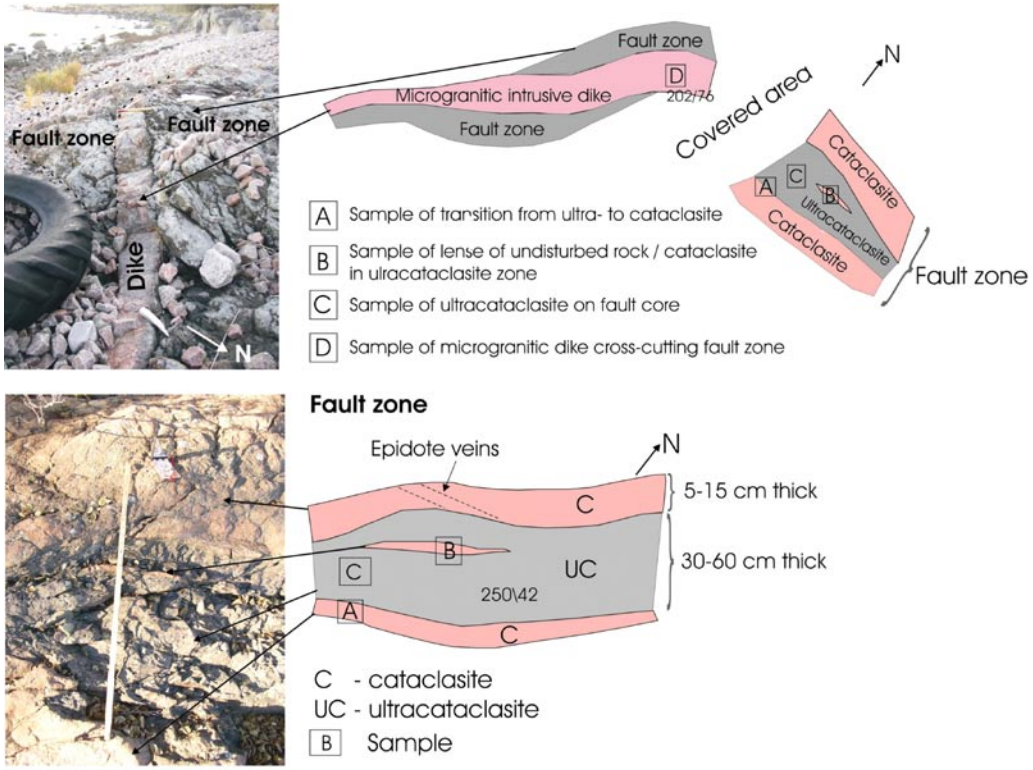

Figure 5-24. *Ultracataclastic fault crosscut by a dyke at locality PSM007646, along the coast of Ävrö. Sketches illustrate outcrop structural relationships and fault rock distribution.*

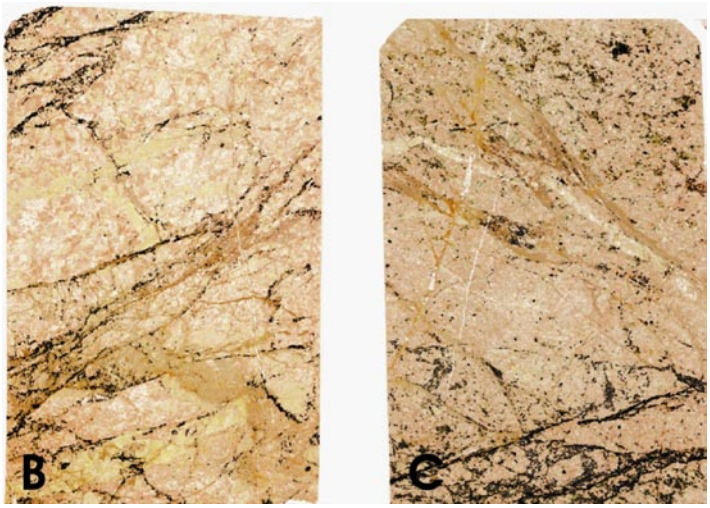

Figure 5-25. *Thin sections illustrating strong strain localization within the cataclasite samples B and C of site PSM007646. Anastomosing, dilatant networks of epidote-decorated fractures and possibly fluidized cataclasites affect pervasively the rock.*

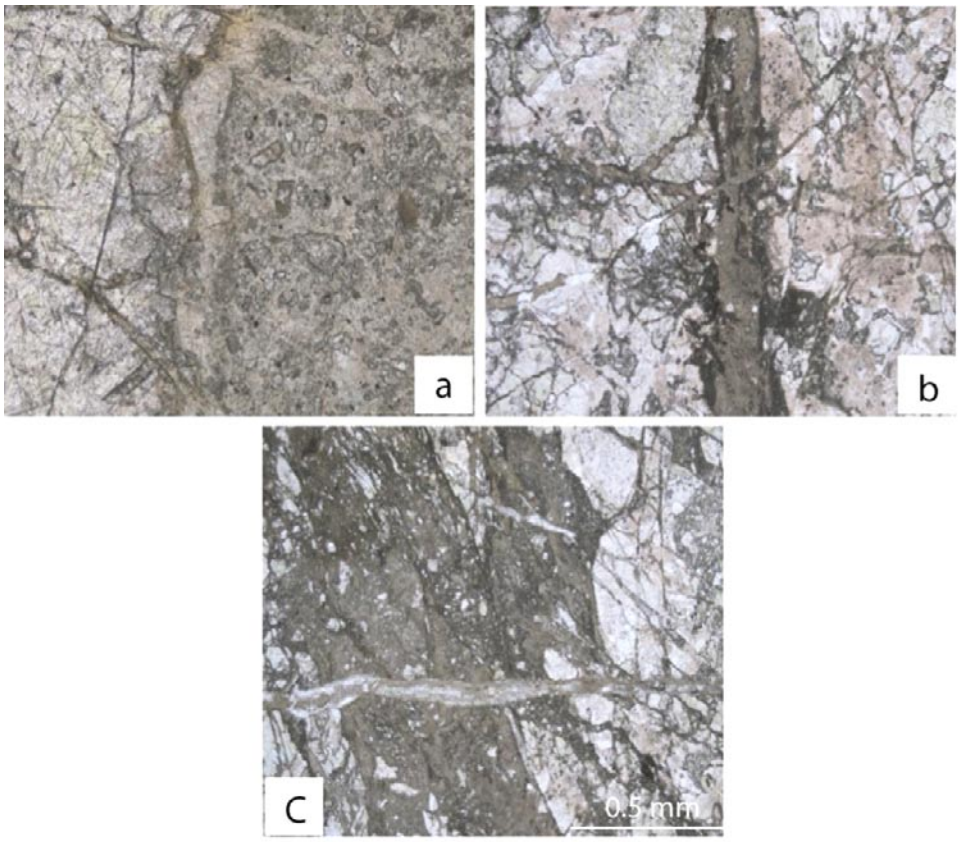

Figure 5-26. *Microstructural features suggesting polyphase brittle deformation with cataclastically-reworked epidote (a), several generations of crosscutting fluidized ultracataclasites (b) and "late" crosscutting calcite veining (c).*

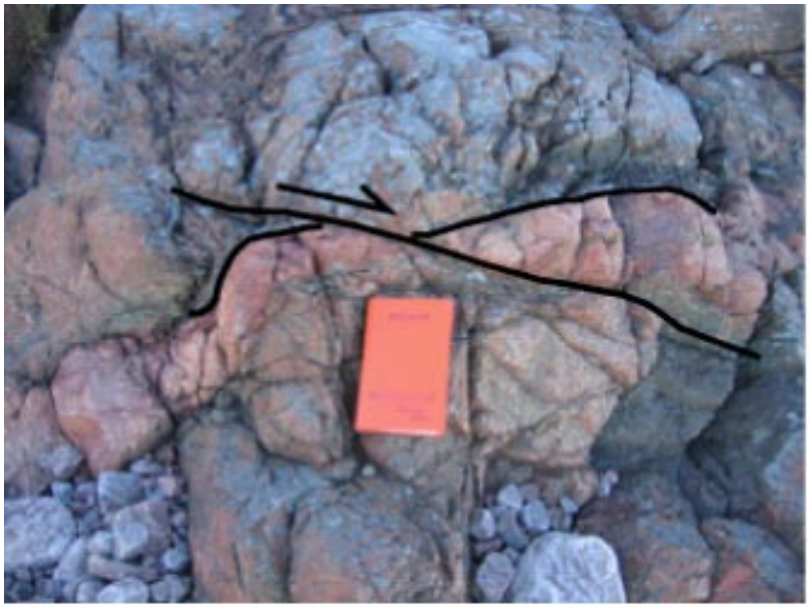

Figure 5-27. *Microgranite dyke offset by c. 0.2 m along a steep, dextral brittle fault.*

PSM007660 (6366841/1551992)

The outcrop contains abundant epidote-coated striated fault planes. The majority consists of steep, NNE-SSW trending planes containing gently S-plunging lineations and displays both sinistral and dextral kinematics. It is worth noting the presence of shallower NW-SE trending planes showing normal kinematics or conjugate strike-slip shear senses (Figure 5-28).

5.1.3 Coastline of Simpevarp

This area is located along the coastline south and east of the Power Plant, towards the port facilities of Oskarshamn.

The host rock south of the Power Plant is a fine- to medium-grained dioritoid. North-eastward, a medium- to coarse-grained quartz-monzodiorite and the Ävrö granite characterize the area. Both rock types host numerous dykes of medium- to coarse-grained and pegmatitic granite. Several fracture and fault trends are present, with N-S and E-W structures as the most prominent ones. NE-SW and NNE-SSW fractures are subordinate.

PSM007639 (6366157/1552167)

Several striated fault planes were observed and measured at the outcrop and clear slickensides provided kinematic constraints. Fault surfaces are generally coated by epidote, some also contain lenses of calcite.

Slickensides appear both as fibrous epidote and as groves in the fault surfaces. It is worth noting the presence of a prominent population of striated faults dipping moderately to the S, SSE or SSW (Figure 5-29). Slip-lines show them to be dip-slip faults at times with an oblique component. Slip-criteria indicate they are both normal and reverse faults. The outcrop also contains a population of steep, N-S oriented faults. Slickensides on these faults suggest they are basically strike-slip faults. Unfortunately no crosscutting relationships were observed, thus hampering the establishment of a relative chronology within the sequence of faulting episodes.

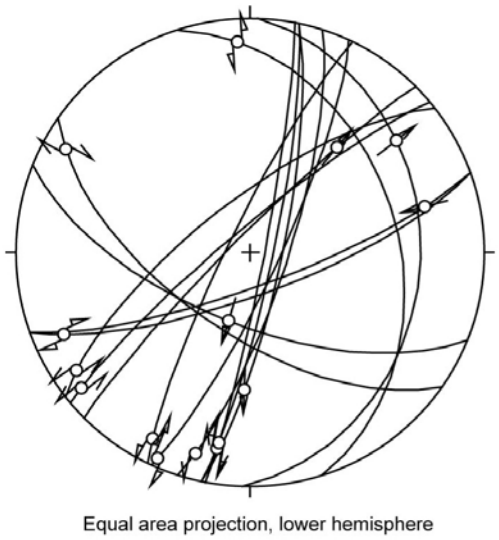

Figure 5-28. *Stereoplot of PSM007660 fault slip data.*

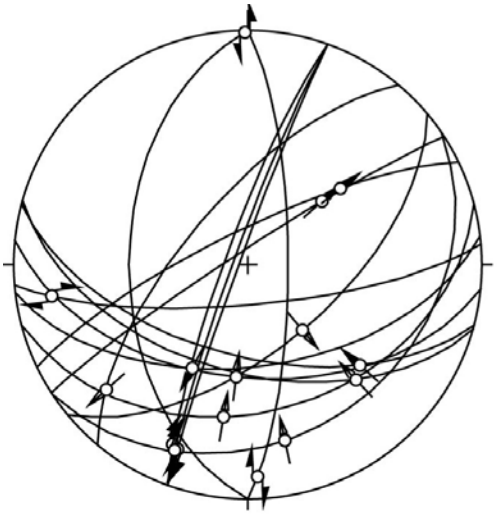

Figure 5-29. *Stereoplot of PSM007639 fault slip data.*

PSM007647 (6365222/1551104)

The granite outcrop is characterized by a strong, systematic fracture pattern. The spatial distribution of the fractures suggests that the dominant system of ENE trending fractures and faulted surfaces (labeled C in Figure 5-30) represents the master fault set of a sinistral Riedel system. Figure 5-30 provides the full orientation of the faults measured and the suggested kinematic interpretation, whereby R are sinistral Riedels genetically linked to C and R' are the corresponding dextral Antiriedels.

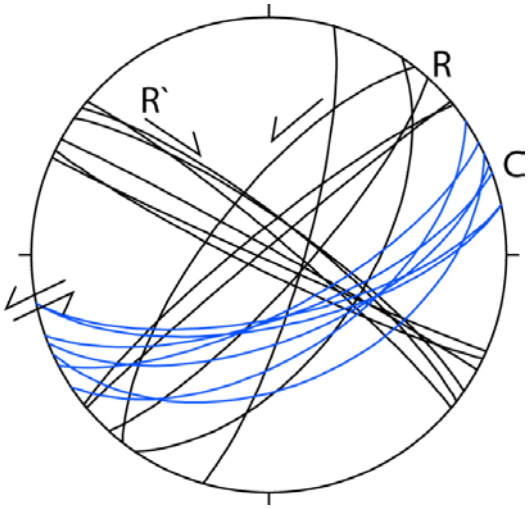

Figure 5-30. *Orientation of fractures measured at PSM007647. Blue great circles (C) are interpreted as master fractures, R and R' as genetically linked Riedels and Antiriedels. The fracture spatial arrangement suggests sinistral kinematics for the C planes.*

PSM007648 (6365337/1552294)

The outcrop is characterized by a rather complex fracture orientation pattern, with both steep and shallow sets of fracture planes (Figure 5-31).

PSM007649 (6365430/1552372)

A fault-rock barren, NS trending fault is found at PSM007649. A highly fractured fault core and a very sharp transition to the surrounding undeformed host rock characterize the outcrop (Figure 5-32). The geometry of secondary faults and fractures associated with the main NS fault suggests sinistral kinematics.

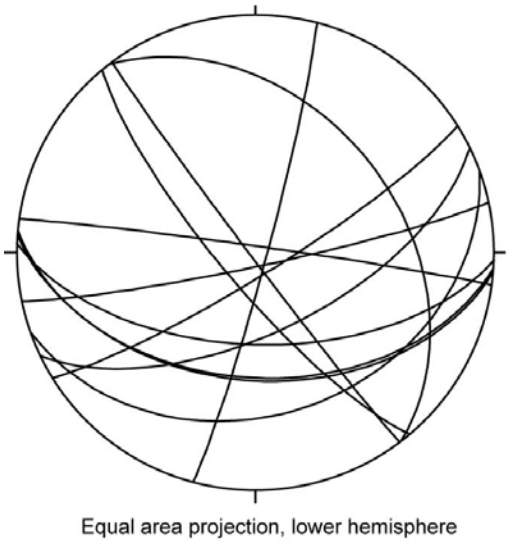

Figure 5-31. *Orientation of fractures at PSM007648.*

Figure 5-32. *View to the north (left) and to the south (right) of the NS trending sinistral brittle fault. The person on the left stands between the main fault strand (in front of the person) and a prominent sinistral Riedel.*

A different set of slightly shallower, WSW-ENE trending fractures is also pervasive at the outcrop scale. No clear crosscutting relationships were observed (Figure 5-33).

PSM007650 (6365573/1552301)

Two moderately SSW dipping normal faults were observed at this outcrop (Figure 5-34).

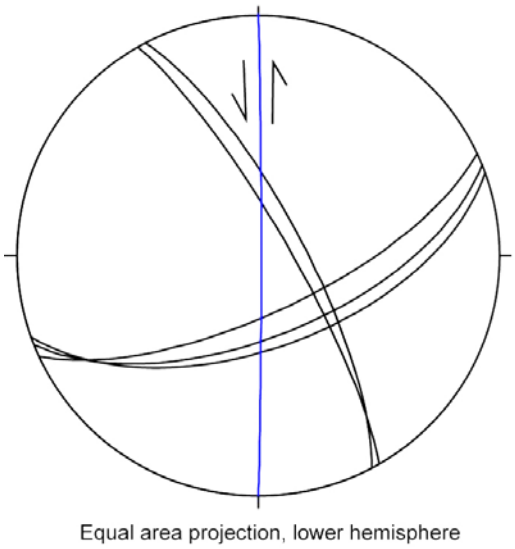

Figure 5-33. *Orientation of the NS brittle fault (in blue), its sinistral Riedels and the WSW-ENE trending set of fractures.*

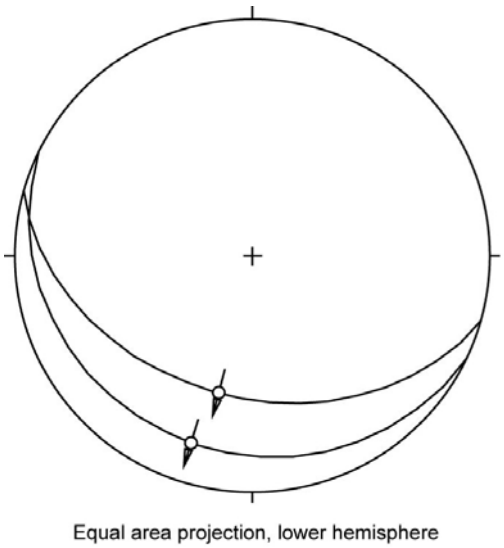

Figure 5-34. *Stereoplot of PSM007650 fault slip data.*

PSM007651 (6365560/1552264)

Several SSW moderately dipping fracture planes were identified (Figure 5-35). They are all epidote-coated. Unfortunately neither slickenlines nor kinematic indicators were observed.

PSM007652 (6365989/1552684)

At PSM007652 there occurs a significant NS subvertical fracture zone that bears a S-plunging series of slickenlines (Figure 5-36). It is a sinistral fault on the basis of slickensides and cogenetic Riedel structures.

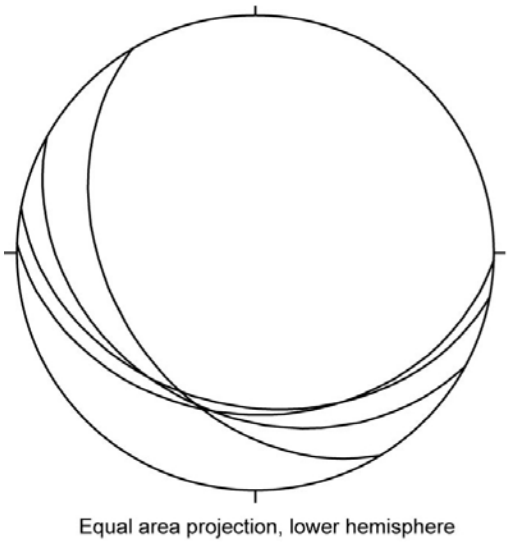

Figure 5-35. *Orientation of fractures at PSM007648.*

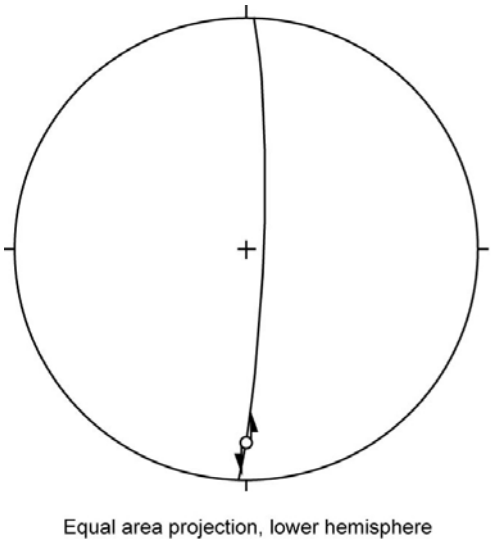

Figure 5-36. *Fault slip data for site PSM007652.*

PSM007654 (6365944/1552592)

The outcrop is worth mentioning for the presence of extensive networks of dilatant fractures that are very likely the result of hydrofracturing processes in response to high-pressure fluids (Figure 5-37).

PSM007655 (6365905/1552386), PSM007656 (6366036/1552430)

A possible set of steep conjugate strike-slip faults characterizes the outcrop (Figure 5-38).

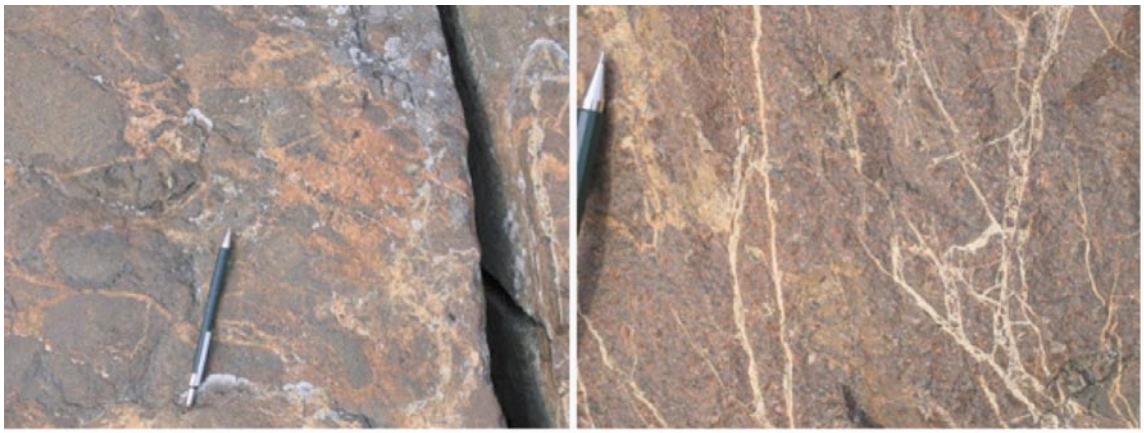

Figure 5-37. *Network of randomly oriented dilatant hydrofractures.*

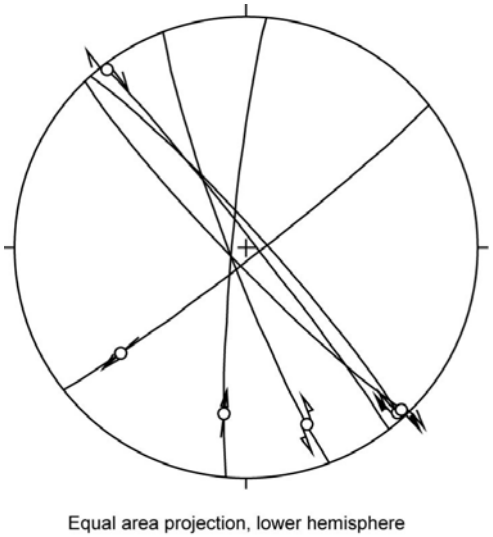

Figure 5-38. *Fault slip data for site PSM007655.*

PSM007657 (6366198/1552727)

The deformed outcrop consists of a NE-SW striking strike-slip brittle fault (Figure 5-39). The actual deformation zone has a lensoidal shape and attains a maximum width of c. 0.5 m (Figure 5-40). The sidewalls of the strongly deformed fault core contain slickenlines plunging 08° toward 218 and are locally epidote-coated. The fault core contains a complete transition from proto- to ultracataclasites and numerous epidote veins and epidote-coated fault planes. Fractures within the core are subvertical and strike c. 020.

Figure 5-39 shows the orientation of the fault zone and suggests sinistral kinematics (at least as far as the latest strain increment is concerned), reconstructed on the basis of the orientation of the associated Riedel fractures. The stereonet on the right hand side plots instead the two individual fault planes that were defined kinematically. More constraints on the fault's kinematics are provided by a c. 0.45 m thick granite dyke (Figure 5-40) that is deformed and offset sinistrally across the fault zone by c. 3 m.

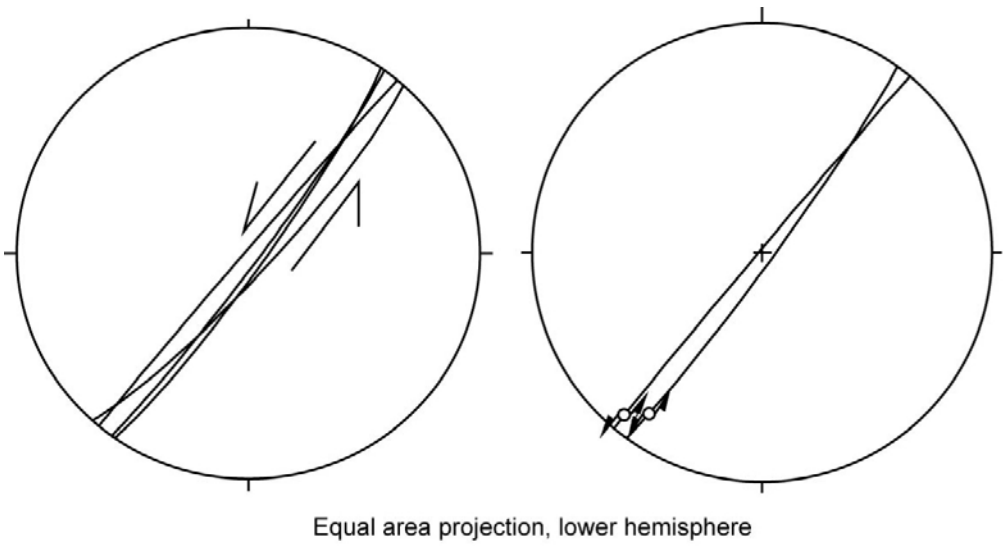

Figure 5-39. *Orientation and kinematics of sinistral fault planes at PSM007657.*

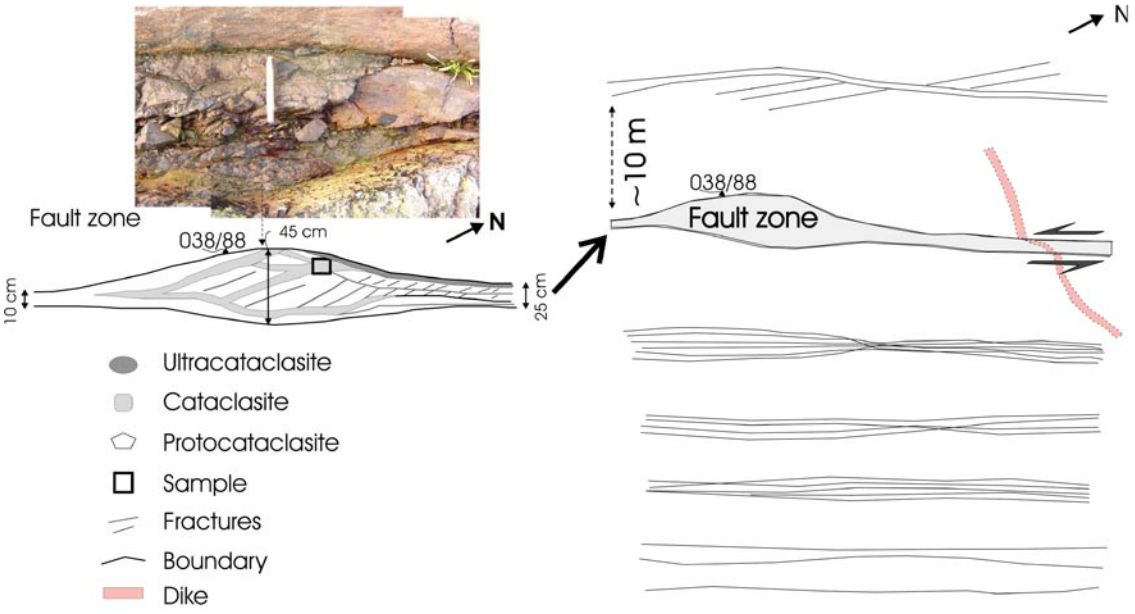

Figure 5-40. *Sketch of the structural relationships of the fault at PSM007657. The fault offsets sinistrally a granitic dyke by c. 3 m.*

Figure 5-41a illustrates the progressive textural transition from the almost undeformed granitic host rock to an ultracataclasite containing highly irregular and poorly sorted clasts derived from mechanical fragmentation of the protolith. Detailed microscopic analysis demonstrates that the ultracataclasite is only one of the many stages of a complex fault rock evolution. Figure 5-41b depicts a millimetric fragment floating in an extremely fine-grained ultracataclastic ground mass. The clast is itself a fragment of a cataclastic rock and this in turn implies multiple brittle events, whereby the product of an earlier faulting episode has then been reworked during a later subsequent episode of brittle deformation. Reactivation of the same fault strand is therefore demonstrated. Figure 5-41c zooms into the result of probably the latest deformation phase that has affected the outcrop. A stretched calcite fibres vein cuts across the thin section. Eight different median lines indicate multiple vein growth phases and the straight calcite crystal boundaries, orthogonal to the vein walls, point to orthogonal dilation. As seen in other examples, calcite veining is consistently a late episode within the brittle deformation history of the whole area.

5.1.4 Äspö

PSM007659 (6367495/1551540)

At outcrop PSM007659 at Äspö three small-scale faults were measured (Figure 5-42). They strike NNW and NNE with dextral kinematics and a third fault strikes N-S and has oblique slip with top to the NNW kinematics.

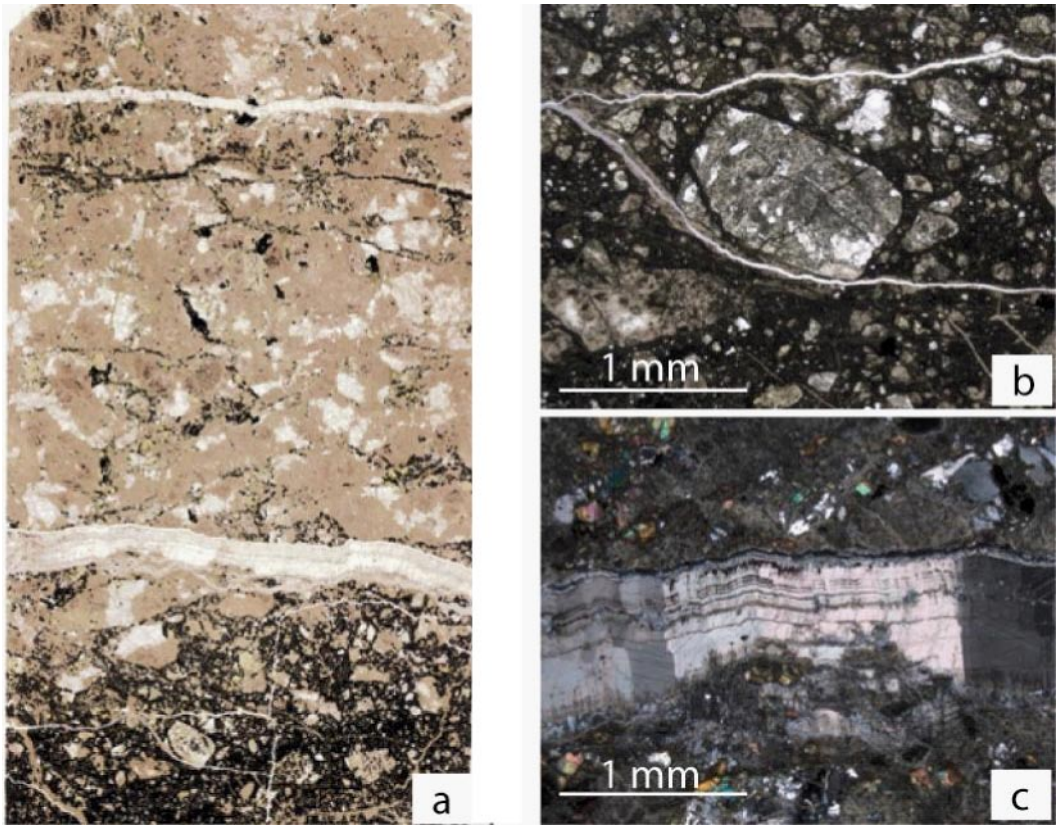

Figure 5-41. *Microphotographs of fault rocks of PSM007657. The ultracataclasite shows evidence of at least two distinct cataclastic events (b). Late calcite veins crosscut the ultracataclasite (c).*

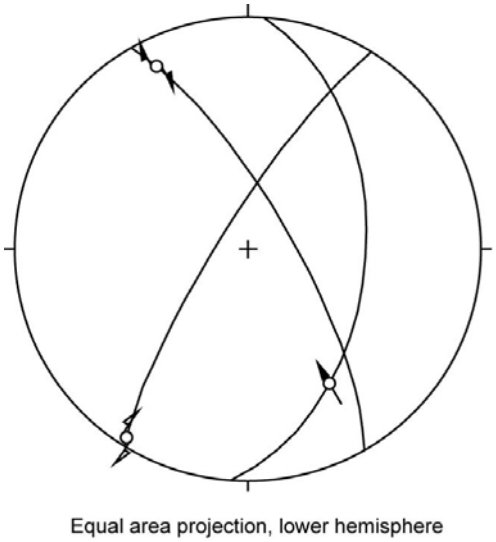

Figure 5-42. *Fault slip data for PSM007659.*

5.1.5 Summary and discussion of field data

Figure 5-43 is a summary of the most significant geometric and kinematic field observations made during this study. Stereonets are numbered for ease of reference.

An important point to stress before attempting a critical analysis of the data is that the observations made refer only to the last local increment of strain. Our study has documented that many faults and fractures of the area have undergone severe reactivation during long-lived structural histories. Apparent kinematic and geometrical inconsistencies may thus find an explanation in the repeated tectonic activity affecting the same structures at different times and under the influence of variably oriented stress fields.

Moreover, although this study focussed on the geometric and kinematic analysis of "so-called" brittle structures, the detailed study of the outcrops has indicated that these very structures may differ significantly even though they were all formed within the same brittle regime. Brittle-ductile shear zones with and without associated fault rocks, brittle faults and fractures with significant displacements and no displacement, late fracturing and jointing decorated by very low-temperature and low-grade minerals, hydrofractures and hydro-breccias: they all indicate that multiple episodes of deformation took place within a broadly-defined brittle regime under different environmental and physical conditions. When attempting a coherent, consistent reconstruction we need therefore to bear in mind these factors, so as to minimize the risk of correlating structures and assigning them to specific events based only on geometrical and kinematic considerations, disregarding age, formation conditions and complex, multiphase reactivation events.

The Laxemar area is dominated by several conjugate sets of subvertical strike-slip fractures and faults that can be correlated to the regional lineaments shown on the lineament map of Figure 5-43. Stereonets 1 and 2 show the presence of a sinistral NS trending set (stereonet 1), a dextral ENE-WSW dextral set (stereonet 1) plus their respective Riedel shears and a well defined family of fractures trending ESE-WNW (stereonet 2) whose kinematics could unfortunately not be determined directly in the field. A possibility is that they may be the conjugate set of the dextral ENE-WSW trending fractures shown in stereonet 1, which would require them to have sinistral kinematics.

Moving eastward, the overall fracture/fault orientation pattern changes progressively, with a set of NNE-SSW and NE-SW trending lineaments becoming the dominant structural features in the Simpevarp area and offshore. This transition is gradual and involves a smooth change in orientation. It has to be stressed that the change in the fracture pattern orientation may be linked to the presence of the intervening NE-SW trending sinistral mylonite belt (stereonet 4), i.e. the Äspö shear zone, which may have played a role in controlling the orientation of later brittle structures.

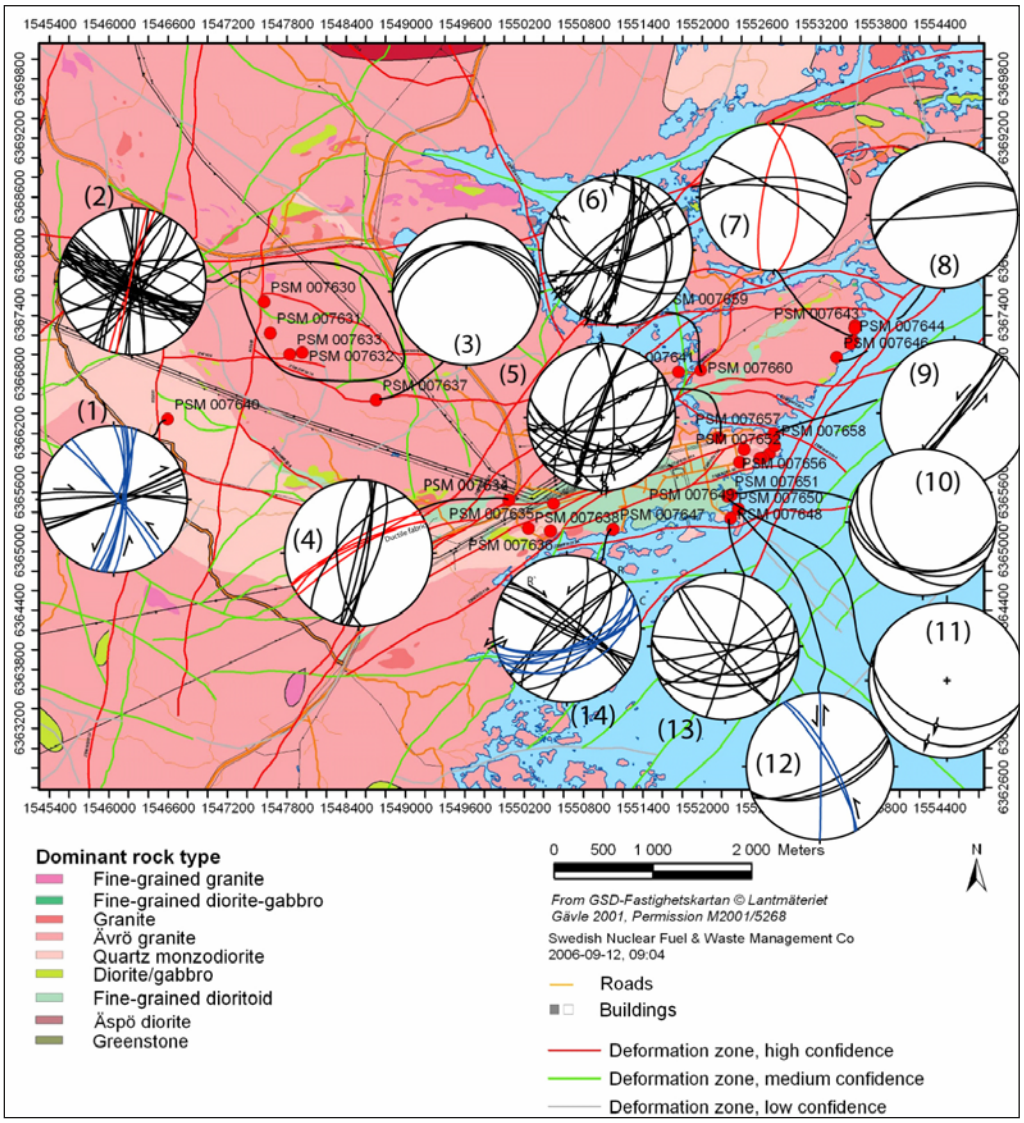

Figure 5-43. *Summary of field structural observations.*

Selected outcrops (stereonet 9) indicate sinistral kinematics for the NE-SW trending faults. Other localities (stereonets 7 and 12) contain dextral NS trending fractures/faults. EW trending steep faults with dextral kinematics are shown in stereonets 7 and 8.

Stereonet 14 shows a complex pattern of fractures that have been assigned to a system of sinistral ENE-WSW trending fractures.

Of great interest is the identification of a set of small-scale, moderately to gently SSW and NNE dipping fault planes that are either normal or reverse faults. They occur in Laxemar (stereonet 3) as well as in the Simpevarp Peninsula (stereonet 5) and along the coastline (stereonets10, 11 and 13).

Time relationships among the fractures/faults identified are difficult to constrain, although the general impression is that flat lying structures generally postdate the steep structures.

It is clear that no obvious simple orientation and kinematic pattern emerges from the data presented and discussed. The introduction to this section warned about the risks of attempting simple correlations at the sub regional scale, due to the long-lived tectonic history of the area and the severe reactivation of the structures. More structural information and the cautious analysis of a larger dataset are therefore needed before we can draw any robust conclusion.

5.2 Drill cores

Several drill core sections were examined (Table 5-1) with the aim of characterizing deformation zones (DZ) in greater detail from a geometric, kinematic and fault rock point of view according to step 2 in the method description SKB MD 810.003 (SKB internal description). The drill cores and the relative depth intervals inspected are listed in Table 5-1 and their location is shown in Figure 5-44.

Table 5-1. List of drill cores inspected during this study.

Drill core	Inspected section (m) – core orientation	Single hole interpretation reference
KSH03A	160–275–126°/57°	/Ehrenborg and Stejskal 2004, Hultgren et al. 2004/
KLX04	873–973–002°/85°	/Mattson et al. 2005/
KLX06	368–390–340°/60°	/Mattson 2005/
KLX07A	111–180; 604–659; 816–838 169°/50°; 174°/52°; 174°/51°	/Carlsten et al. 2006b/
KLX07B	120–175–171°/85°	/Carlsten et al. 2006b/
KLX08	100–165; 218–252; 760–781 199°/60°; 206°/60°; 212°/58°	/Carlsten et al. 2006c/
KLX10	389–432,5; 471–499 270°/85°; 270°/85°	/Carlsten et al. 2006a/

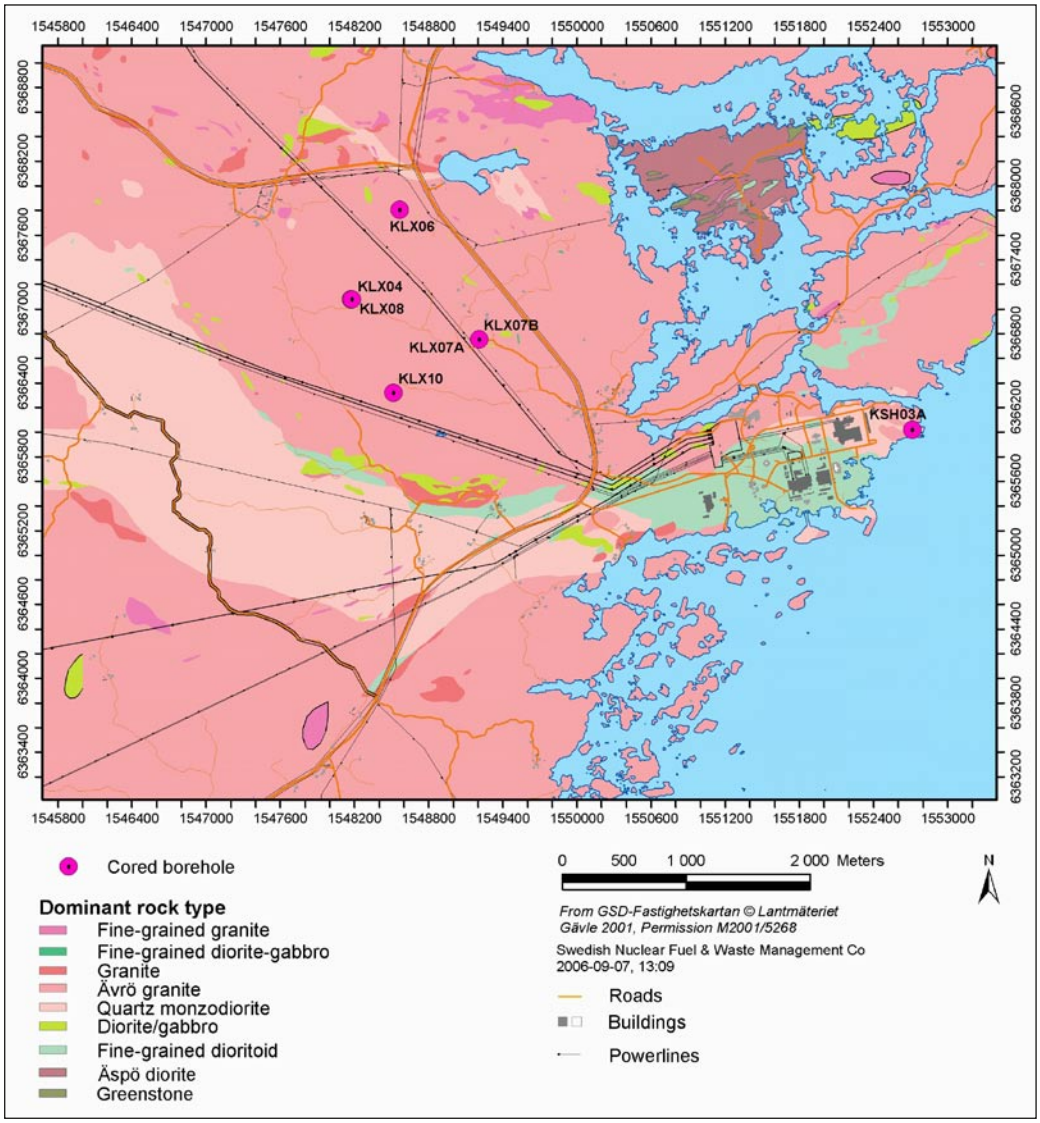

Figure 5-44. *Location of the studied drill cores.*

5.2.1 Drill core KSH03A (160–275 m)

This interval of KSH03A is a 115 m long series of transition zone containing several fault cores (Figure 5-45). The section is described as DZ 1 in the single-hole interpretation by /Ehrenborg and Stejskal 2004, Hultgren 2004/. The whole of the transition zone is in general characterized by a high fracture frequency. A large variety of fault rocks are present, resulting in extensive crushed rock intervals. These are not continuous enough to be classified as a single fault core.

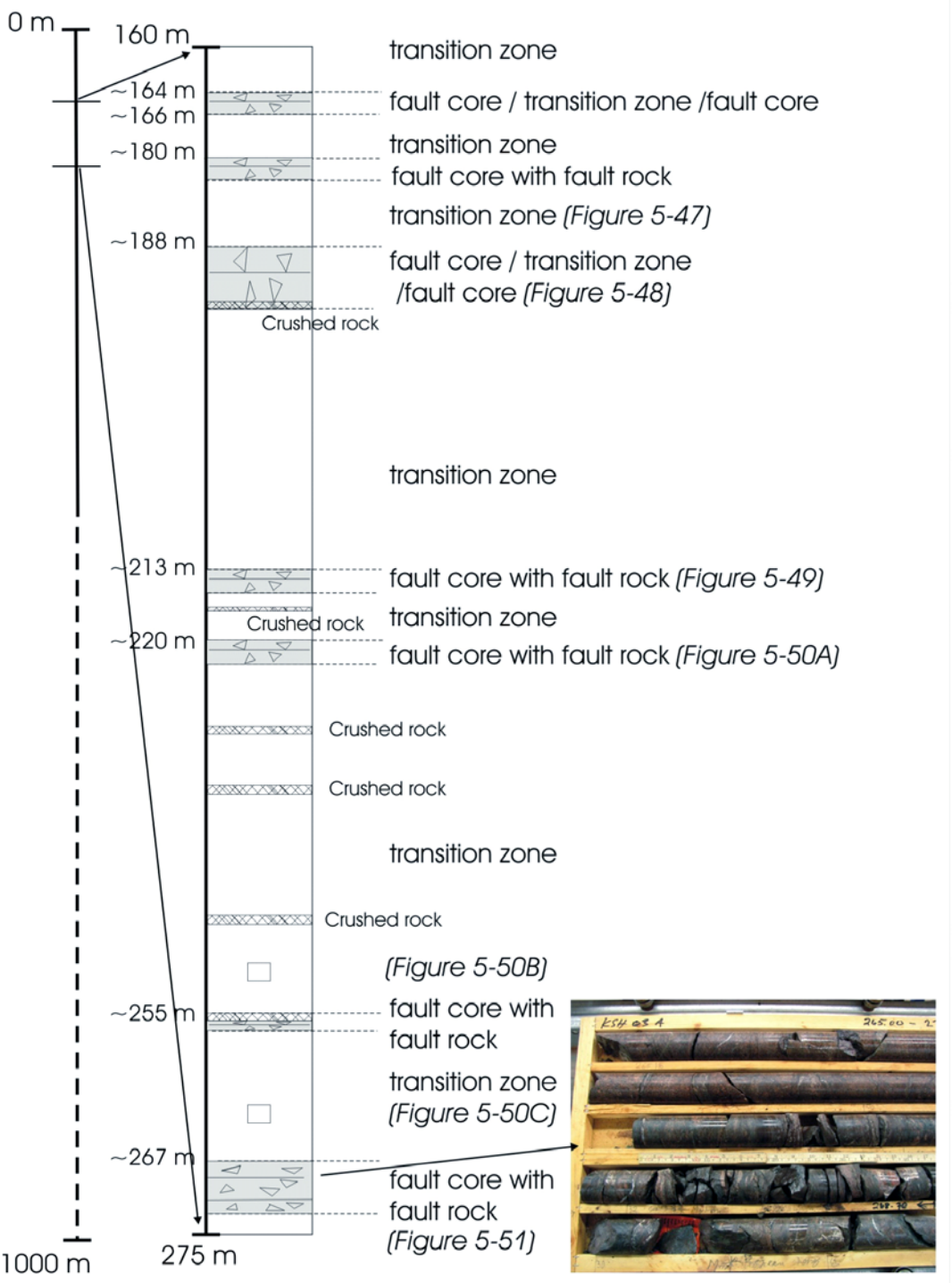

Figure 5-45. *Schematic illustration of the logged depth interval of KSH 03A. The inspected interval corresponds to DZ 1 in the single-hole interpretation by /Ehrenborg & Stejskal 2004, Hultgren et al. 2004/.*

The following are only a few examples of fault rocks occurring in some of the individual fault cores and transition zones, and reflect the structural complexity encountered in this section. In the transition zone, at adjusted length 187 m, there occurs a cataclasite band that is itself brittly offset along discrete fault segments decorated by red gouge (Figure 5-46). Figure 5-46 shows at least three generations of fault rock, the earliest being a protocataclasite (1, Figure 5-46) containing fragments of the granite host rock. This is in turn crosscut by a green cataclasite with calcite and chlorite fragments (2, Figure 5-46). The latest stage is a thin red gouge horizon that offsets the others sinistrally (3, Figure 5-46).

At approximately 191 m the fault core consists of, amongst others, a cemented breccia (Figure 5-47). The breccia contains fragments of an older cataclasite and is cemented by laumontite and epidote. Adjacent to this there is an earlier cataclasite and strands of gouge (Figure 5-47).

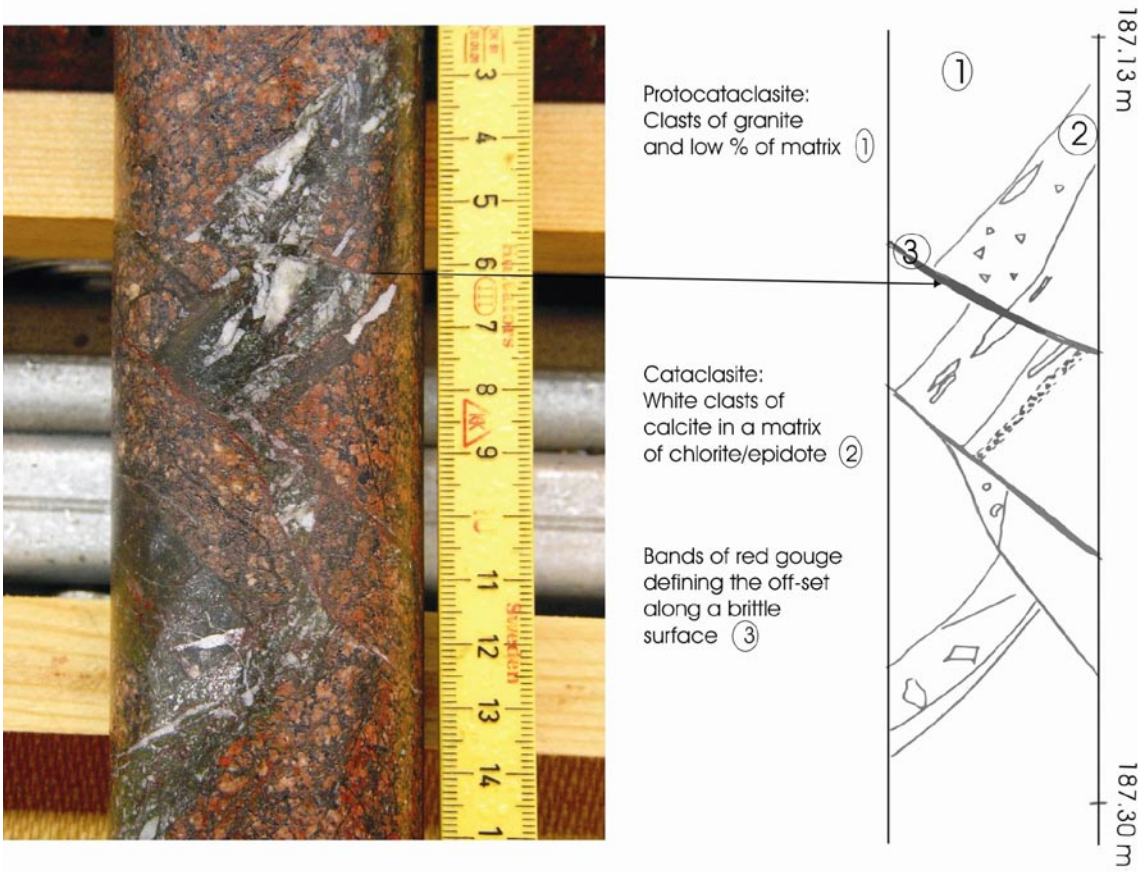

Figure 5-46. *Example of three distinct phases of brittle deformation, the oldest of which is a protocataclasite containing granite fragments and low percentage of matrix (1). This is in turn crosscut by a dilatant cataclasite containing calcite fragments in a chlorite/epidote matrix (2). This is in turn truncated by thin veins of red gouge or ultracataclasite (3), indicating sinistral offset.*

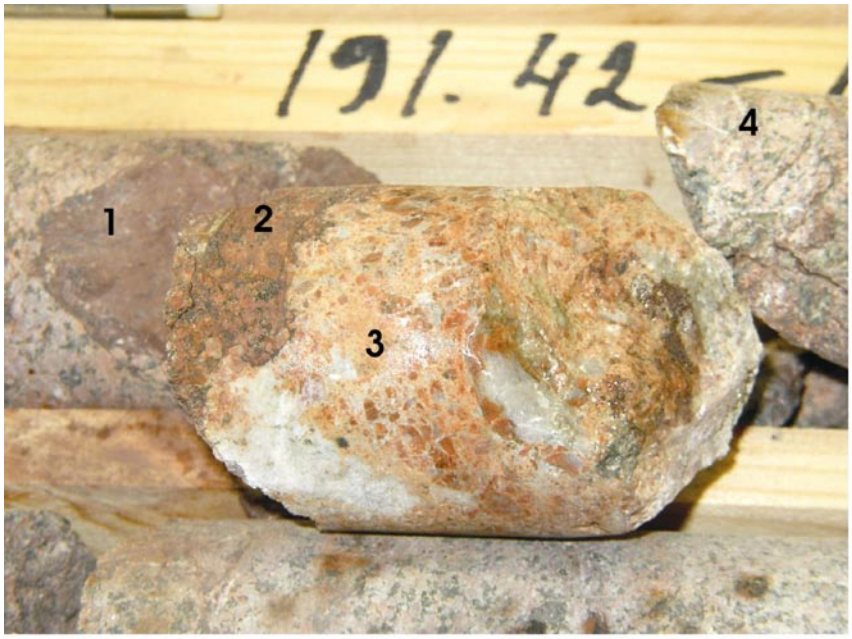

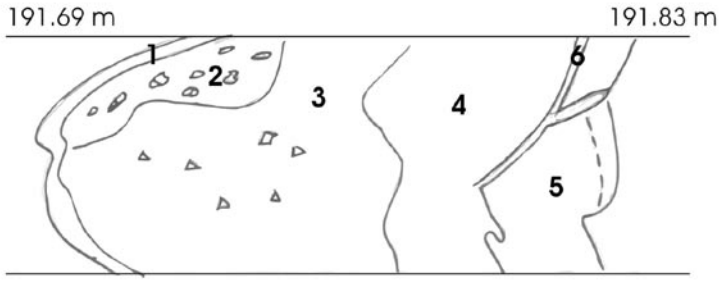

1- Red gouge / ultracataclasite. Close to 100% matrix.
2- Red cataclasite with granite fragments of 0.1/3 mm in size. ~40% matrix
3- Breccia cemented with laumontite. Fragments of cataclasite are angulare and range from 1 to 3 mm size. ~70% matrix.
4- Cataclasite
5- Laumontite / calcite
6- Green gouge / ultracataclasite. Very fine grained, possibly ~100% matrix.

Figure 5-47. *Complex crosscutting relationships among several generations of cataclasites and breccias.*

A fault core at depth 212.87–215.80 m consists of a very complex alternating sequence of cataclasites, undeformed lenses of host rock and ultracataclasites. The thickness of the individual fault rock occurrences varies. This fault core presents evidence for several faulting events, whereby, for example, a 3–4 cm thick zone of epidote and quartz-rich cataclasite is cut by a less than 1 cm wide zone of dark red carbonate-cemented breccia, in which the former fault rock appears as mm-size fragments (Figure 5-48). There are also calcite-filled veins outside the fault. This complex relationship is also visible at the thin section scale where the latest deformation stage is shown by a calcite-filled vein crosscutting the other structures (Figure 5-48).

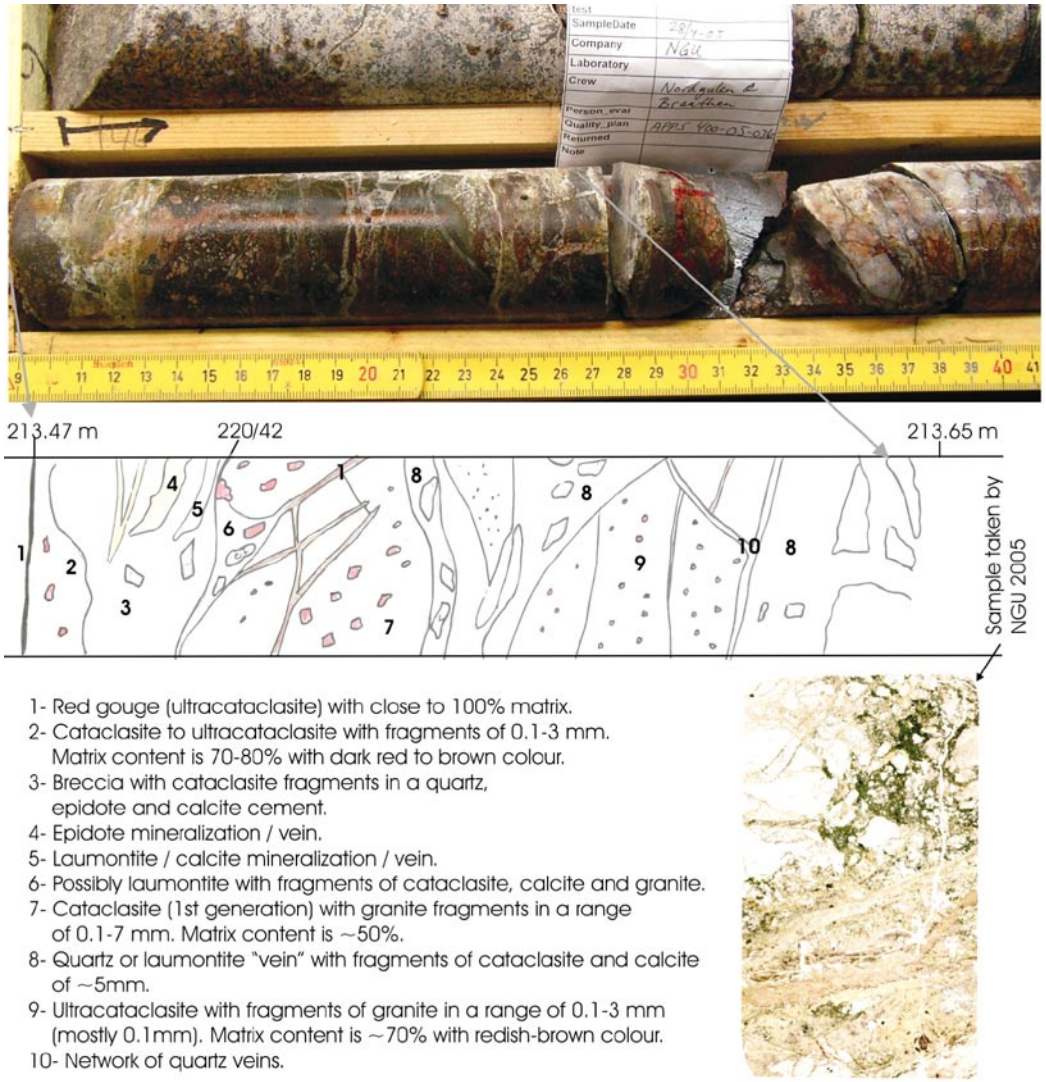

Figure 5-48. *Illustration from drill core KSH03A, depth 213 m. A ~ 30 cm wide fault zone presents evidence of several faulting events. A 3–4 cm thick zone of epidote-quartz (?) bearing cataclasite (locally stained in pink) is cut by a narrow zone of dark red carbonate-cemented breccia, in which the former fault rock appears as mm-sized fragments. A network of calcite-filled veins also cuts the cataclasite. Several generations of cataclasites are amalgamated, including cemented breccias, and are subsequently crosscut by veins of different minerals. The scanned thin section photo of a representative sample is shown to the right.*

At depth 221.5 m there is a 3–4 cm thick red gouge horizon (Figure 5-49A), which is very distinct and exceptionally thick for the drill cores investigated during this study. It is non-cohesive, compared to that found at 246.85 m. Its thin section shows that the fault rock forms a progressive transition from a proper gouge (black) to an ultracataclasite containing fragments of cataclasite and granite (Figure 5-49A).

At depth 246.85 m a cohesive band of gouge and ultracataclasite is in sharp contact with a protocataclasite (Figure 5-49B). These ultracataclasite bands are abundant in transition zones. The thin section shows that it is dominated by an ultracataclastic component, with very fine matrix and small particle size. Some gouge (black) is interfingered with the ultracataclasite (Figure 5-49B).

A laumontite-cemented breccia, containing cataclasite clasts, occurs at depth 261.40 m (Figure 5-49C). The thin section shows several phases of structural reworking, with an early cataclasite characterized by poorly sorted and angular clast and a later crosscutting vein (Figure 5-49C).

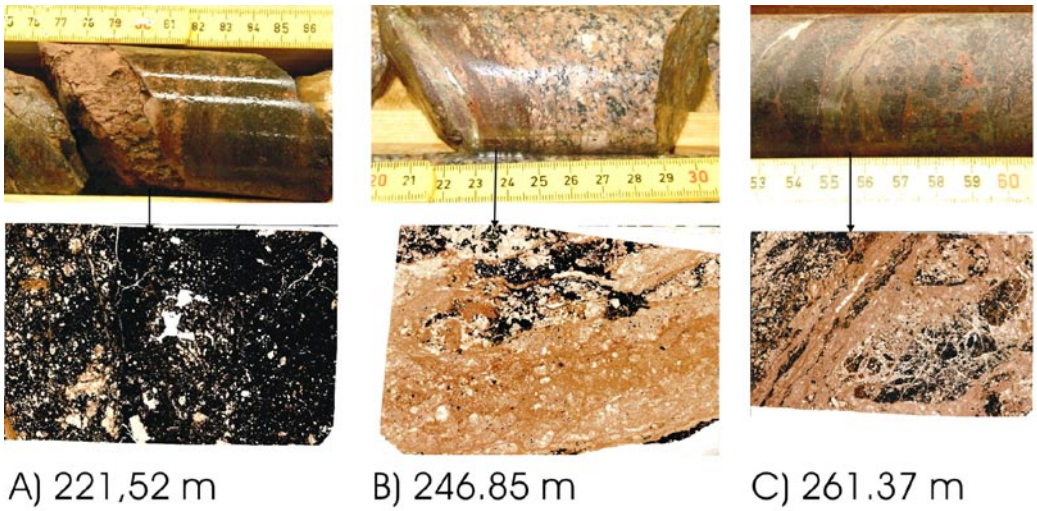

Figure 5-49. *Samples of A) red gouge, B) band of ultracataclasite and gouge, and C) cemented breccia. Scanned thin sections of samples show A) Gouge (black) and ultracataclasite with fragments of cataclasite and granite. B) Ultracataclasite with fragments of cataclasite and granite, with some gouge (black), and C) fragments of cataclasite cemented in laumontite, with a network of anastomosing dilatant ultracataclasites.*

Within the lower part of the analysed depth interval there is a fault core showing evidence of several faulting events and a progressive textural evolution from undeformed medium-grained pink granite to a cataclasite and finally to a strongly foliated cataclasite/phyllonite (Figure 5-50). Figure 5-50A shows several generations of crosscutting cataclasites forming at the expenses of the pink granite. A foliated cataclasite/phyllonite, with a strong planar fabric reminiscent of a mylonitic rock, follows in the sequence and is shown in Figure 5-50B. It is important to observe that no clasts of the foliated cataclasite/phyllonites are found in the cataclasite defining the beginning of the deformation zone, implying that the foliated rock postdates the development of the cataclasite. This strongly foliated cataclasite/phyllonite evolves progressively into an only moderately foliated cataclasite (Figure 5-50C), before the final transition back into undeformed rock.

In this fault core there occurs also a narrow sliver of sandstone. The relation between the fault core and the sandstone is not obvious.

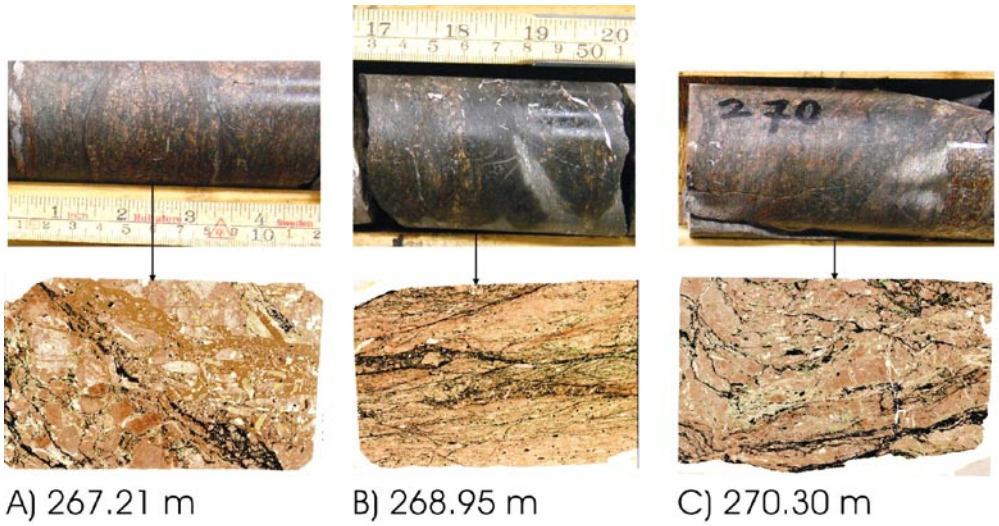

Figure 5-50. *Samples of A) cataclasite, B) strongly foliated cataclasite/phyllonite and C) foliated cataclasite. Below are thin sections from the relative samples. A) Cataclasite showing several phases of deformation in the form of multiple, crosscutting cataclasite generations. B) Strongly foliated cataclasite with distinct foliated fabric defined by opaque minerals and phyllosilicates and C) foliated cataclasite.*

Figure 5-51 shows the orientation of all structural elements measured in the drill core interval and, to the right, fault slip data for fault planes that could be constrained kinematically.

The drill core section under discussion lacks statistically significant amounts of striated surfaces, and this hampers any meaningful analyses of the observed kinematic pattern. However, we can recognize some preferential orientations in the stereonets of Figure 5-51. Sets of moderately NW, SW and SSW dipping planes are the most common features observed. The foliated cataclasites of Figure 5-50 dip consistently to the NW, and ultracataclastic bands and gouge layers dip also NW. Steep late fractures and laumontite-calcite veins crosscut the moderately dipping structures and strike subvertical NE-SW.

The kinematic analysis of the moderately dipping planes suggests a predominantly normal kinematics with top-to-SW, W and NW sense of movement.

5.2.2 Drill core KLX04 (870–970 m)

This section corresponds to DZ 6 in the single-hole interpretation /Mattson et al. 2005/. Drill core KLX04 intersects an approximately NNW-SSE-striking and gently E-ENE and W-WSW dipping fault zone. Several fault cores, commonly containing fault rocks, and their respective adjacent transition zones, characterize this section (Figure 5-52). Transition zones show increased fracture frequency towards the fault cores and occurrences of strands and thin bands of cataclasites and gouge. Red staining is common in the transition zones.

Examples of fault rocks in this interval are protocataclasites, cataclasites, ultracataclasites, gouge and cemented breccias. Figure 5-53A shows a brecciated cataclasite, with fragments of cataclasite and ultracataclasite ripped off and cemented by late calcite to form a now cohesive fault rock. The scanned thin section reflects the same sequence, with a primary cataclasite subsequently dilated and crosscut by calcite veins. Figure 5-53B shows a complex assemblage of fault rocks, from a foliated cataclasite, to the left in the middle core, to ultracataclasites, gouge and again cataclasites containing granite fragments. The very fine-grained matrix seems to consist mainly of epidote. In addition, there are some narrow zones of a very distinct red gouge (Figure 5-53B).

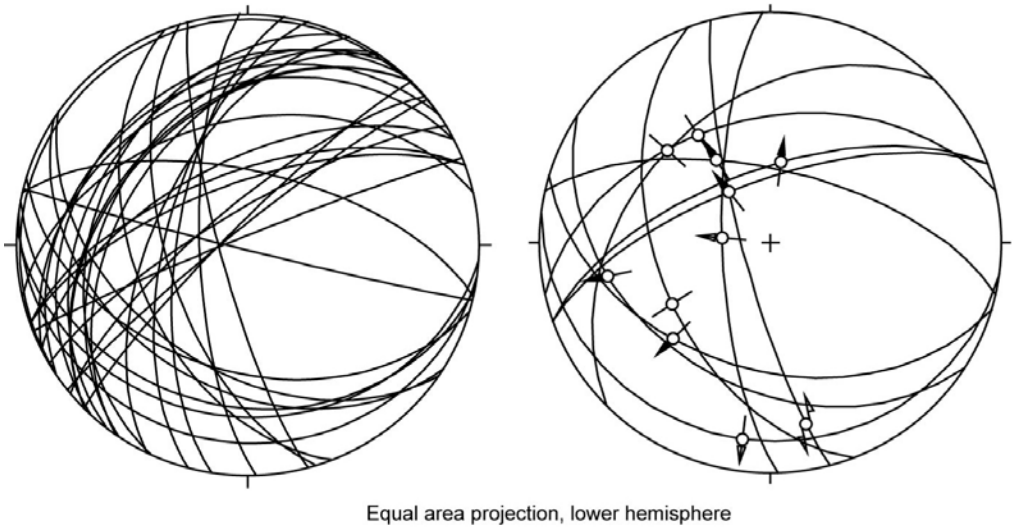

Figure 5-51. *Fracture orientation and kinematics observed in the drill core section.*

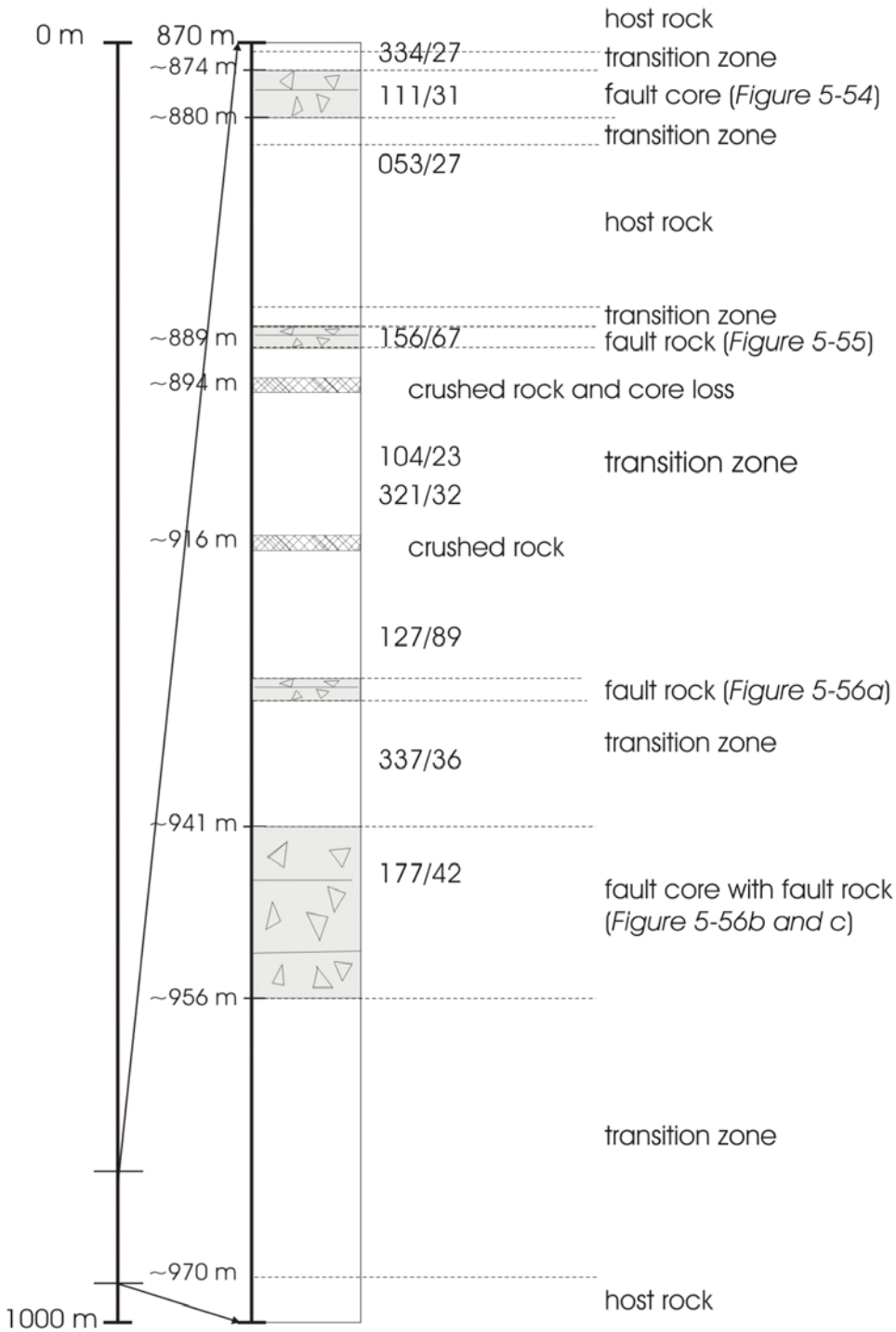

Figure 5-52. *Schematic illustration of the 870–970 m interval studied in KLX04. The orientation of specific structural features is also reported according to the right hand rule convention. The section corresponds to DZ 6 in the single-hole interpretation /Mattson et al. 2005/.*

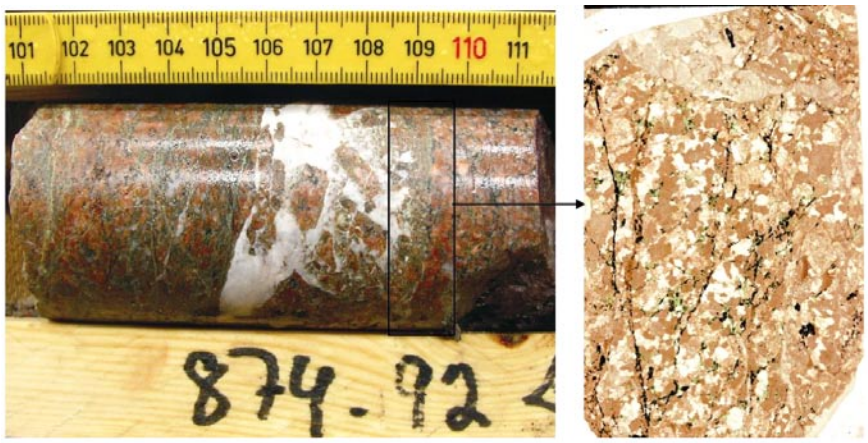

A) 874.70 m

B) 876.30 m

Figure 5-53. *Samples from A) cemented breccia and B) red gouge/ultracataclasite. Scanned thin sections of the samples are shown to the right.*

Figure 5-54 shows four distinct fault rock occurrences, with complex crosscutting relationships. Epidote veins crosscut a protocataclastic zone. These are in turn brittly offset along a band of cemented breccia. The breccia contains elongated, strongly reworked fragments of cataclasite and epidote, which are cemented together by chlorite and/or epidote matrix. This is in turn crosscut by ultracataclasite/gouge (to the left end of Figure 5-54), with abundant epidote in the matrix and only dispersed fragments of cataclasite, epidote and calcite. Calcite cemented all fragments.

Figure 5-55 shows even more fault rock variations in this section. An epidote-rich cataclasite (A) illustrates the superposition of two possible faulting events, identified by a cataclasite/ultracataclasite containing a fine-grained epidote matrix and a brecciated cataclasite cemented by epidote, respectively. Figure 5-55B shows a cataclasite with two distinct structural imprints, with the latest stage infilled by calcite veining. The black injection is formed by very fine-grained material, possibly gouge or a fluidized ultracataclasite, whereas the surrounding cataclasite consists of reworked granite fragments. The cataclasite is in turn crosscut by a thin band of ultracataclasites, later injected by a pervasive calcite vein network. Figure 5-55C shows a chlorite-rich cataclasite crosscut by a distinct red gouge (Figure 5-55C).

The section logged is dominated by gently-dipping fracture planes and slickensided surfaces (Figure 5-56). The relatively low dip angle of the measured planes generates a rather confused stereonet that indicates no strong preferred planar orientation. It is important to observe the predominance of relatively flat-lying fractures and fault planes in the whole section, with only

Figure 5-54. *Several generations of proto- to ultracataclasites and cemented breccias. The thin section to the left shows overall rock dilation, subsequently infilled by calcite. On the left-hand side of the calcite there occurs an ultra-/cataclasite, whereas protocataclasites are found on the right side. A cataclasite with abundant epidote in the matrix is visible in the thin section to the right. Strands of epidote-decorated ultracataclasites and fragments of an earlier cataclastic rock form an anastomosing network.*

a few steep structures observed. Kinematically constrained gently to moderately dipping planes indicate either normal or reverse kinematics, with prevalence of down- or up-dip movements and scarcity of oblique kinematics (Figure 5-56).

A few steep and subvertical NW-SE and NE-SW striking fracture planes indicate mostly sinistral kinematics.

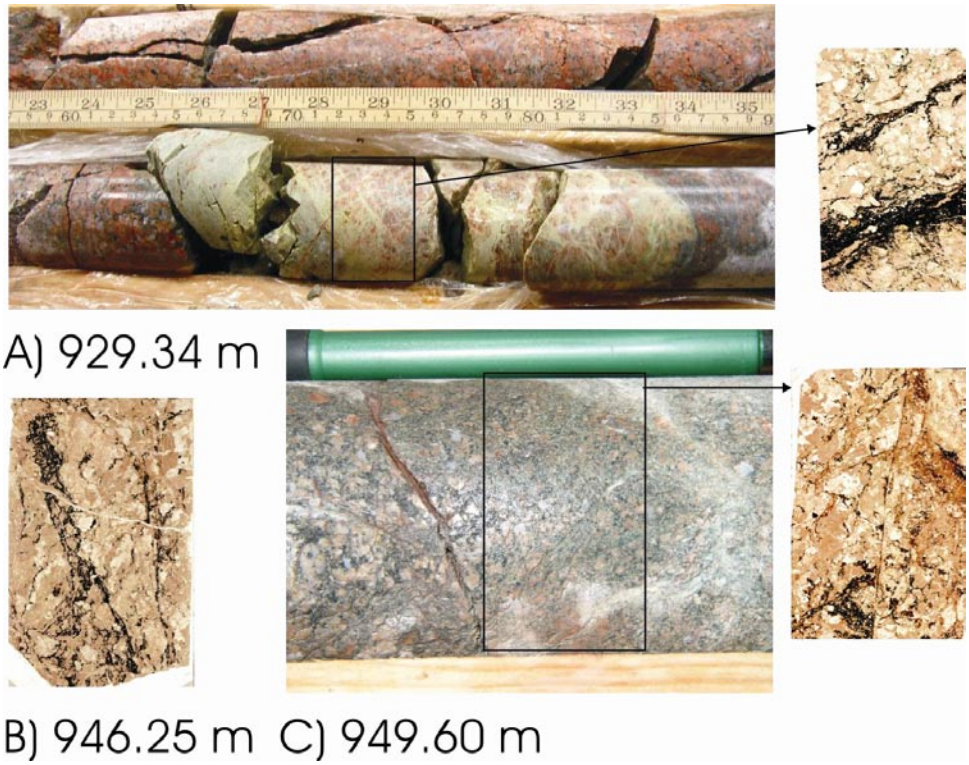

Figure 5-55. *Samples of A) epidote rich cataclasite, B) cataclasite and C) chlorite rich cataclasite. Scanned thin sections of samples show A) a progressive fault rock evolution from cataclasite (top), to gouge (black), and ultracataclasite (bottom). B) Two generations of cataclastic reworking, and C) brittle micro-scale faults and a network of fine strands of ultracataclasite and gouge overprinting an older cataclasite.*

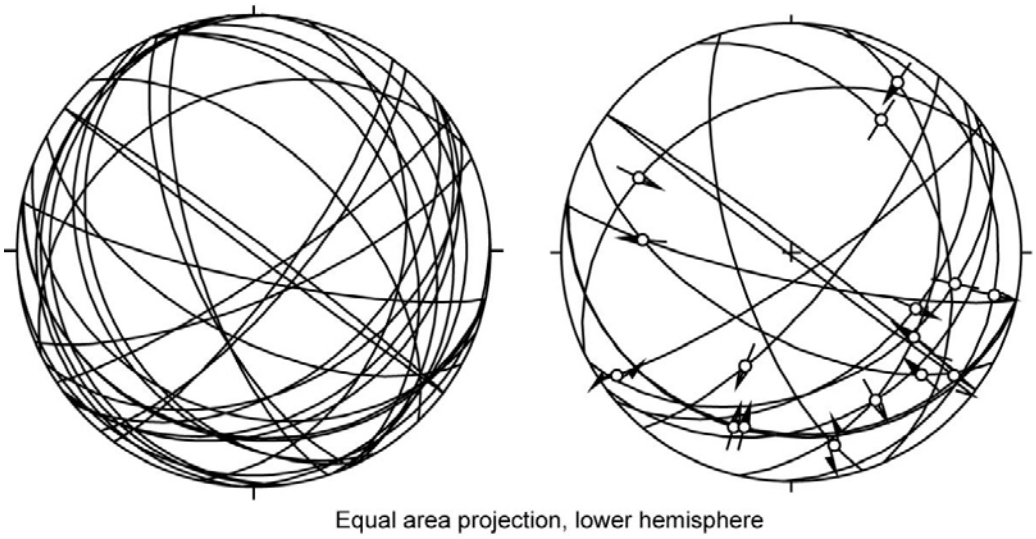

Figure 5-56. *Orientation of fracture planes and striated surfaces with relative kinematics measured in the drill core section.*

5.2.3 KLX06 (368–390 m)

This section (297–425 m) corresponds to DZ 2 in the single-hole interpretation /Mattson 2005/. At depth interval 290–435 m, KLX06 intersects a spectacular fault, striking approximately E-W and dipping steeply to the south; the fault presents brittle-ductile deformation features. The section contains a narrow zone of crushed rock and a distinct fault core containing brittle fault rocks

(Figure 5-57) that overprint a rather pervasive foliation. The transition zone consists of foliated granites with localized brittle-ductile deformation bands. The fault core consists of protomylonites, cataclasites and red gouge (Figure 5-57). The protomylonites are affected by later brittle deformation as suggested by the presence of mylonitic fragments in the crosscutting cataclasites.

Figure 5-58 shows the orientation of the deformation zone under discussion and two gently W-plunging stretching lineations defined by chlorite.

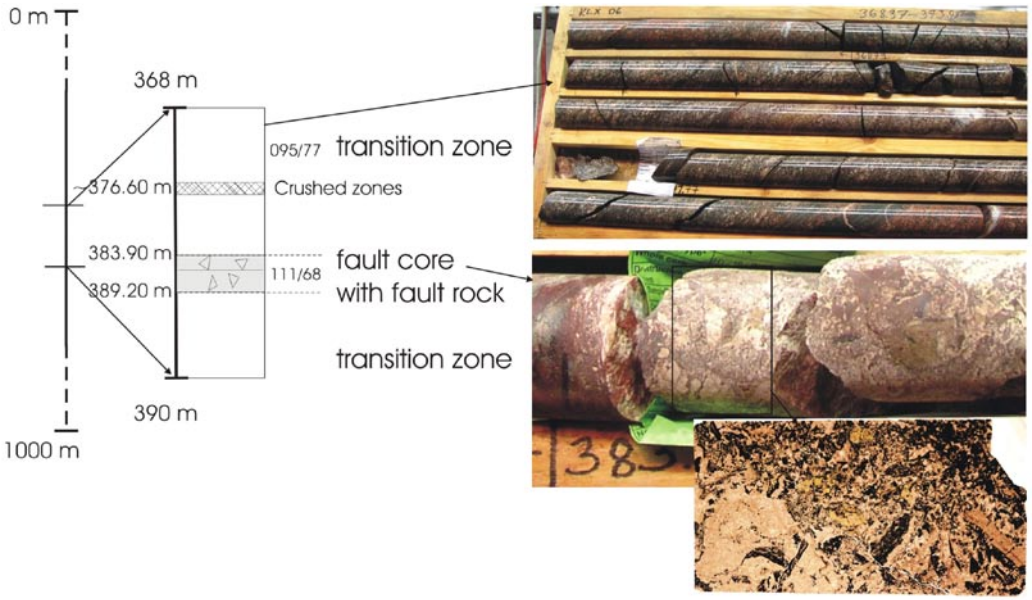

Figure 5-57. *Schematic illustration of the logged section with right hand rule orientation of chosen structural features. To the right, thin section of a cataclastic sample at depth ~ 384,7 m. This depth interval corresponds to DZ 2 in the single-hole interpretation.*

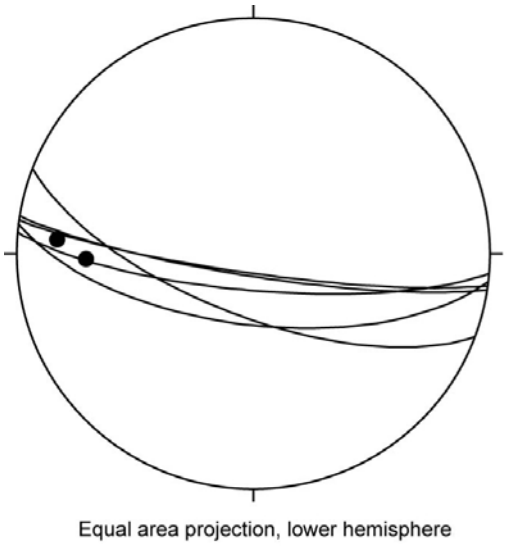

Figure 5-58. *Orientation of the brittle-ductile shear zone that characterizes the 368–390 m depth interval of KLX06. Solid dots show the azimuth of two chlorite-defined stretching lineations.*

5.2.4 Drill core KLX07A

Depth interval 111–180 m

This section corresponds to DZ 1 and 2 in the single-hole interpretation /Carlsten et al 2006b/. This KLX07A section is characterized by a relatively thin fault core defined by fault rock occurrences and two narrow zones of crushed rock (Figure 5-59). The fault core consists of cataclasites and protocataclasites. The thin section sample is from a band of red gouge sandwiched by cataclasites. The thin section shows that the cataclasite is formed by angular fragments of granite and anastomosing bands of ultracataclasite/gouge (black) containing a few small fragments of cataclasite (Figure 5-59). The remaining part of the section is defined as a weak transition zone containing several occurrences of thin bands (mm-cm) of cataclastic rocks (Figure 5-59). As an example we report an ultracataclasite with an epidote matrix and fragments of granite, as shown in Figure 5-59. There is also some indication of dilation with mineral growth on the edges of the band.

Cataclasite-decorated fracture planes dip at a gentle angle to the NW (Figure 5-60) and the NE. Subvertical laumontite, chlorite and epidote fractures crosscut all previous structures in a NNE-SSW and WSW-ENE direction (Figure 5-60). The stereonet of Figure 5-60 shows two moderately S-dipping red great circles. They represent the orientation of two almost parallel fault sets that offset with complex normal and reverse kinematics thin strands of red gouge-ultracataclasites (Figure 5-60). No clear crosscutting relationships between normal and reverse faults could be established.

Depth interval 604–659 m

This section is described as DZ 10 in the single-hole interpretation /Carlsten et al. 2006b/. It is characterized by fresh granites with only sporadic occurrences of fault rock (Figure 5-61), such as networks of cataclasite strands, commonly interfingered with bands of gouge and ultracataclasite, as shown in Figure 5-61. A c. 4–5 cm thick ultracataclasite band containing a chlorite and epidote matrix, in which are dispersed angular fragments of granite, occurs at depth 645 m. A calcite vein injected into this band, possibly during a later reactivation stage. Cataclasites are dark, fine-grained and contain fragments of granite (Figure 5-61). A one-metre thick zone of crushed rock occurs at the bottom of the section.

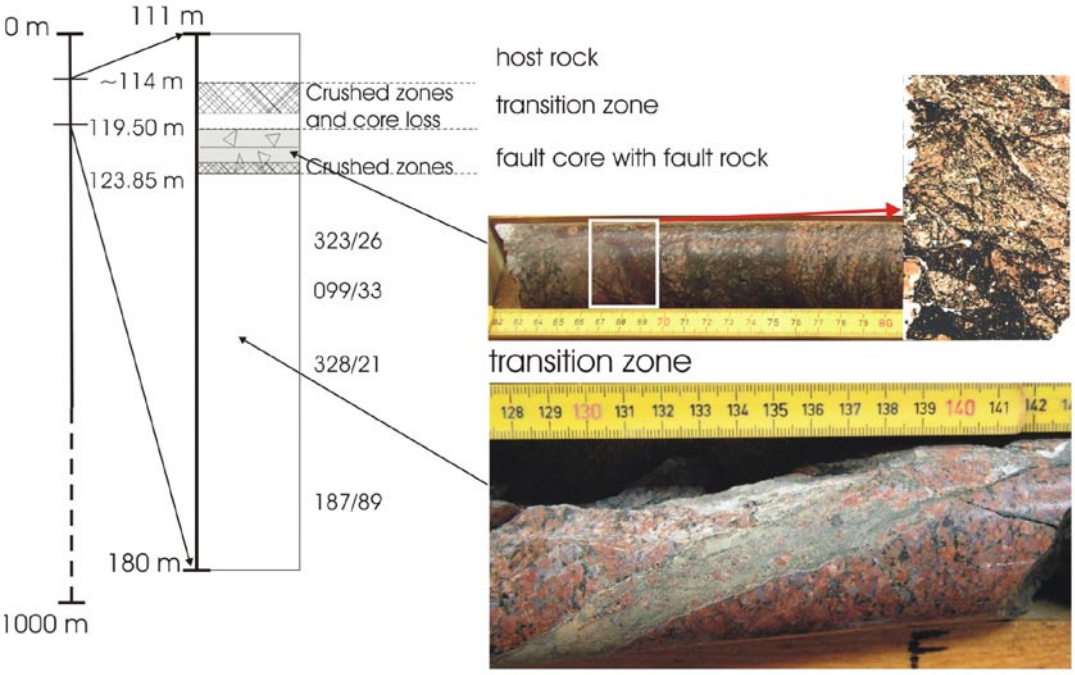

Figure 5-59. *Structural log of the inspected section and location of thin section sample. Chosen structural features' orientations are shown according to the right hand rule. The sample at depth ~ 119.70 m is made of by ultracataclasites offset by a later crosscutting fault. The section corresponds to DZ 1 and DZ 2 of the single-hole interpretation /Carlsten et al. 2006b/.*

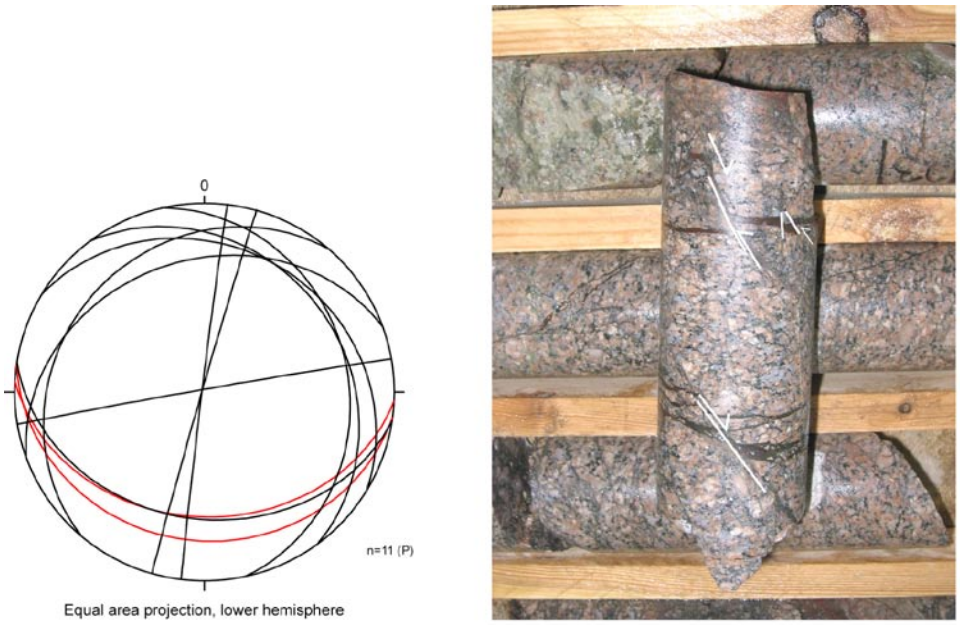

Figure 5-60. *Orientation of fracture and fault planes (gently to moderately dipping great circles) and veins (subvertical planes) observed in KLX07A. The photograph shows subparallel normal and reverse faults cutting across thin gouge/ultracataclastic layers. A complex reactivation history is inferred.*

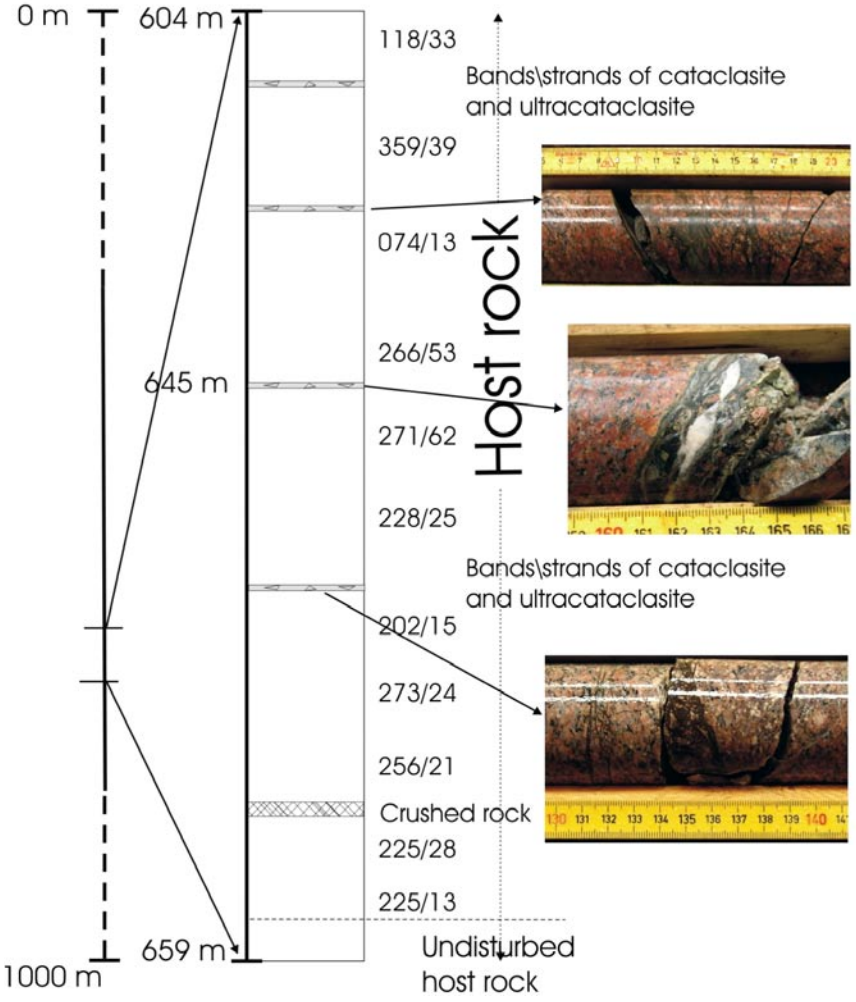

Figure 5-61. *Schematic illustration of section 604–659 m. It corresponds to DZ 10 of the single-hole interpretation. Chosen structural features' orientations are shown according to the right hand rule.*

Relatively flat lying cataclastic and ultracataclastic bands characterize the interval. Figure 5-62 shows them plotted as red great circles, dipping 25–35° to the NW, N and NE. Only two surfaces could be constrained kinematically and provided reverse sense of shear. Epidote and quartz veins (black great circles) have very shallow planar attitudes.

Depth interval 816–838 m

This section is described as DZ 13 in the single-hole interpretation. It is a relatively short interval and is generally characterized by undisturbed rock with the exception of a significant crushed or highly fractured zone containing fault rock occurrences with abundant epidote veining (Figure 5-63**)**. The predominant fault rocks characterising the fault zone at depth 831 m are mylonites and some volumetrically minor cataclasites (Figure 5-63). The thin section analysis shows a penetrative mylonitic fabric overprinted by thin strands of ultracataclasite (brownish red lines).

The mylonitic fabric dips rather steeply to the E-ENE. One NE-dipping fault surface containing top-to-E normal kinematics is also shown. (Figure 5-64).

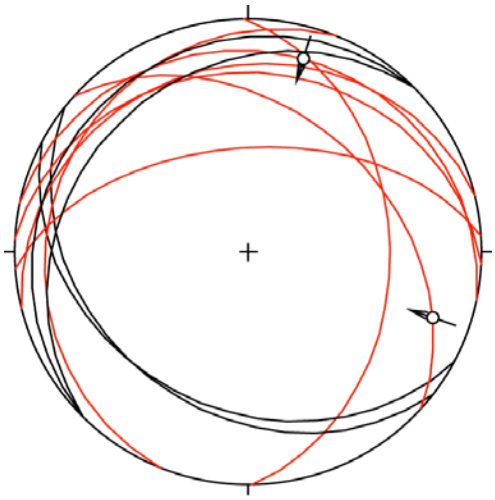

Figure 5-62. *Orientation of cataclastic and ultracataclastic bands (red great circles) and quartz and epidote veins (black circles) for depth interval 604–659 of KLX07A.*

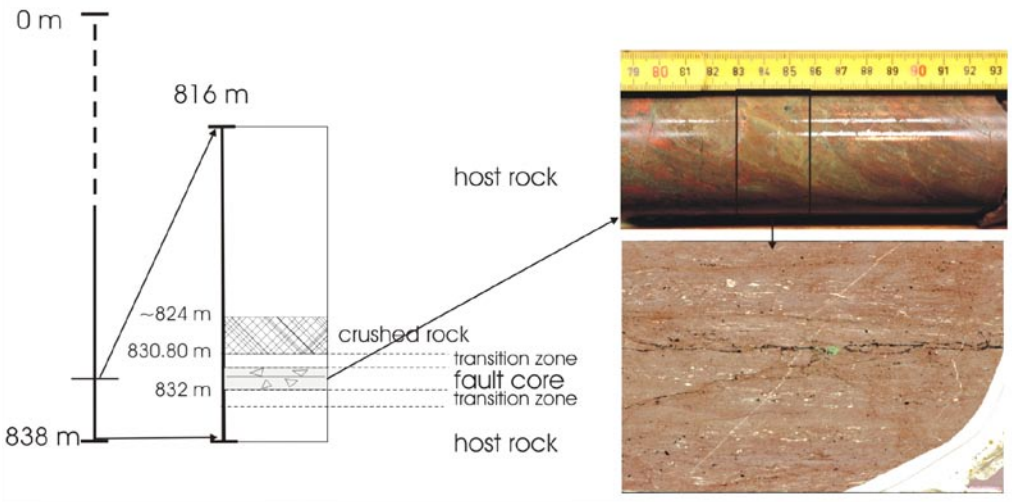

Figure 5-63. *Schematic illustration of studied section and thin section of a strongly foliated mylonitic rock locally reworked into an ultracataclasite (brownish-red and black bands). The deformation zone corresponds to DZ 13 of the single-hole interpretation. Chosen structural features' orientations are shown according to the right hand rule.*

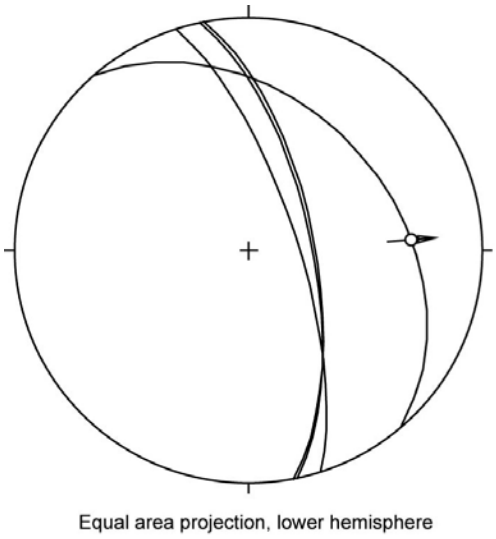

Figure 5-64. *Orientation of the mylonitic fabric in KLX07A, depth interval 816–838 m.*

5.2.5 Drill core KLX07B (120–175 m)

This section corresponds to DZ 3 in the single-hole interpretation /Carlsten et al. 2006b/. The core section contains mainly undisturbed rock, except for a minor fault zone consisting of fault and crushed rocks at depth 130 m (Figure 5-65). Fault rocks are protocataclasites, cataclasites and ultracataclasites. Thin sections show A) cataclasites with angular granite fragments and some fine-grained matrix (black) and abundant epidote, and B) ultracataclasites/gouge (black) with fragments of cataclasite (Figure 5-65). The gouge has very sharp contacts to the ultracataclastic bands sandwiching it.

Cataclastic bands dip at shallow to moderate angle to the NNE-NE, and gouge occurrences are concordant (black and red great circles in Figure 5-66, respectively). Two slickensided fault surfaces, also with moderate dip in the same direction, constrain a top-to-NNE extension episode (Figure 5-66). The steep W-dipping plane plots a discrete brittle-ductile shear zone decorated by quartz and epidote with a distinctive S/C fabric.

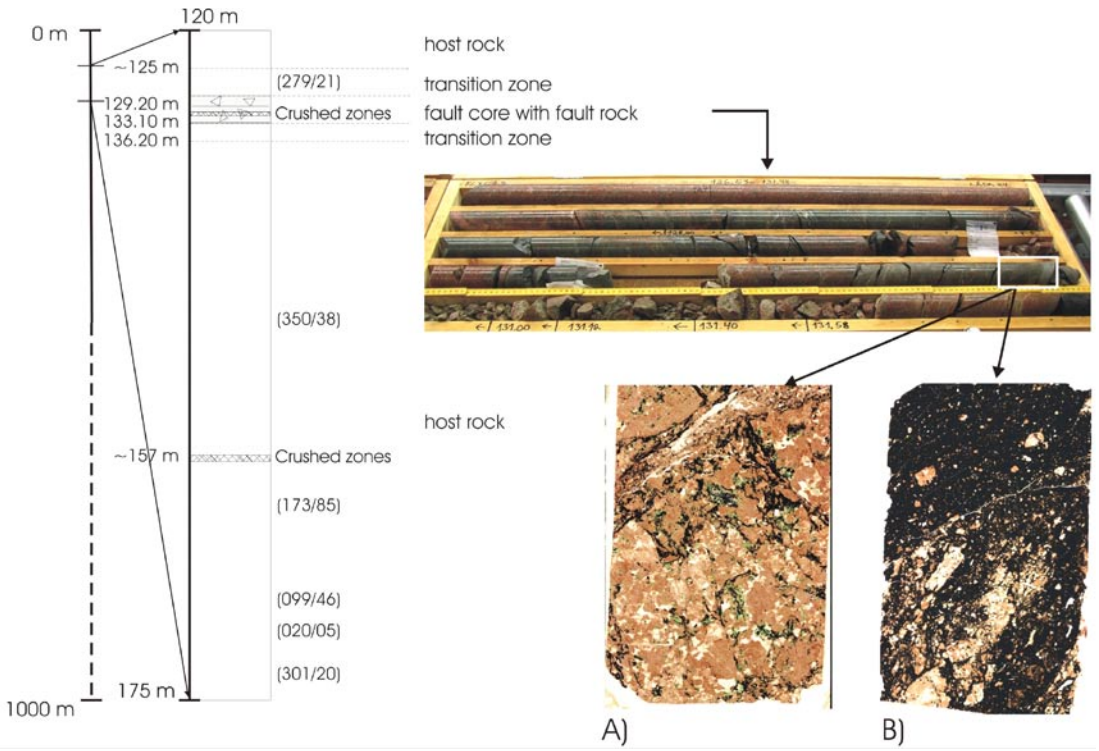

Figure 5-65. *Structural log of KLX07B logged and pictures illustrating the fault zone occurring at depth 130.92 m. A) Scanned thin section of cataclasite with network of finer-grained ultracataclasites and gouge (black), and abundant epidote. B) Scanned thin section of gouge (black)/ultracataclasite with clasts of cataclasite. The section corresponds to DZ3 in the single-hole interpretation /Carlsten et al. 2006b/. Chosen structural features' orientations are shown according to the right hand rule.*

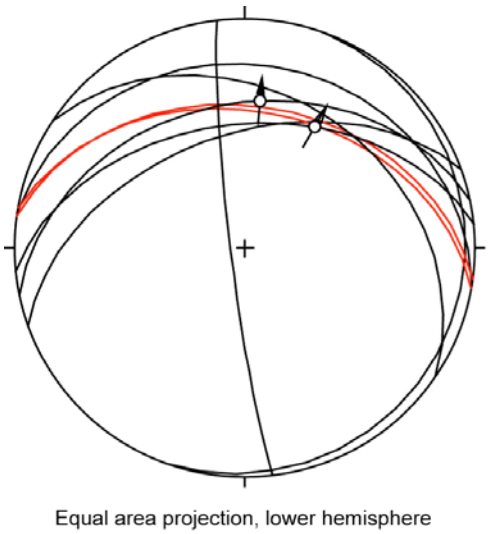

Figure 5-66. *Orientation of cataclastic occurrences in KLX07B (black great circles), gouge layers (red circles) and striated planes with top-to-NNE normal kinematics.*

5.2.6 Drill core KLX08

Depth interval 100–165 m

This section corresponds to DZ 1 and 2 in the single-hole interpretation /Carlsten et al. 2006c/. A complex transition zone characterizes the logged interval with both variations in bedrock types and occurrences of narrow fault rock-containing fault cores (Figure 5-67). The transition zone has in general a relatively high fracture frequency and numerous strands of cataclasites, ultracataclasites and gouge. Locally there occur cemented breccias, as shown in Figure 5-67 at an approximate depth of 150 m. The breccia at depth 152 m seems more porous and non-cemented. These breccias are very thin, 2–3 cm in thickness at the most.

The deformation zone contains a few striated planes that dip shallowly to the SW or NE. Slickenlines are mostly defined by chlorite and calcite. Kinematic indicators show predominantly reverse shear along these planes.

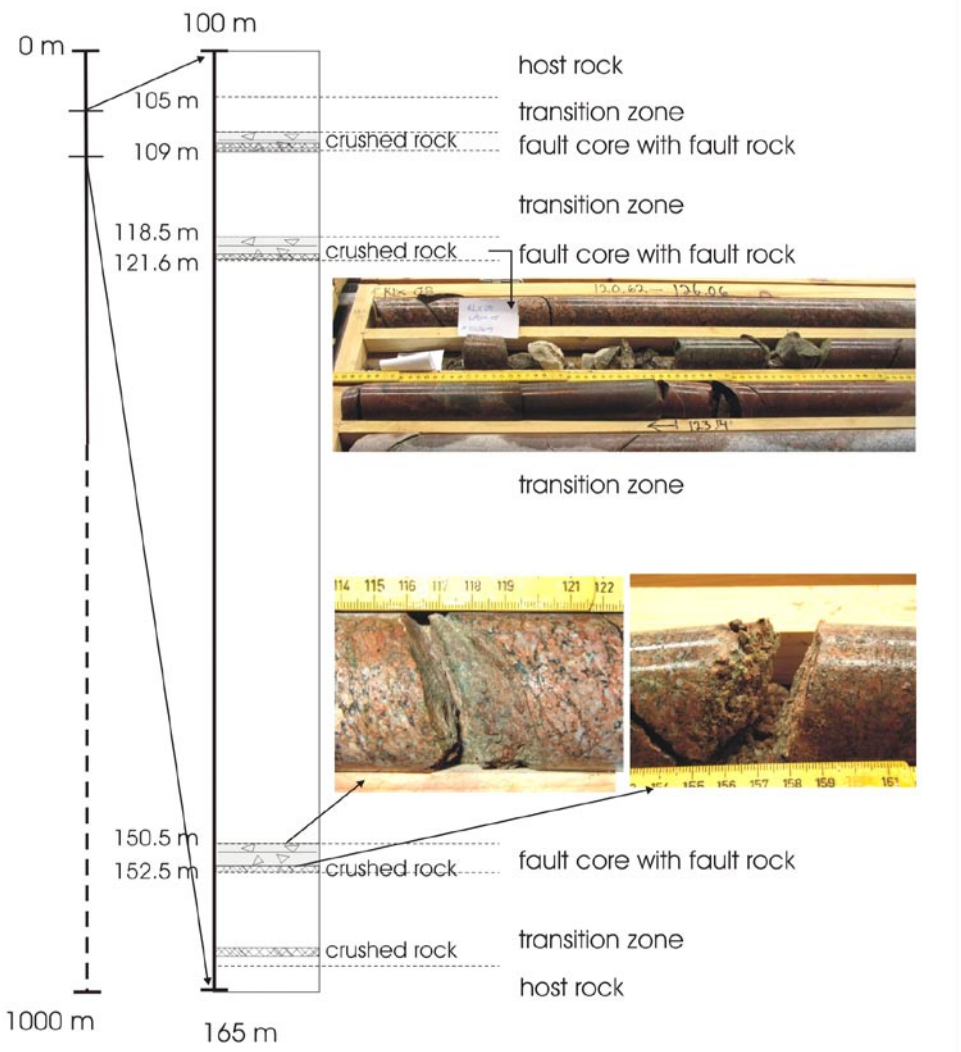

Figure 5-67. *Schematic illustration of the mapped section. The section contains DZ 1 and DZ 2 of the single-hole interpretation.*

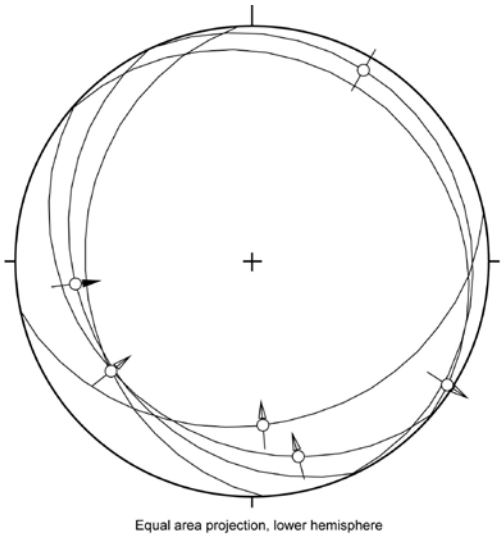

Figure 5-68. *Striated planes found in the depth interval 100–165 m of drill core KLX08.*

Depth interval 218–252 m

This section corresponds to DZ 3 and 4 in the single-hole interpretation /Carlsten et al. 2006c/. The logged interval begins with a ~ 2 metres core loss, a transition to crushed rock and a possible breccia (Figure 5-69). The core loss was possibly due to the occurrence of non-cohesive fault rock, such as breccia. The rest of the section is characterized by relatively undisturbed rock, with only a narrow fault core formed by crushed cataclasites and a few occurrences of thin cataclasite bands in the transition zone.

Apart from one subvertical reverse fault plane, all crush zones (240/23, 161/20) and the orientation of the breccia horizon at the top of the section (207/26 for the upper contact and 296/25 for the lower) dip gently to SW, NE and predominantly to the NW (Figure 5-70).

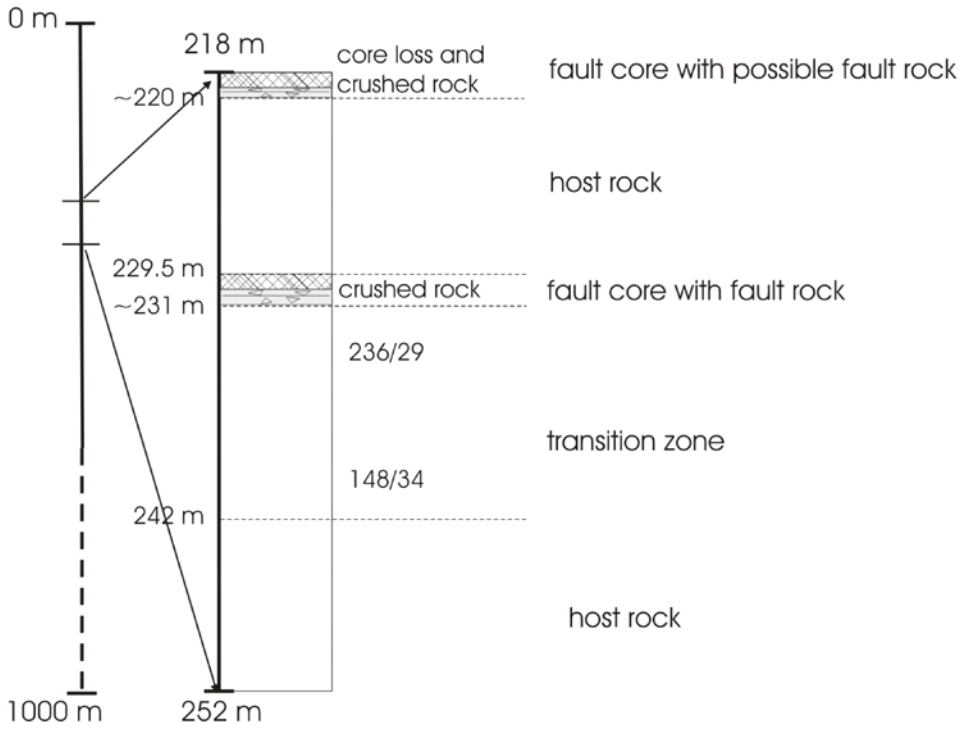

Figure 5-69. *Schematic illustration of the section under discussion. The fault cores are very narrow and the logged section consists predominantly of undeformed rock. DZ3 and DZ 4 of the single-hole interpretation are contained within this depth interval.*

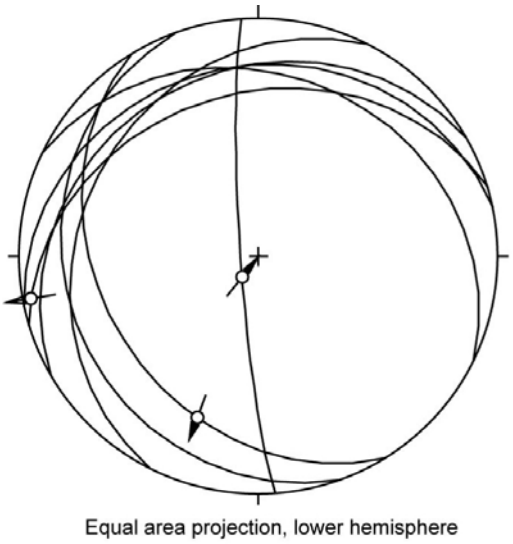

Figure 5-70. *Shallow dips characterize crush zones and brecciated horizons within interval 218–252 m of KLX08.*

Depth interval 760–781 m

It is a short and complex section with a narrow fault core (Figure 5-71). The fault core is located at a lithological contact, with predominantly mafic rocks in the hanging wall and granitic rocks in the footwall. The fault rock is comprised of a complex association of cataclasites, ultracataclasites and gouge (Figure 5-72**)**. These fault rocks bear evidence of multiple reactivation. The ultracataclasite/gouge that occurs in the core of the zone, which is brown to green in colour, contains fragments of cataclasite, granite, calcite crystals, chlorite and epidote (Figure 5-72). The broad deformation zone core has interfingered ultracataclasites and even finer-grained gouge (Figure 5-72) and there are ghosts of layering/foliation.

Figure 5-73 shows the orientation of the margins of the complex structure that dip consistently NW at high angle. A slickensided surface immediately above the upper contact provides indication about a possible dextral plus north side up kinematics for the structure.

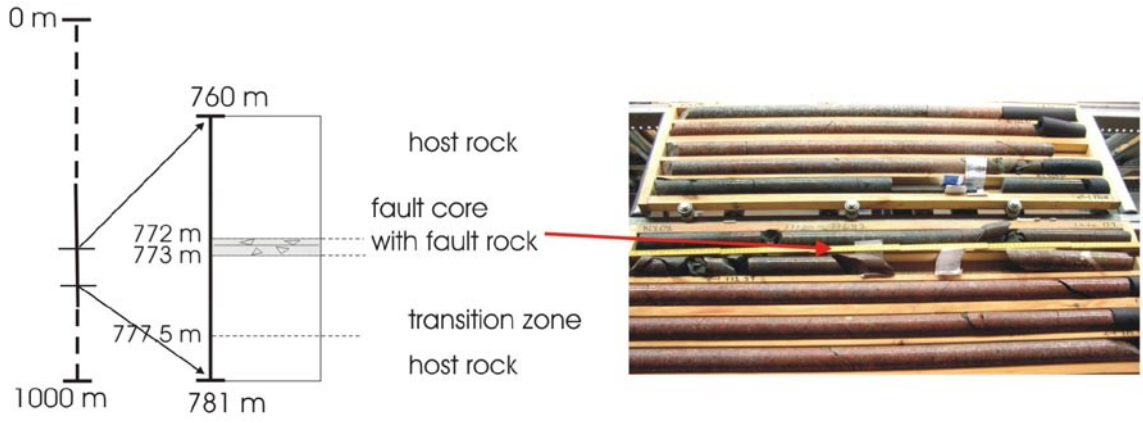

Figure 5-71. *Schematic illustration of the mapped section. This section is described as DZ 9 in the single-hole interpretation. A detailed figure of the fault rock is shown in Figure 5-72.*

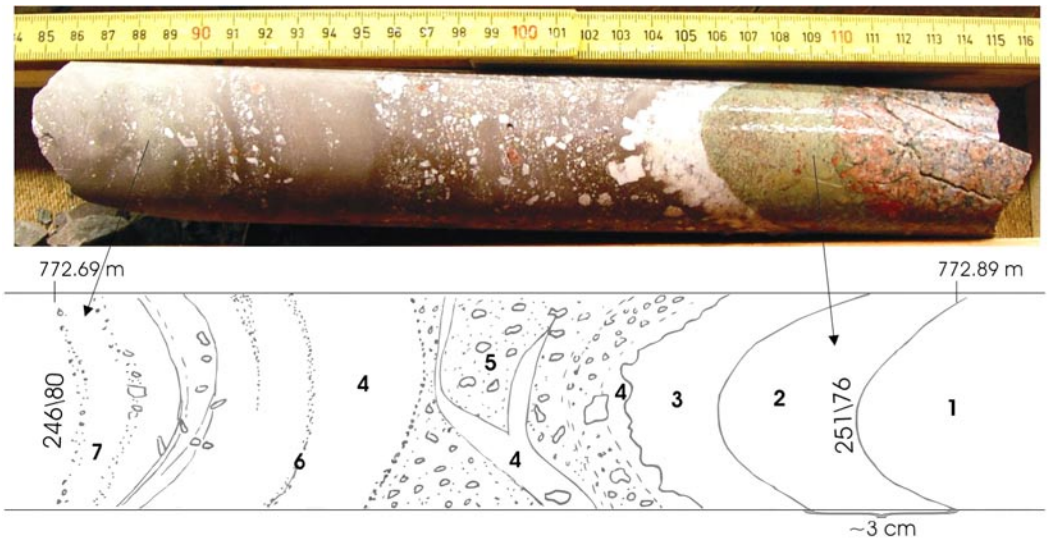

1- Protocataclasite with transition to cataclasite with granite clasts.
2- Epidote "vein" with caltaclasite clasts, possibly epidite cemented cataclasite with high % matrix.
3- Growth of calcite minerals.
4- Gouge / ultracataclasite, brown colour. Close to 100% matrix
5- Cataclasite with clasts of calcite, granite, epidote and abundant cataclasite. The clasts range in size of 1 cm to 0.1 mm. Matrix 60-70%.
6- Clasts of calcite, epidote, granite and cataclasite with great variation in size.
7- Ultracataclasite / gouge with chlorite as dominant matrix content.

Figure 5-72. *Complex fault rock occurrence with several generations of cataclasites, epidote and calcite veining.*

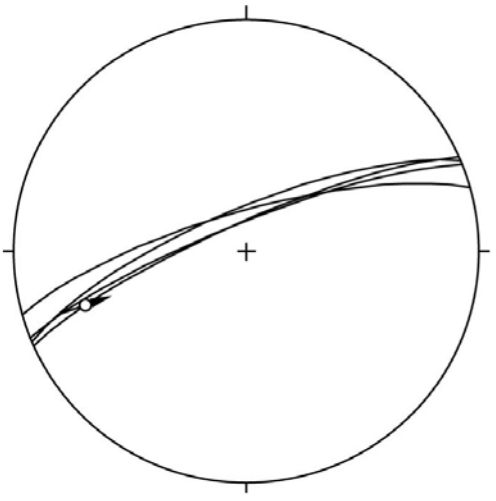

Equal area projection, lower hemisphere

Figure 5-73. *Orientation of the structure illustrated in Figure 5-72.*

5.2.7 Drill core KLX10 (389–432 m and 471–499 m)

KLX10 389–432.5 m

In the single-hole interpretation this section is described as DZ 6 /Carlsten et al. 2006a/. A deformation zone defined by relatively steep, pervasive fractures characterizes this section (Figure 5-74). The fractures run parallel to the core axis. These fractures have the character of joints, many with millimetric aperture, and they tend to follow and exploit an older sealed network of calcite (?) veins with a similar orientation. Examples of these joints are shown in the upper picture in Figure 5-74. In the last few metres of the section the fracture frequency decreases and there occurs a progressive transition to undisturbed rock. Joints strike consistently E/ESE-W/WNW (Figure 5-75).

In the section there are a few occurrences of fault rocks in thin bands (maximum thickness 5 cm). These are not distinctive enough to form a fault core. This section differs in character from all other sections studied.

KLX10 471–499 m

This section is described as DZ 7 in the single-hole interpretation /Carlsten et al. 2006a/. It is characterized by an extremely low fracture frequency and undisturbed rock (Figure 5-74). The only exceptions are 3–4 small intervals of altered rock, with pervasive red staining and isolated occurrences of millimetric cataclastic bands. Examples are shown in the bottom picture of Figure 5-74.

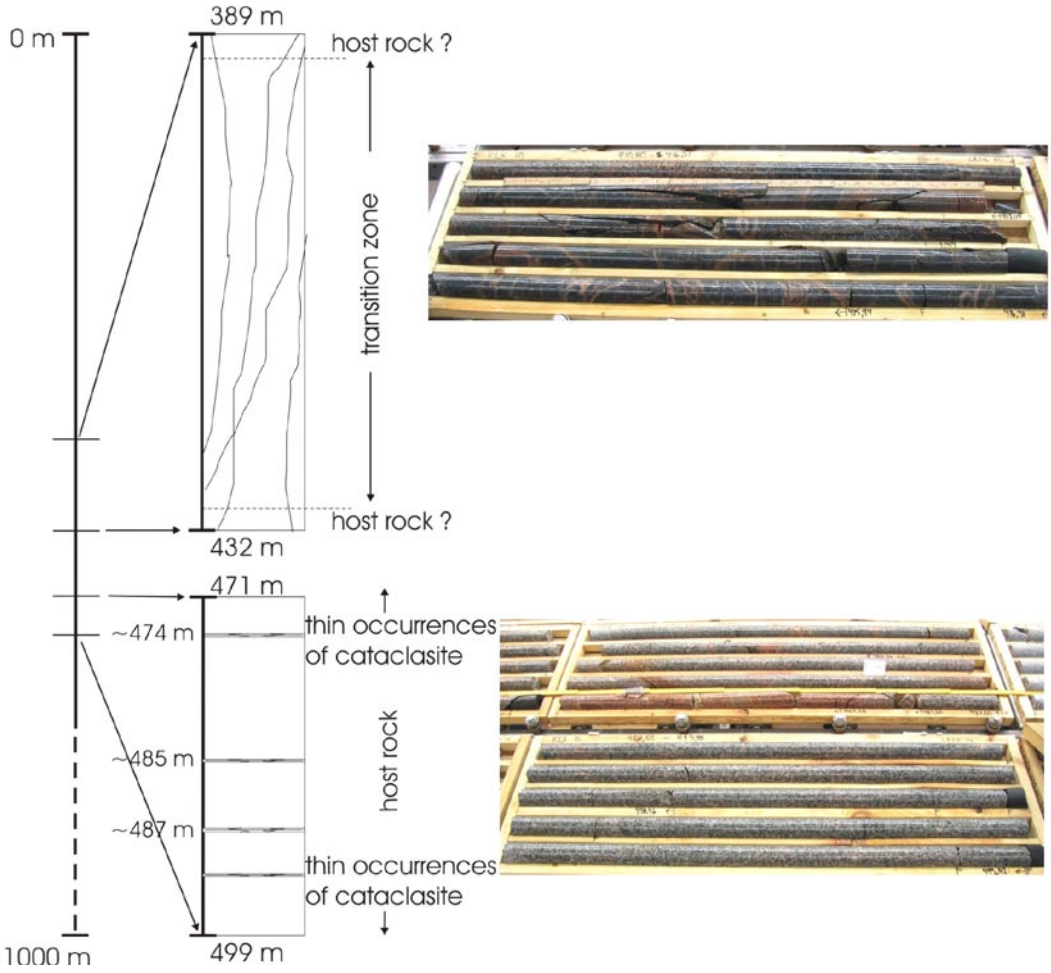

Figure 5-74. *Schematic illustration of the sections logged in drill core KLX10.*

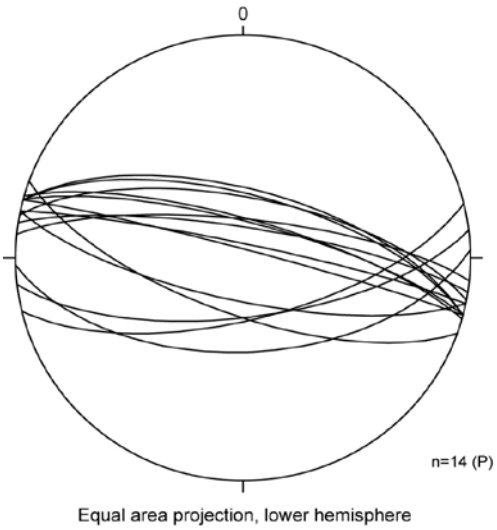

Figure 5-75. *A strong E/ESE-W/WNW joint preferred orientation is observed in depth interval 389–432 of KLX10.*

5.2.8 Summary and discussion of drill core data

Most of the drill cores studied during this project intersect fault planes decorated by cohesive fault rocks, predominantly cataclasites. Foliated cataclasites, phyllonites and mylonites do occur, but only very sporadically, confirming the result of the field study. Fault gouge (both cohesive and non-cohesive) is abundant and very distinct, and commonly occurs in the central part of fault cores. Green gouge is not common, but when it occurs it is usually in association with the red gouge. Non-cohesive fault rocks, such as breccias, were not identified in any core, but they might be lacking due to mechanical problems during the recovery of faulted, incohesive drill cores leading to core losses. Field observations, however, never showed any significant presence of breccias in the area.

The deformation zones identified, studied and characterized during this project contain evidence for a complex, tectonic activitiy, with several generations of crosscutting cataclastic rocks indicating multiple faulting events, and polyphase reactivation. It is difficult to assign specific kinematics to the different events.

Fault rocks observed in the drill cores are comparable to fault rocks observed in the field.

6 References

Braathen A, 1999. Kinematics of brittle faulting in the Sunnfjord region, western Norway. Tectonophysics 302, 99–121.

Braathen A, Gabrielsen R H, 2000. Bruddsoner i fjell – oppbygning og definisjoner. Gråstein, 7, 1–20. Norges geologiske undersøkelse, ISSN 0807-4801.

Braathen A, Osmundsen P T, Nordgulen Ø, Roberts D, Meyer G B, 2002. Orogen-parallel extension of the Caledonides in northern Central Norway: an overview. Norwegian Journal of Geology, 82, 225–241.

Braathen A, Osmundsen P T, Gabrielsen R, 2004. Dynamic development of fault rocks in a crustal-scale detachment; an example from western Norway. Tectonics, 23, TC4010, doi:10.1029/2003TC001558.

Caine J S, Evans J P, Forster C B, 1996. Fault zone architecture and permeability structure. Geology, 24, 11, 1025–1028.

Carlsten S, Wahlgren C H, Hultgren P, Mattsson H, Stanfors R, 2006a. Geological single-hole interpretation of KLX10, HLX20 and HLX35. SKB P-06-174, Svensk Kärnbränslehantering AB.

Carlsten S, Wahlgren C H, Hultgren P, Mattsson H, Stanfors R, 2006b. Geological single-hole interpretation of KLX07A, KLX07B, HLX34 and HLX35. SKB P-06-175, Svensk Kärnbränslehantering AB.

Carlsten S, Wahlgren C H, Hultgren P, Mattsson H, Stanfors R, 2006c. Geological single-hole interpretation of KLX08. SKB P-06-176, Svensk Kärnbränslehantering AB.

Cronquist T, Forssberg O, Hansen L M, Koyi S, Vestgård J, Wikholm M, 2006. Oskarshamn site Investigation. Detailed outcrop mapping on drillsite KLX11. SKB P-06-06, Svensk Kärnbränslehantering AB.

Davis G H, Reynolds S J, 1996. Structural geology of rock and regions. 776 pp.

Ehrenborg J, Stejskal V, 2004. Boremap mapping of core drilled boreholes KSH03A and KSH03B. Oskarshamn site investigation. SKB P-04-132, Svensk Kärnbränslehantering AB.

Evens J P, Forster C B, Goddard J V, 1997. Permeability of fault-related rocks, and implications for hydraulic structure of fault zones. Journal of Structural Geology, 19, 1393-1404.

Gudmundsson A, Berg S S, Lyslo K B, Skurtveit E, 2001. Fracture networks and fluid transport in active fault zones. Journal of Structural Geology 23, 343–353.

Higgings M W, 1971. Cataclastic Rocks. Geological Survey Professional Paper, 687, 1–97.

Hultgren P, Stanfors R, Wahlgren C H, Carlsten S, Mattsson H, 2004. Oskarshamn site investigation. Geological single-hole interpretation of KSH03A, KSH03B, KLX02, HAV09, and HAV10. SKB P-04-231, Svensk Kärnbränslehantering AB.

Mattson H, 2005. Interpretation of geophysical borehole measurements from KLX06. Oskarshamn site investigation. SKB P-05-44, Svensk Kärnbränslehantering AB.

Mattson H, Thunehed H, Keisu M, 2005. Intepretation of geophysical borehole measurements and compilation of petrophysical data from KLX01, KLX03, KLX04, HLX21, HLX22, HLX23, HLX24, HLX25, HLX26, HLX27 and HLX28. Oskarshamn site investigation. SKB P-05-34, Svensk Kärnbränslehantering AB.

Munier R, Stanfors R, Milnes A G, Hermanson J, Triumf C A, 2003. Geological Site Descriptive Model. A strategy for the development during site investigations. SKB R-03-07, Svensk Kärnbränslehantering AB.

Nordgulen Ø, **Braathen A, Corfu F, Osmundsen P T, Husmo T, 2002.** Polyphase kinematics and geochronology of the Kollstraumen detachment, north-central Norway. Norwegian Journal of Geology, 82, 299–316.

Osmundsen P T, Braathen A, Nordgulen Ø, Roberts D, Meyer G B, Eide E A, 2003. The Nesna shear zone and adjacent gneiss-cored culminations, North-central Norwegian Caledonides. Journal of the Geological Society, London 160*,* 1–14.

Persson Nilsson K, Bergman T, Eliasson T, 2004. Oskarshamn site investigation. Bedrock mapping 2004 – Laxemar subarea and regional model area. Outcrop data and description of rock types. SKB P-04-221, Svensk Kärnbränslehantering AB.

Petit J P, 1987. Criteria for the sense of movement on fault surfaces in brittle rocks. Journal of Structural Geology 9, 597–608.

Rowe C D, Moore J C, Meneghini F A, McKeirnan W, 2005. Large-scale pseudotachylytes and fluidized cataclasites from an ancient subduction thrust fault, Geology, 33, 937–940.

Röshoff K, Cosgrove J, 2002. Sedimentary dykes in the Oskarshamn-Västervik area. A stydy of the mechanism of formation.

Sibson R H, 1977. Fault rocks and fault mechanisms. J Geol Soc London, 133, 191–213.

Wahlgren C H, Ahl M, Sandahl K A, Berglund J, Petersson J, Ekström M, Persson P O, 2004. Oskarshamn site investigation. Bedrock mapping 2003 – Simpevarp subarea. Outcrop data, fracture data, modal and geochemical classification of rock types, bedrock map, radiometric dating. SKB P-04-102, Svensk Kärnbränslehantering AB.

Wahlgren C H, Bergman T, Persson Nilsson K, Eliasson T, Ahl M, Ekström M, 2005. Oskarshamn site investigation. Bedrock map of the Laxemar subarea and surroundings. Description of rock types, modal and geochemical analyses. SKB P-05-180, Svensk Kärnbränslehantering AB.

Appendix

List of localities and samples

List of studied field localities.

Field localities			Swedish grid, RT 90	
Name	Northing (m)	Easting (m)	Accuracy	Area
PSM 007630	6367536	1547573	8 metres	Laxemar
PSM 007631	6367218	1547636	10 metres	Laxemar
PSM 007632	6367018	1547958	7 metres	Laxemar
PSM 007633	6367002	1547836	6 metres	Laxemar
PSM 007634	6365518	1550051	8 metres	Laxemar
PSM 007635	6365232	1550249	6 metres	Laxemar
PSM 007636	6365205	1550473	8 metres	Laxemar
PSM 007637	6366534	1548707	7 metres	Laxemar
PSM 007638	6365484	1550505	8 metres	Laxemar
PSM 007639	6366157	1552167	6 metres	Simpevarp
PSM 007640	6366342	1546600	5 metres	Laxemar
PSM 007641	6366825	1551768	5 metres	Ävrö
PSM 007642	6367295	1553551	11 metres	Ävrö
PSM 007643	6367266	1553550	9 metres	Ävrö
PSM 007644	6367141	1553530	6 metres	Ävrö
PSM 007645	6367113	1553507	6 metres	Ävrö
PSM 007646	6366972	1553367	6 metres	Ävrö
PSM 007647	6365222	1551104	8 metres	Simpevarp
PSM 007648	6365337	1552294	6 metres	Simpevarp
PSM 007649	6365430	1552372	6 metres	Simpevarp
PSM 007650	6365573	1552301	8 metres	Simpevarp
PSM 007651	6365560	1552264	6 metres	Simpevarp
PSM 007652	6365989	1552684	6 metres	Simpevarp
PSM 007653	6365948	1552622	8 metres	Simpevarp
PSM 007654	6365944	1552592	8 metres	Simpevarp
PSM 007655	6365905	1552386	7 metres	Simpevarp
PSM 007656	6366036	1552430	8 metres	Simpevarp
PSM 007657	6366198	1552727	6 metres	Simpevarp
PSM 007658	6366076	1552736	5 metres	Simpevarp
PSM 007659	6367495	1551540	11 metres	Äspö
PSM 007660	6366841	1551992	9 metres	Ävrö

List of field rock samples and thin sections.

Location	Sample ID	Field rock type identification	Thin section	SEM analysis
PSM 007633	A	Fault rock	Yes	
PSM 007634	A	Mylonite/cataclasite	Yes	
	B	Cataclasite	Yes	
	C	Mylonite/cataclasite	Yes	
	D	Mylonite	Yes	
PSM 007637	A	Cataclasite	Yes	
	B	Cataclasite	Yes	
	C	Cataclasite	Yes	
	D	Cataclasite	Yes	SEM
	E	Cataclasite	Yes	SEM
	E-E	Cataclasite	Yes	
	F	Cataclasite	Yes	
	G	Cataclasite	Yes	
	H	Cataclasite	Yes	
	I	Host rock?	Yes	
	J	Fault rock	Yes	
	K	Fault rock	Yes	
	L	Fault rock	Yes	
	M	Fault rock	Yes	
	N	Fault rock	Yes	
	O	Fault rock	Yes	
	P	Fault rock	Yes	
	Q	Fault rock	Yes	
PSM 007640	A	Joint sedimentary infill	Yes	
PSM 007644	A	Cataclasite	Yes	
	B	Mylonite	Yes	SEM
PSM 007646	A	Fault rock	No	
	B	Cataclasite	Yes	SEM
	C	Ultracataclasite	Yes	
	D	Dike for zircon dating	No	
PSM 007653	A	Ultrabreccia / Hydrofracture injection (pseudotachylyte)?	Yes	
PSM 007657	A	Cataclasite / ultracataclasite	Yes	SEM

Drill core information.

ID-code	Inclination (degrees)	Bearing (degrees)	Northing (m)	Easting (m)	Coordinate system
KLX02	–85.000	358.120	6366768.985	1549224.090	RT90–RHB70
KLX03	–74.930	199.040	6366112.590	1547718.920	RT90–RHB70
KLX04	–84.720	1.620	6367077.190	1548171.940	RT90–RHB70
KLX05	–65.160	190.050	6365633.340	1548909.410	RT90–RHB70
KLX06	–65.230	328.810	6367806.640	1548566.880	RT90–RHB70
KLX07A	–60.040	174.180	6366752.090	1549206.860	RT90–RHB70
KLX07B	–85.002	174.330	6366753.135	1549206.758	RT90–RHB70
KLX08	–60.250	199.170	6367079.100	1548176.710	RT90–RHB70

Deformation zones: Drill core “secup” and “seclow”.

ID code	From depth (m)	To depth (m)	Deformation zone
KLX03	722.5	814	DZ1
KLX04	227	230	DZ1
KLX04	254	258	DZ2
KLX04	295	298	DZ3
KLX04	325	326	DZ4
KLX04	346	355	DZ5
KLX04	873	973	DZ6
KLX06	200	260	DZ1
KLX06	297	425	DZ2
KLX07A	105	147	DZ1
KLX07A	167.9	168.3	DZ2
KLX07A	184.8	185.4	DZ3
KLX07A	604	654.7	DZ10
KLX07A	816.8	835.5	DZ13
KLX07B	124	172	DZ3
KLX08	100	131	DZ1
KLX08	150.32	159	DZ2
KLX08	211.5	220	DZ3
KLX08	769	778	DZ9
KLX10	396	416	DZ6
KLX10	478	486	DZ7
KSH03A	162	275	DZ1

List of drill core thin sections.

Sample ID	Borehole	Låda	Depth from	Depth to	Comment
KLX04/1	KLX04	143	874,660	874,780	
KLX04/2	KLX04	143	876,270	876,400	
KLX04/3	KLX04	146	889,390	889,480	
KLX04/4	KLX04	146	889,480	889,620	
KLX04/5	KLX04	153	929,290	929,390	
KLX04/6	KLX04	157	946,190	946,350	
KLX04/7	KLX04	157	949,560	949,680	
KSH03A/1	KSH03A	24	221,526	221,613	Gouge
KSH03A/2	KSH03A	29	246,850	246,924	Ultracataclasite
KSH03A/3	KSH03A	32	261,370	261,500	Hydraulic breccia-cataclasite
KSH03A/4	KSH03A	33	267,210	267,265	Transition phyllonite-cataclasite
KSH03A/5	KSH03A	33	268,985	269,045	Pervasively foliated phyllonite
KSH03A/6	KSH03A	33	270,295	270,325	Cataclasite
KLX07A/1	KLX07A	4	119,570	119,770	Ultra-cataclasite with crosscutting faults
KLX07/2	KLX07	132	831,460	831,520	
KLX07B/1a	KLX07B	24	130,800	130,887	Ultracataclasite-gouge
KLX07B/1b	KLX07B	24	130,800	130,887	Ultra-cataclasite
KLX06/1	KLX06	52	384,051	384,100	